Technische Universität München

Fakultät für Medizin

TUT

The Role of FRA1 and SUMOylation
in Pancreatic Cancer

Christian Andreas Schneeweis

Vollständiger Abdruck der von der Fakultät für Medizin der Technischen Universität München

zur Erlangung eines

Doktors der Naturwissenschaften (Dr. rer. nat.)

genehmigten Dissertation.

Vorsitz: Prof. Dr. Susanne Kossatz

Prüfer*innen der Dissertation:

     1.   Prof. Dr. Günter Schneider
     2.   Prof. Dr. Bernhard Küster

Die Dissertation wurde am 20.10.2022 bei der Technischen Universität München eingereicht

und durch die Fakultät für Medizin am 21.02.2023 angenommen.

Table of Contents

List of Figures

List of Tables

Abbreviations

°C	Degree Celsius
4-OHT	4-hydroxytamoxifen
AML	Acute myeloid leukemia
AP-1	Activator protein 1
APS	Ammonium-persulfate
ATP	Adenosine triphosphate
AUC	Area-under-the-curve
BET	Bromodomain and extra-terminal proteins
bp	Base pairs
BRCA1	Breast cancer 1, early onset
BRCA2	Breast cancer 2, early onset
BSA	Bovine Serum Albumin
bZIP	Basic leucine zipper
Cas9	CRISPR-associated protein 9
CDKN2A	Cyclin Dependent Kinase Inhibitor 2A
cDNA	Complementary DNA
cm	Centimeter
CO_2	Carbon dioxide
CRE	cAMP-responsive elements
CRISPR	Clustered Regularly Interspaced Short Palindromic Repeats
Ct	cycle threshold
DAPI	4′,6-diamidino-2-phenylindole
DDR	DNA damage repair
dH2O	distilled water

DMEM	Dulbecco's Modified Eagle's Medium
DMSO	Dimethyl sulfoxide
DNA	Deoxyribonucleic acid
DNase	Deoxyribonuclease
dNTP	Deoxynucleotide Triphosphate
E-box	Enhancer box
EDTA	Ethylenediaminetetraacetic acid
EGFR	Epidermal Growth Factor Receptor
EMT	Epithelial-to-mesenchymal
ERK	extracellular signal-regulated kinases
ERKi	ERK inhibitor
et al.	et alii (and others)
EtBr	Ethidium bromide
EtOH	Ethanol
FBS	Fetal bovine serum
FDA	US Food and Drug Administration
Flp	Flippase
FOLFIRINOX	Fluorouracil, leucovorin, irinotecan, and oxaliplatin
FOSL1	FOS-related antigen 1
Fra1	FOS-related antigen 1
FSF	Frt-Stop-Frt
g	Gram
GAP	GTPase-activating protein
GAPDH	Glyceraldehyde 3-phosphate dehydrogenase
GFP	Green fluorescent protein
GG	Di-Glycine
GI_{50}	half-maximal growth inhibitory concentration
GSEA	Gene set enrichment analysis
GTP	Guanosine triphosphate
h	Hours
H_2O	Water

HDAC	Histone deacetylase
HEPES	4-(2-hydroxyethyl)-1-piperazineethanesulfonic acid
HRP	Horseradish peroxidase
HRR	homologous recombination repair
HSP90	Heat shock protein 90
IFN1	type 1 interferon
k	kilo
kb	Kilobase-pairs
KC	$Ptf1a^{Cre/+}; LSL\text{-}Kras^{G12D/+}$
KCF	$Ptf1a^{Cre/+}; LSL\text{-}Kras^{G12D/+}; Fra1^{lox/lox}$
kDa	Kilodalton
kg	Kilogram
KRAS	KRAS proto-oncogene, GTPase
LSL	LoxP-stop-LoxP
m	milli
M	Molar
mA	Milliampere
MAX	MYC-associated factor X
MEK	Mitogen-activated protein kinase kinase
MEKi	MEK inhibitor
mg	Milligram
min	Minute
mL	Milliliter
mm	Millimeter
mM	Millimolar
mRNA	messenger-RNA
MTT	3-(4,5-dimethylthiazol-2-yl)-2,5-diphenyltetrazolium bromide
mut	Mutated
MYC	MYC proto-oncogene, bHLH transcription factor
MYC^{ER}	fusion protein of MYC and Estrogen receptor (ER) ligand binding domain
n =	Number =

n	nano
NEM	N-ethylmaleimide
NF1	Neurofibromin 1
ng	Nanogram
nm	Nanometer
nM	Nanomolar
NSCLC	non-small-cell lung cancer
NTRK	Neurotrophic tyrosine receptor kinase
p	Phospho
PAGE	Polyacrylamide gel electrophoresis
PanIN	Pancreatic intraepithelial neoplasia
PARP	Poly (ADP-ribose) polymerases
PBS	Phosphate buffered saline
PBS-T	Phosphate Buffered Saline with Tween ® 20 (0.1%)
PCR	Polymerase chain reaction
PDAC	Pancreatic ductal adenocarcinoma
PDEC	Primary pancreatic ductal epithelial cells
Pdx1	Pancreatic and duodenal homeobox 1
PI	Propidium Iodide
PI3K	Phosphatidylinositol 3-kinase
PML	Promyelocytic leukemia
POLO trial	Pancreas Cancer Olaparib Ongoing trial
PP2A	Protein phosphatase 2A
PPT	Pancreatic primary tumor
PROTAC	PROteolysis TArgeting Chimeras
PS	Phosphatidylserine
Ptf1	Pancreas transcription factor 1
PTM	Post-translational modifications
PTPN11	protein tyrosine phosphatase SHP2
PVDF	Polyvinylidene fluoride
qPCR	quantitative PCR

R26	Rosa 26
RAF	rapidly accelerated fibrosarcoma
RAFi	RAF inhibitor
RAS	Rat sarcoma
RBD	Ras-binding domain
RNA	Ribonucleic acid
RNase	Ribonuclease
ROS	Reactive oxygen species
RRID	Research Resource Identifiers
RT	Room temperature
RTK	Receptor tyrosine kinase
SAE	SUMO1-activating enzyme
SD	Standard Deviation
SDS	Sodium dodecyl sulfate
SDS-PAGE	Sodium dodecyl sulphate–polyacrylamide gel electrophoresis
SENP	SUMO1/sentrin specific peptidase
Ser	Serine
shRNA	Small hairpin RNA
SNIP1	Smad nuclear interacting protein 1
SNP	Single-nucleotide polymorphism
STR	Short Tandem Repeat
SUMO	Small ubiquitin-like modifier
SUMOi	SUMOylation inhibitor
TAE	Tris Acetate EDTA
TEMED	N,N,N',N'-Tetramethylethylenediamine
Thr	Threonine
TP53	Tumor protein p53
TRE	TPA-responsive element
TRIS	Tris-(hydroxymethyl)-amino methane
Trp53	Transformation related protein 53
TSO	Template Switch Oligo

Tyr	Tyrosine
U	Unit
UBC9/UBE2I	Ubiquitin Conjugating Enzyme E2
UBE2I	Ubiquitin Conjugating Enzyme E2
UV	Ultra violet
V	Volt
v/v	Volume per volume
w/v	Weight per volume
WT	Wild type
μ	micro
μg	Microgram
μL	Microliter
μm	Micrometer
μM	Micromolar
x g	relative centrifugal force (times gravity)

Abstract

Pancreatic ductal adenocarcinoma (PDAC) is an almost universally fatal disease with a five-year survival rate of 10% that is projected to become the second leading cause of cancer-related deaths in the Western world within the next decade. Whereas targeted therapies have greatly improved survival for other tumor types, cytotoxic chemotherapies are still standard-of-care for PDAC and targeted therapies have largely failed to show clinical benefit. This underscores the need to identify therapeutic targets for PDAC and stratify patients accordingly.

The transcription factors FRA1 and MYC are critical signaling nodes engaged by mutant KRAS, which is the major oncogenic driver of PDAC. Functions of both transcription factors were analyzed in this study.

FRA1 is activated upon induction of oncogenic KRAS in pancreatic ductal epithelial cells. To study its role in tumor maintenance and therapy response in more detail, isogenic FRA1 gain- and loss-of-function models were generated. A growth-promoting role of FRA1 was observed in PDAC cells. However, FRA1-deficient cells were viable and acute perturbation of FRA1 affected cellular growth only slightly. To identify inhibitors that synergize with loss of FRA1, isogenic FRA1-proficient and -deficient PDAC cells were screened with a drug library, which revealed that perturbation of FRA1 sensitizes to MAPK pathway inhibitors. This finding was validated by viability and clonogenic assays and across different gain- and loss-of-function genetic models. Western blot analysis demonstrated increased phosphorylation of ERK upon loss of FRA1, suggesting a heightened dependence on this pathway that might explain the increased susceptibility of FRA1-deficient cells to MAPK pathway inhibitors.

The MYC oncogene is a major driver of PDAC, whose amplification is linked to a worse survival. In a gene set enrichment analysis (GSEA), MYC-amplified tumors showed an enrichment of SUMOylation gene signatures. SUMOylation is a dynamic post-translational modification that controls a variety of cellular processes such as transcription, signaling, DNA repair or mitotic progression. In a panel of human PDAC cells, cells with high MYC protein expression tended to show increased levels of SUMO-conjugated proteins in Western Blots

and activation of the SUMOylation machinery was observed upon overexpression of MYC. To determine whether the increased SUMOylation was a targetable vulnerability of high MYC expressing PDAC cells, a large panel of murine and human PDAC cells was screened with a SUMOylation inhibitor. This showed that MYC-high cells were more sensitive to SUMO inhibitors. Furthermore, genetic overexpression of MYC sensitized PDAC cells to SUMO inhibition. At the cellular level, SUMO inhibition caused arrest at the G2/M phase of the cell cycle, increased polyploidy and subsequent apoptosis, indicating that mitotic progression is a vulnerability especially in MYC-high PDAC cells that can be targeted by SUMO inhibitors.

Zusammenfassung

Mit einer 5-Jahres-Überlebensrate von 10% ist das duktale Adenokarzinom des Pankreas (pancreatic ductal adenocarcinoma: PDAC) eine fast immer tödliche verlaufende Erkrankung. Laut Prognosen, wird es innerhalb der nächsten Dekade die zweithäufigste krebsbedingte Todesursache in der westlichen Welt sein. Während zielgerichtete Therapien in anderen Tumorarten die Überlebensrate stark erhöht haben, ist die zytotoxische Chemotherapie immer noch die Standardtherapie für PDAC. Klinische Studien mit zielgerichteten Therapien für PDAC waren bisher weitestgehend erfolglos. Aus diesem Grund ist es wichtig therapeutische Zielstrukturen im PDAC zu identifizieren und Patienten dementsprechend zu stratifizieren.

Die Transkriptionsfaktoren FRA1 und MYC sind wichtige Signalknotenpunkte, die vom mutierten KRAS, dem hauptsächlichen onkogenen Treiber im Pankreaskarzinom, aktiviert werden. Funktionen beider Transkriptionsfaktoren werden in dieser Arbeit analysiert.

FRA1 wird in den duktalen Zellen des Pankreas aktiviert, wenn onkogenes KRAS genetisch angeschaltet wird. Um die Funktion von FRA1 für die Aufrechterhaltung des Tumors sowie das Ansprechen auf Therapien genauer zu untersuchen, wurden isogene Zellkulturmodelle entwickelt um FRA1 in PDAC Zellen genetisch an- oder auszuschalten. Damit konnte eine wachstumsfördernde Funktion von FRA1 in PDAC Zellen gezeigt werden. Allerdings, waren auch FRA1-defiziente Zellen noch lebensfähig und die akute Perturbation von FRA1 hatte nur geringfügige Auswirkungen auf das Zellwachstum. Um Inhibitoren zu finden, die eine synergistische Wirkung mit der Inhibition der FRA1-Expression haben, wurde ein Screening mit einer Wirkstoff-Sammlung in isogenen FRA1-profizienten und -defizienten Zellen durchgeführt. Dabei zeigte sich, dass FRA1-defiziente Zellen sensitiver gegenüber Inhibitoren des MAPK Signalwegs waren. Diese Beobachtung konnte in weiteren Analysen der Zellviabilität- und des klonogenen Wachstums sowie mit weiteren genetischen Modellen bestätigt werden. Im Western Blot zeigte sich eine erhöhte Phosphorylierung von ERK nach Ausschaltung von FRA1, was auf eine verstärkte Abhängigkeit von diesem Signalweg

hindeutet und die erhöhte Vulnerabilität von FRA1-defizienten Zellen gegenüber Inhibition des MAPK Signalweges erklären könnte.

Das MYC Onkogen ist ein wichtiger Treiber in PDAC. PDAC Patienten mit MYC Amplifikation haben eine geringere Überlebensrate. Mit Hilfe einer Genexpressionsanalyse, der sogenannten gene set enrichment analysis (GSEA), konnte gezeigt werden, dass MYC-amplifizierte Tumore erhöhte Gensignaturen für SUMOylierung aufzeigten. SUMOylierung ist eine dynamische post-translationale Modifizierung, die für die Kontrolle wichtiger zellulärer Prozesse wie der Transkription, DNA Reparatur oder mitotische Progression von entscheidender Bedeutung ist. Humane PDAC Zellen mit hoher MYC Proteinexpression zeigten in Western Blot Analysen tendenziell höhere Level an SUMO-konjugierten Proteinen. Des Weiteren aktivierte die Überexpression von MYC verstärkt die SUMOylierungs-Maschinerie. Um Herauszufinden, ob die erhöhte SUMOylierung von PDAC Zellen mit hoher MYC Expression eine therapeutische Vulnerabilität darstellt, wurde eine große Zahl muriner und humaner PDAC Zellen mit einem SUMO Inhibitor gescreent. Dabei zeigte sich, dass Zellen mit hoher MYC Aktivität sensitiver gegenüber SUMO Inhibition waren. Des Weiteren führte genetische Überexpression von MYC in den Zellen zu einer erhöhten Suszeptibilität. Auf der zellulären Ebene verursachte SUMO Inhibition einen Arrest in der G2/M Phase des Zellzyklus und führte zu einer erhöhten Polyploidie und letztendlich Apoptose. Dies deutet darauf hin, dass die mitotische Progression eine Vulnerabilität insbesondere von PDAC Zellen mit erhöhter MYC Expression darstellt, die sich therapeutisch nutzen lassen könnte.

1   Introduction

1.1   Pancreatic Cancer

Pancreatic ductal adenocarcinoma (PDAC) arises from the exocrine glands of the pancreas and constitutes more than 90% of pancreatic cancers. Despite recent treatment advances, pancreatic cancer is still one of the deadliest cancers with a five-year-survival rate around 10% compared to 67% for all cancers combined (Siegel et al., 2021). While incidences for most other tumors have been declining for the last years due to better diagnostics and targeted therapies, incidences of PDAC have been on the rise (Siegel et al., 2021). By the end of this decade, PDAC is projected to become the second leading cause of cancer related deaths in the United States and Germany (Quante et al., 2016; Rahib et al., 2014; Rahib et al., 2021), underscoring the dire unmet clinical needs.

This is mainly due to late diagnosis and the lack of adequate treatment options. Unlike for other tumors, no targeted therapies are currently standard-of-care treatments for PDAC.

So far, the only curable treatment of PDAC is resection, but due to the general late diagnostics, only a minority of patients (~20%) is available for surgery, while the majority of patients has advanced stage disease, with around 50% of the patients already showing metastatic cancer at diagnosis (Werner et al., 2013).

Current standard-of-care regimen like FOLFIRINOX (fluorouracil, leucovorin, irinotecan, and oxaliplatin) or Gemcitabine/nab-Paclitaxel have greatly improved survival, but the relatively low response rates especially in patients with metastatic PDAC and the high toxicities associated with these aggressive polychemotherapies limit its effectiveness as a treatment option (Ducreux et al., 2019).

1.1.1 Oncogenic KRAS in pancreatic cancer

Oncogenic mutations of KRAS occur in over 90% of PDAC patients (Biankin et al., 2012; Witkiewicz et al., 2015) and are considered to be the main driver of PDAC tumorigenesis (Waters and Der, 2018). The most common activating mutations of KRAS in PDAC are in Codon 12 (G12D (40%), G12V (33%), G12R (15%), G12C (1%) and G12S), codon 13 (7%) and codon 61 (1-2%), which render KRAS refractory to GTPase-activating protein (GAP)-induced guanosine triphosphate (GTP) hydrolysis and shift the equilibrium to an active GTP-bound state (Buscail et al., 2020).

Mutant KRAS drives the formation of pre-neoplastic lesions such as pancreatic intraepithelial neoplasia (PanIN), which are the most common precursor lesions of PDAC. Other lesions include intraductal papillary mucinous neoplasms or mucinous cystic neoplasms (Hruban et al., 2007). During carcinogenesis, PDAC acquires additional mutations (Hruban et al., 2000) with inactivating mutations in *CDKN2A*, *TP53* and *SMAD4* being the most prevalent ones (Hayashi et al., 2021). The mutational landscape of PDAC is very complex and heterogeneous (Hayashi et al., 2021; Knudsen et al., 2016), with most other mutations occurring at a low prevalence of less than 10% (Biankin et al., 2012; Jones et al., 2008; Waddell et al., 2015; Witkiewicz et al., 2015).

1.1.2 Subtypes of Pancreatic Cancer

The genetic heterogeneity of PDAC presents a major challenge to develop targeted precision therapies. Molecular subtyping of pancreatic cancer therefore holds the promise for better patient stratification and more tailored subtype driven therapies. Two main subtypes of PDAC – a "classical-pancreatic" and a "squamous/basal-like" lineage – have consistently been identified (Collisson et al., 2019; Raphael et al., 2017). A study published in 2020, which included metastatic Stage IV disease, further divided the two subtypes into Classical A/B and Basal A/B plus a fifth subtype that was termed "Hybrid" (Chan-Seng-Yue et al., 2020). The classical subtype contains mostly well-differentiated tumors and is enriched in Stage I/II of the

disease, while especially the Basal-like-A subtype was found to be enriched in Stage IV disease and highly chemoresistant (Chan-Seng-Yue et al., 2020). Classical tumors resemble pancreatic precursors and show an upregulation of pancreatic endodermal lineage specifying transcription factors such as GATA6 (Chan-Seng-Yue et al., 2020; Collisson et al., 2019; Collisson et al., 2011; O'Kane et al., 2020).

The squamous subtype (Bailey et al., 2016) – which has also been termed as basal-like (Moffitt et al., 2015) or quasi-mesenchymal (Collisson et al., 2011) – is associated with a poor prognosis and characterized by a loss of endodermal identity through hypermethylation of genes that determine pancreatic endodermal cell fate such as *GATA6* and *HNF4A* (Bailey et al., 2016; Collisson et al., 2019). Squamous tumors are enriched for mutations in *TP53* and *KDM6A*. They are marked by activation of the MYC pathway, increased expression of TP63ΔN and TGF-β signaling, as well as inflammation, hypoxia response and metabolic reprogramming (Bailey et al., 2016). These differences in molecular signaling and therapy response between subtypes indicate that better patient stratification and tailored therapies could provide benefit for PDAC treatment.

1.2 Targeted therapies for pancreatic cancer

While targeted therapies have shown great benefits in other solid tumors such as melanoma, colorectal and lung cancer, no such molecularly informed treatments are currently standard-of-care for PDAC (Nevala-Plagemann et al., 2020). The Epidermal Growth Factor Receptor (EGFR) inhibitor Erlotinib in combination with gemcitabine was the first approved targeted therapy for PDAC, but it showed only marginal benefit compared to gemcitabine alone and only a specific subtype responded significantly (Moore et al., 2007).

1.2.1 KRAS inhibition

The growing use of next-generation sequencing has opened up new opportunities for precision therapy in PDAC (Nevala-Plagemann et al., 2020). Oncogenic mutations in KRAS are the most common mutations in PDAC and have led to considerable efforts to target mutant KRAS (Buscail et al., 2020; Waters and Der, 2018). Despite intensive research and efforts over more than three decades to target KRAS, it has been long considered "undruggable". Recently, however, novel inhibitors have been developed that target mutant $Kras^{G12C}$, which have shown promising effects against $KRAS^{G12C}$-mutant cancers *in vitro* and *in vivo* (Canon et al., 2019; Hallin et al., 2020). Several $KRAS^{G12C}$-inhibitors are currently in clinical trials (Moore et al., 2020) and the first $KRAS^{G12C}$-inhibitor sotorasib (AMG510) was granted accelerated approval by the US Food and Drug Administration (FDA) in May 2021 based on promising phase 2 clinical trial data in patients with $KRAS^{G12C}$-mutated non-small-cell lung cancer (NSCLC) (Skoulidis et al., 2021). AMG 510 also showed efficacy *in vitro* and *in vivo* against the $KRAS^{G12C}$-mutant pancreatic cancer cell line MiaPaCa-2 (Canon et al., 2019). However, $KRAS^{G12C}$ is a relatively rare mutation in PDAC (~1-2%)(Bailey et al., 2016; Biankin et al., 2012; Witkiewicz et al., 2015), so that only a small subset of PDAC patients might benefit from such inhibitors. Other strategies will therefore be needed to target the more common KRAS mutations such as G12D or G12V (Moore et al., 2020). For example, exosomes loaded with small interfering RNAs that target $KRAS^{G12D}$, which suppressed tumor growth in preclinical models, are currently under investigation in clinical trials (NCT03608631) (Kamerkar et al., 2017). Furthermore, indirect approaches to pharmacologically target all KRAS mutants – such as pan-KRAS SOS1 inhibitors that block the interaction of the guanine-nucleotide exchange factor (GEF) SOS1 with guanosine diphosphate (GDP)-bound KRAS and thus prevent the nucleotide exchange and GTP loading of KRAS – as well as direct pan-KRAS inhibitors and degraders are currently being developed and investigated (Hofmann et al., 2022).

1.2.2 Precision oncology identifies targetable alterations in pancreatic cancer

While the most common mutations in PDAC (*KRAS, TP53, CDKN2A, SMAD4*) are currently not actionable alterations, sequencing studies have revealed low-prevalence aberrant genetic

alterations that are targetable with currently available anticancer therapies in 17-48% of PDACs (Aguirre et al., 2018; Aung et al., 2018; Semaan et al., 2021; Singhi et al., 2019). Findings from the "Know Your Tumor" program showed that approximately 25% of patients had highly actionable genomic alterations and that those who received matched therapy had significantly longer median progression-free and overall survival than those who received unmatched therapy (Pishvaian et al., 2018a; Pishvaian et al., 2020).

The targetable genomic alterations can be broadly divided into two main categories: alterations in the RTK/RAS/MAPK pathway in KRAS wild type tumors and mutations in the DNA damage repair pathway (Singhi et al., 2019).

PDAC with wild type KRAS are found in approximately 10% of patients and 38% of those had genomic alterations in the RTK/RAS/MAPK pathway, especially BRAF alterations and kinase fusions, which are rarely found in KRAS-mutant tumors (Singhi et al., 2019). Another study found *BRAF* in-frame deletions or insertions in 10% of wild-type KRAS tumors and demonstrated a partial response in one patient to the MEK 1/2 inhibitor Trametinib (Aguirre et al., 2018).

There is only limited clinical data regarding the targeted treatment of kinase fusions. However, several small studies in PDAC patients with gene fusions in *NTRK* or *ROS* (Pishvaian et al., 2018b), *ALK* (Singhi et al., 2017) and *NRG1* (Heining et al., 2018) have shown clinical benefits and NTRK inhibitors have received regulatory approval in a tissue-agnostic indication for advanced solid cancers with NTRK fusions, which encompasses <1% of PDAC patients (Nevala-Plagemann et al., 2020).

1.2.3 Targeting DNA damage repair

Patients with mutations in DNA damage repair (DDR) pathways are the second subset of patients that could benefit from targeted therapies (Nevala-Plagemann et al., 2020; Perkhofer et al., 2021). Whole-genome sequencing has identified the existence of a subtype, which was

termed "unstable", in about 14% of PDAC that is characterized by a large number (>200) of structural chromosomal variation events (Waddell et al., 2015). This indicates a defective DNA maintenance machinery, particularly in the homologous recombination pathway, in this subtype and potential sensitivity to DNA damaging therapeutics. Tumors from the unstable subtype were characterized by a BRCA mutational signature and sensitivity to platinum therapy (Waddell et al., 2015). Germline and somatic mutations in *BRCA1*, *BRCA2* and *PALB2* were detected in 14% of patients. However, an unstable genome or BRCA mutational signature was present in 24% of patients, indicating that these might be candidates for therapeutics targeting DDR deficiency (Dreyer et al., 2017; Waddell et al., 2015). Poly (ADP-ribose) polymerases (PARP) are key enzymes in DDR that function as DNA damage sensors, recruit the DNA repair machinery and stabilize replication forks during repair (Lord and Ashworth, 2017; Pilie et al., 2019). PARP inhibitors "trap" PARP in a complex with the DNA strand, leading to accumulation of single strand breaks and stalled replication forks. This induces a DNA damage response, which is normally repaired via homologous recombination repair (HRR). However, cancer cells deficient for HRR such as those with mutations in *BRCA1/2* fail to repair the DNA damage, which eventually causes double strand breaks leading to cell death (Lord and Ashworth, 2017; Pilie et al., 2019). This concept, whereby a defect in either one of two genes has little effect, while the combined defects in both genes causes cell death, is known as synthetic lethality and PARP inhibition in BRCA1/2-deficient cancers is a prime example with clinical relevance (Lord and Ashworth, 2017). Results from the POLO (Pancreas Cancer Olaparib Ongoing) trial demonstrated that the concept of synthetic lethality is also applicable to pancreatic cancer (Golan et al., 2019). In this randomized, double-blind, placebo-controlled, phase 3 study, patients with a germline BRCA mutation and metastatic pancreatic adenocarcinoma that had not progressed during first-line platinum-based chemotherapy were randomized to receive the PARP inhibitor Olaparib or placebo. The response rate in the Olaparib group was 23% and the median progression-free survival was significantly longer (7.4 months vs. 3.8 months) than in the placebo group, while no difference in overall survival was observed (Golan et al., 2019). As a result, Olaparib gained approval by the FDA in December

2019 for maintenance treatment of adult patients with germline BRCA-mutated metastatic pancreatic adenocarcinoma, whose disease has not progressed on first-line platinum-based chemotherapy regimen (FDA, 2019). These data suggest that PARP inhibitors could provide substantial benefit for a subset of PDAC patients with germline BRCA mutation, which was detected in 7.5% of the 3315 patients screened for entry in the POLO trial (Golan et al., 2019). In a follow-up study, however, overall survival was similar and therefore only a fraction of BRCA-mutated PDAC benefits (Golan et al., 2021). Whether the larger subset (~24%) of PDAC patients with DDR deficiencies beyond BRCAness (Dreyer et al., 2017) could benefit from PARP inhibitors as well is currently unclear (Nevala-Plagemann et al., 2020).

1.2.4 Targeting KRAS effector pathways

These examples underscore the potential and feasibility of precision oncology to identify small subsets of patients that could benefit from tailored targeted therapies. However, novel therapeutic strategies are urgently needed to benefit the large majority of patients for whom there are currently no adequate targeted therapies available. Despite the recent progress in the development of KRAS inhibitors (Moore et al., 2020), there are still no drugs available that target the most common mutant variants in pancreatic cancer. And even in the case of $KRAS^{G12C}$ inhibitors, diverse acquired resistance mechanisms are already being detected in patients (Awad et al., 2021), which further underscores the urgent need to better understand the complex KRAS-signaling driver network and identify critical signaling nodes for novel targeted therapies.

Oncogenic KRAS engages a complex and dynamic downstream signaling network, including signaling pathways such as RACGEF-RAC1, RALGEF-RAL and especially RAF-MEK-ERK and PI3K-AKT-MTOR (Eser et al., 2014; Waters and Der, 2018).

1.2.5 PI3K pathway inhibition

Phosphatidylinositol 3-kinase (PI3K) is a major effector pathway of RAS, regulating, among others, cellular growth, survival and metabolism (Castellano and Downward, 2011). Mice harboring mutations in the Ras-binding domain (RBD) of the PI3K catalytic subunit p110α that block binding with RAS-GTP are highly resistant to RAS-induced tumorigenesis (Castellano and Downward, 2011). In pancreatic cancer, AKT is found to be overexpressed in approximately 60% of cancers, which is associated with poor prognosis (Schlieman et al., 2003). Genetic deletion of *Pdk1* completely blocked PanIN and tumor formation in a mouse model of PDAC, thus underscoring the essential role for PI3K-PDK1-AKT signaling in the KRAS-driven tumorigenesis in the pancreas (Eser et al., 2013). Furthermore, tumor growth was efficiently blocked by a clinically available pan class I PI3K inhibitor (Eser et al., 2013), thus underscoring the clinical relevance of this signaling pathway in PDAC.

1.2.6 MAPK pathway inhibition

The other main effector pathway of oncogenic KRAS is the RAF-MEK-ERK signaling cascade. RAF kinase is activated upon binding of RAS-GTP to its amino-terminal RBD and subsequently activates MEK1 and MEK2 by phosphorylation, which in turn phosphorylate and activate ERK1 and ERK2 serine/threonine kinases (Shaul and Seger, 2007; Waters and Der, 2018). Activated ERK can then phosphorylate – in a highly context dependent manner – hundreds of cytosolic and nuclear substrates such as MYC or the AP-1 family of transcription factors that control key cellular processes that are critical in tumorigenesis (Yoon and Seger, 2006). The central role of the RAF-MEK-ERK pathway in PDAC is highlighted by recent sequencing studies that show that a large percentage of KRAS wild-type tumors has activating mutations in genes of the RAF-MEK-ERK cascade (Singhi et al., 2019; Witkiewicz et al., 2015). $BRAF^{V600E}$ mutations, for example, which were detected in 3% of PDAC samples, were mutually exclusive with KRAS mutations (Witkiewicz et al., 2015). Expression of BRAF^{V600E} in the mouse pancreas was sufficient to induce PanIN formation and resulted in PDAC formation upon concomitant expression with mutant TP53 (Collisson et al., 2012).

Whereas RAF and MEK inhibitors have been very effective in the treatment of BRAF-mutated melanoma (Savoia et al., 2019), clinical trials with MEK inhibitors in PDAC patients have largely failed to show any benefit so far (Infante et al., 2014; Van Cutsem et al., 2018). And while there are currently more than 40 inhibitors of the PI3K-AKT-MTOR pathway in clinical development, clinical trials with PI3K inhibitors in solid tumors have also largely been disappointing, primarily due to limited single-agent activity, problematic toxicities and lack of biomarkers for adequate patient selection (Hanker et al., 2019; Janku et al., 2018).

1.2.7 Combination therapies

The failure of MEK and PI3K pathway inhibitors in PDAC – despite ample preclinical evidence of the importance of these pathways in KRAS-mutant cancers – highlights the need for novel therapeutic strategies. The effector pathways downstream of oncogenic KRAS are not simple linear signaling cascades, but embedded in a complex KRAS signaling network that is characterized by feedback and feedforward loops within the pathways as well as extensive cross-signaling between KRAS effectors (Eser et al., 2014). This well documented intra- and inter-connectedness of the KRAS signaling network severely limits the efficacy of any mono-targeted approach due to rapid adaptive rewiring of the oncogenic signaling pathways (Lake et al., 2016; Ryan et al., 2015). Efficacy of RAF or MEK inhibitors is often limited by reactivation of ERK signaling due to increased upstream signaling to MEK (Poulikakos and Solit, 2011; Ryan et al., 2015; Yaeger and Corcoran, 2019) or activation of alternative signaling pathways such as PI3K (Wee et al., 2009). Combination therapies have been developed to overcome resistance to single agent therapies and shown promising results. One strategy involves targeting of multiple nodes of the same signaling cascade – so called "vertical inhibition" – to overcome feedback re-activation. This vertical inhibition strategy has been proven successful in BRAF mutant melanoma, where it is an approved therapy as it has been shown that RAF + MEK inhibitor combination has a better clinical response and lower toxicities than BRAF inhibitor treatment alone (Savoia et al., 2019). In KRAS mutant cancers, CRAF knockdown

sensitizes cells to MEK inhibition (Lito et al., 2014). In KRAS mutant PDAC models, low dose vertical inhibition of RAF plus ERK was refractory to ERK reactivation mechanisms and showed strong synergistic effects, leading to apoptotic death, while each inhibitor alone only had cytostatic effects (Ozkan-Dagliyan et al., 2020). Building on the success of combined RAF and MEK inhibition in melanoma, Xue et al. (2017) demonstrated that compared to double combination of MEK and ERK inhibitors, a concurrent triple targeting of RAF + MEK + ERK in BRAF-mutant melanomas and lung cancers delayed onset of resistance and resulted in stronger tumor suppression, while showing lower toxicity. In EGFR mutant non-small cell lung cancer, a multiple low dose therapy consisting of RAF+MEK+ERK or EGFR+RAF+MEK+ERK inhibitor combinations blocked MAPK pathway signaling and proliferation, while minimizing therapeutic resistance and associated toxicities (Fernandes Neto et al., 2020).

Circumvention of kinase inhibition by adaptive reprogramming of the kinome often via upregulation of receptor tyrosine kinases (RTKs) is another reason for the limited clinical success of targeted therapies (Duncan et al., 2012). RTKs such as EGFR (Ardito et al., 2012; Navas et al., 2012) and IGFR1 (Appleman et al., 2012) are critical for the KRAS-driven pancreatic carcinogenesis. Combined ablation of *Egfr/Raf1* resulted in complete regression in a subset of PDACs (Blasco et al., 2019), however, intriguingly, the effect seems to have been independent of MAPK signaling activity. In organoid models of pancreatic cancer, hyper-activation of ErbB signaling was observed upon MEK and AKT blockade and pan-ERBB inhibition synergized with MEK antagonists, resulting in tumor regressions in orthotopic xenograft models (Ponz-Sarvise et al., 2019). Another study showed activation of AXL, PDGFRa, and HER1-2 receptor tyrosine kinases upon MEK inhibition and only combined inhibition of all three activated RTKs in conjunction with MEK induced antitumor activity (Pettazzoni et al., 2015). The RTKs that drive the feedback activation upon MEK inhibition in KRAS-mutant cells are diverse and dependent on context, making MEKi/RTKi combination therapies challenging (Fedele et al., 2018; Lu et al., 2019). However, the protein tyrosine phosphatase SHP2 (PTPN11) acts as a signal transducer between RTKs and RAS and is required for RAS/ERK pathway activation by most RTKs. It thus presents a common resistance

mechanism to MEK inhibitors that can be pharmacologically targeted by combining MEKi with SHP2 inhibitors, which was shown to be synergistic in several PDAC models (Fedele et al., 2018; Lu et al., 2019; Ruess et al., 2018).

In addition to the vertical feedback signaling, therapy resistance is also mediated by the complex cross-signaling between the effector pathways downstream of KRAS (Mendoza et al., 2011). Inhibition of one KRAS effector pathway is compensated by activation of another signaling node, thus severely limiting the effectiveness of any mono-targeted approach (Collisson et al., 2012; Hassan et al., 2018). Combined inhibition of the MEK-ERK and PI3K-MTOR pathways has shown benefit in preclinical models of KRAS-mutant cancers (Alagesan et al., 2015; Engelman et al., 2008), but have largely failed in clinical trials due to the associated toxicities (Bedard et al., 2015; Grilley-Olson et al., 2016).

The pre-clinical success of these combination therapies suggests further development and refinement of these strategies for treatment of PDAC. Novel approaches such as multiple low-dose treatment or alternate and intermittent dosing strategies could help to achieve effective antitumor activity with limited toxicity (Settleman et al., 2021).

1.3 The transcription factor FRA1

The FOS-related antigen 1 (FRA1 or FOSL1) is a 271 amino acids transcription factor encoded by the *FOSL1* gene at the 11q13 locus. It belongs to the FOS family of transcription factors together with FOS, FOSB and FOSL2 that can form dimeric complexes with JUN family members to form the AP-1 (activator protein 1) complex. AP-1 is a dimeric transcription factor complex comprising members of the JUN, FOS, ATF and MAF protein families, with JUN and FOS being the most important in mammals (Eferl and Wagner, 2003). Unlike the JUN family, which can form JUN-JUN homodimeric complexes, FOS family members can only form heterodimeric complexes with JUN family members. AP-1 recognizes and binds to specific DNA sequences – such as the TPA-responsive element (TRE) and with lower affinity the cAMP-responsive elements (CRE) – on promoter or enhancer sites of target genes to regulate

various cellular processes involved in tumorigenesis such as cell proliferation, metastasis, differentiation and apoptosis (Angel et al., 1987). It is still not entirely understood how AP-1 controls gene transcription, but it has become increasingly clear that AP-1 principally binds to distal transcriptional enhancers rather than proximal to transcription start sites (Bejjani et al., 2019). A 2021 study indicates that FRA1 also preferably binds to distal enhancers and that it has both repressive as well as activating functions, with however moderate effects on most of the genes (Bejjani et al., 2021). Depending on the context, both oncogenic and tumor-suppressive properties of AP-1 have been described (Eferl and Wagner, 2003). Like the other AP-1 proteins, FRA1 has a basic leucine zipper (bZIP) domain, which enables it to form heterodimeric complexes with JUN family members (Cohen et al., 1989).

FRA1 is transcriptionally regulated by growth factors, cytokines and oncogenic signaling pathways (Talotta et al., 2020). RAS/MEK/ERK, PKC, PI3K, WNT/beta-catenin, IL-6/STAT3 and SIRT1 all have been shown to regulate FRA1 expression (Jiang et al., 2020). Out of these factors, the MAPK pathway is one of the major regulators of FRA1. It not only activates FRA1 at the transcriptional level, but also stabilizes FRA1 post-translationally through phosphorylation. FRA1 is an inherently instable protein with a short half-life due to its C-terminal destabilizer domain of 30-40 amino acids (Basbous et al., 2007). Within the destabilizing domain are two serine residues, Ser252 and Ser265 that can be phosphorylated by Erk1/2-pathway kinases, which stabilizes FRA1 and thus antagonizes its proteasomal degradation (Basbous et al., 2007).

FRA1 is overexpressed in many cancers such as breast, lung, colorectal and pancreatic cancer, where it has been shown to regulate cell proliferation, apoptosis and metastasis (Jiang et al., 2020; Talotta et al., 2020; Young and Colburn, 2006). *FRA1* was among the most downregulated mRNA transcripts upon inhibition of mutant KRAS with the KRAS[G12C] inhibitor ARS-1620, underscoring its tight connection to mutant KRAS (Janes et al., 2018; Lou et al., 2019). In addition, it has been identified to be among the most significant preferential dependencies of KRAS mutant compared to wild type cancer cell lines in a recent analysis of

genome-scale CRISPR-Cas9 loss-of-function screens from over 500 cancer cell lines from the Cancer Dependency Map (https://www.depmap.org) (Waters et al., 2021). Knockdown of FRA1 in RAS-transformed thyroid cells decreased proliferation and induced arrest in the G2 phase of the cell cycle as well as cell death associated with mitotic defects (Casalino et al., 2007). Correspondingly, FRA1 has been linked to regulation of the mitotic machinery in KRAS-driven lung and pancreatic cancer (Vallejo et al., 2017a; Vallejo et al., 2017b). Vallejo et al. (2017a) identified FRA1 to belong to a 8-gene core signature of mutant KRAS-related genes across tumors, out of which FRA1 was the only gene whose high expression was linked with a poorer prognosis in both lung and pancreatic cancer patients with mutant KRAS. In the pancreatic context, genetic inhibition of *Fra1* inhibited acinar-to-ductal metaplasia progression as well as proliferation of human and murine pancreatic cancer cells (Vallejo et al., 2017a). In a large scale CRISPR-Cas9 screen in pancreatic carcinoma cell lines, loss of fitness upon genetic targeting of FRA1 was observed in 16 out of 41 cell lines and based on these findings, FRA1 was designated as a "priority therapeutic target" in pancreatic carcinoma (Behan et al., 2019). In addition to its role in cell proliferation, FRA1 has also been linked to metastasis in PDAC. Dai et al. (2021) identified FRA1 in an *in vivo* screen as a SMAD4 target and went on to show that FRA1 drives metastatic colonization to the lung. This fits to the well described roles of FRA1 as a key regulator of epithelial-to-mesenchymal (EMT) plasticity (Dhillon and Tulchinsky, 2015) (Talotta et al., 2020) and metastasis in other tumor entities such as breast cancer (Desmet et al., 2013).

1.4 SUMOylation

Reversible post-translational modifications (PTM) such as phosphorylation, acetylation or ubiquitylation are highly dynamic molecular regulation mechanisms that control timing, activity, localization and interaction of almost all physiological processes. Among these PTM, small ubiquitin-like modifier (SUMO) are conserved across all eukaryotes and play essential roles in maintaining genome integrity, regulating gene expression and transduction of intracellular

signaling pathways (Seeler and Dejean, 2017). SUMO proteins are small 11kDa proteins that are covalently attached to other proteins in a reversible fashion by an enzymatic cascade similar to the process of ubiquitination. They are synthesized as pre-proteins that are cleaved by a SUMO1/sentrin specific peptidase (SENP) in the maturation step to generate a carboxy-terminal diglycine (GG) motif. In mammals, three major SUMO paralogues (SUMO1, SUMO2 and SUMO3, with SUMO2 and SUMO3 sharing 97% homology) are expressed. In the ATP-dependent activation step, SUMOs are transferred to the SUMO1-activating enzyme subunit 1 (SAE1)–SAE2 heterodimer to form a SUMO-SAE2 thioester. In the subsequent conjugation process, SUMO is then bound via another thioester bond to the E2 conjugating enzyme UBC9 (UBE2I) before being ligated in the last step by SUMO E3 ligases via an iso-peptide bond to a lysine residue on the target protein (Flotho and Melchior, 2013). These targets can be mono-, poly- or multi-SUMOylated and are rapidly deSUMOylated by SENPs, so that only a small fraction of target proteins is SUMOylated at any given time. More than 3000 proteins – corresponding to roughly 18% of the human proteome - have been reported to be SUMO targets (Hendriks and Vertegaal, 2016) and SUMOylation has been shown to be especially crucial for the cellular response to biotic and abiotic stress (Guo and Henley, 2014). The dynamic switch between SUMOylation and deSUMOylation therefore allows the cells to rapidly respond to cellular stress, which is especially important for cancer cells that often face harsh environments such as hypoxia or nutrient deprivation and have higher burdens of replication and DNA damage stress (Seeler and Dejean, 2017).

This explains why the SUMOylation machinery is often upregulated in cancers (Seeler and Dejean, 2017), which makes it an interesting target for cancer therapy (Kroonen and Vertegaal, 2021; Schneeweis et al., 2021). SUMO enzymes are primarily enriched in the nucleus, where they regulate and control nuclear structures and functions such as transcription, DNA damage repair, chromatin remodeling, signaling and cell cycle progression (Zhao, 2018). Genetic depletion or silencing of SUMO pathway components has been linked to mitotic impairment and apoptosis due to the resulting nuclear defects such as multinucleated cells or anaphase bridges (Kroonen and Vertegaal, 2021). In PDAC, SUMOylation has been linked to

chemotherapy response and resistance (Bonacci et al., 2014; Swayden et al., 2019). In the pancreatic cancer cell line MiaPaCa-2, post-translational modifications such as SUMOylation were dynamically altered upon gemcitabine treatment and specifically SUMOylation of Smad nuclear interacting protein 1 (SNIP1) was shown to enhance cell survival (Bonacci et al., 2014). In another study, hypo-SUMOylation of promyelocytic leukemia (PML) protein was associated with resistance to both gemcitabine and oxaliplatin in pancreatic cancer (Swayden et al., 2019).

SUMOylation can be blocked at various steps of the enzymatic cascade and several genetic as well as pharmacological approaches have been shown to inhibit cell proliferation. Genetic targeting of the single E2-conjugating enzyme UBC9 has demonstrated its critical role for cellular fitness as knockdown of UBC9 by shRNAs blocked colony formation in U2OS cells (He et al., 2015) and impaired proliferation in WI38 fibroblasts (Neyret-Kahn et al., 2013). Several compounds such as GSK145, the antibiotic Spectomycin B and 2-D08 that inhibit UBC9 have been identified (Yang et al., 2018). In acute myeloid leukemia (AML) cells, 2-D08 was able to inhibit cell viability as well as colony formation and induced apoptosis in a reactive oxygen species (ROS)-dependent manner possibly through deSUMOylation of NOX2. In the PDAC cell line MiaPaCa-2, treatment with 2-D08 inhibited cell migration in a concentration-dependent manner that correlated with reduced KRAS SUMOylation status (Choi et al., 2018).

Knockdown of SAE2 also inhibits cell proliferation, especially mitotic progression by causing chromosomal segregation defects (Eifler et al., 2018) as well as apoptosis, endoreduplication and senescence (He et al., 2015). In an *in vivo* HCT116 xenograft tumor model, conditional shRNA-mediated knockdown of SAE2 significantly impaired tumor growth (He et al., 2015). Several natural and synthetic inhibitors of SAE1/2 have been identified (Kroonen and Vertegaal, 2021; Yang et al., 2018). Natural compounds such as ginkgolic acid, its structural analog anacardic acid, kerriamycin B, Davidiin and tannic acid have all been shown to inhibit SUMO E1 by blocking the formation of the SAE1/2-SUMO intermediate. However, most of these natural molecules inhibit tumor growth in the micromolar range and have a broad range of targets besides SUMO (Kroonen and Vertegaal, 2021; Yang et al., 2018).

Several synthetic molecules including COH-000, ML-792 and its derivatives ML-93 and TAK-981 have been developed in the recent years to overcome these limitations. COH-000 is a covalent allosteric inhibitor that binds to Cys30 in the Uba2 subunit, thereby inducing conformational changes that block adenylation and lock the enzyme in an inactive state (Lv et al., 2018). COH-000 blocks SUMO E1 activity in the micromolar range and inhibited tumor growth of colorectal cancer cells in vitro and in vivo (Li et al., 2019).

ML-792, ML-93 and TAK-981 on the other hand inhibit SAE activity by forming covalent adducts with SUMO on its C-terminus in an ATP-dependent mechanism that is catalyzed by the enzyme itself (He et al., 2017; Langston et al., 2021). ML-792 works at nanomolar concentrations to decrease cellular protein SUMOylation and shows no cross-reactivity with other closely related E1 enzymes such as the ubiquitylation or NEDDylation pathways (He et al., 2017).

ML-792 induces mitotic disruption and chromosome-segregation failure and inhibits cell proliferation in multiple breast, colon and melanoma cancer cell lines (He et al., 2017). Treatment with ML-792 as well as its derivatives ML-93 and TAK-981 inhibited tumor growth *in vivo* in a colorectal and a hematological xenograft model, with ML-93 and TAK-981 working at lower dosages than ML-792 (Langston et al., 2021). TAK-981 is currently being investigated in Phase 1 clinical trials in patients with hematological and solid tumors (NCT03648372, NCT04074330, and NCT04381650, NCT04776018).

1.5   The MYC oncogene in pancreatic cancer

The oncoprotein MYC is a basic helix-loop-helix leucine zipper transcription factor that functions as a master regulator of metabolism, growth and proliferation of cancer cells by binding as a heterodimer with its dimerization partner protein MAX (MYC-associated factor X) to enhancer (E-) boxes of target genes (Dang, 2012; 2013). MYC is one of the most highly amplified oncogenes in human cancers (Beroukhim et al., 2010) and the sole copy number variation in PDAC (amplified in 14%) that is associated with poor prognosis (Witkiewicz et al.,

2015). Overexpression of MYC alone is sufficient to induce formation of invasive and metastatic PDAC (Lin et al., 2013). MYC also plays a critical role for the KRAS-driven tumorigenesis in the pancreas and functions as an integrator of oncogenic signaling pathways downstream of KRAS (Diersch et al., 2016; Schneeweis et al., 2018). It is upregulated both in early premalignant lesions and advanced PDAC (Lin et al., 2013) and it has been demonstrated that MYC deregulation drives progression of KRAS^{G12D}-induced PanINs to adenocarcinoma (Sodir et al., 2020). The MYC pathway is activated especially in the basal-like/squamous subtype of PDAC, which is characterized by a poor prognosis (Bailey et al., 2016). Activation of the MYC network in PDAC is furthermore linked to an immunosuppressive microenvironment (Muthalagu et al., 2020; Sodir et al., 2020) and metastasis (Maddipati et al., 2021). In addition, MYC is associated with therapeutic resistance in PDAC, both to targeted therapies such as ERK (Waters et al., 2021) or MTOR inhibition (Allen-Petersen et al., 2019) as well as chemotherapeutics such as gemcitabine (Farrell et al., 2017). MYC thus presents a highly relevant therapeutic target in PDAC (Schneider et al., 2021; Wirth et al., 2016). Genetic targeting of MYC impaired the KRAS-driven tumor formation in the pancreas (Saborowski et al., 2014; Walz et al., 2014). Additionally, established PDAC are highly MYC-dependent. Expression of OmoMYC, a dominant-negative allele of MYC, suppressed growth of PDAC cells *in vitro (Jung* et al.*, 2017)* and induced complete tumor regression of pancreatic cancer *in vivo* (Sodir et al., 2020; Sodir et al., 2011). While normal regenerating tissues are also affected by systemic MYC inhibition with OmoMYC, these effects are nevertheless well tolerated, thus indicating the principal feasibility of targeting MYC for cancer therapy (Soucek et al., 2008). However, due to the fact that MYC is a largely unstructured transcription factor unless dimerized with a binding partner, direct therapeutic targeting with small molecule inhibitors has been challenging (Dang et al., 2017; Wolf and Eilers, 2020). Therefore, many efforts have focused on indirect targeting of MYC in PDAC, which can be broadly classified into targeting MYC expression, MYC stability or specific vulnerabilities of MYC-driven tumors (Wolf and Eilers, 2020). Several studies have confirmed the feasibility of indirectly targeting MYC also in PDAC (Schneider et al., 2021; Wirth et al., 2016). MYC transcription is regulated by

bromodomain and extra-terminal (BET) proteins, which can be therapeutically targeted with small-molecule BET inhibitors (Wolf and Eilers, 2020). In a transcriptomic analysis of 55 PDAC patient-derived xenografts, Bian et al. (2017) identified a MYC-high subgroup (30%) – characterized by high expression of MYC transcriptional targets, poor differentiation and shorter survival time – that was particularly sensitive to BET inhibition by the small-molecule compound JQ1. In another study, JQ1 synergized with histone deacetylase (HDAC) inhibitors and suppressed PDAC growth even more potently than BET inhibition alone (Mazur et al., 2015).

In addition to the transcriptional regulation, MYC protein expression is also regulated at the posttranslational level. KRAS signaling in particular has been shown to stabilize the MYC protein through ERK-mediated phosphorylation of MYC at Ser62, which extends its half-life, and through the PI3K pathway, which blocks the phosphorylation of Thr58 by glycogen synthetase-3 thereby preventing MYC degradation (Bachireddy et al., 2005). In PDAC, it has been shown that KRAS suppression causes proteasome-dependent degradation of MYC protein in both ERK1/2-dependent and independent mechanisms (Vaseva et al., 2018). While targeting of ERK1/2 alone is not sufficient to induce loss of MYC due to compensatory upregulation of MEK5-ERK5 signaling, concurrent targeting of ERK1/2 and ERK5 reduces phosphorylation of MYC at Ser62 and synergistically induces proteasome-dependent loss of MYC protein in PDAC cells (Vaseva et al., 2018). Concordantly, activation of the tumor suppressor protein phosphatase 2A (PP2A), which dephosphorylates MYC at Ser62 and thereby destabilizes it, reduced MYC protein expression in PDAC (Allen-Petersen et al., 2019; Farrell et al., 2014).

Other approaches have focused on identifying specific vulnerabilities of MYC-high tumors, as high MYC expression is stressful for the cells and therefore creates critical dependencies on co-factors to cope with the increased cellular stress (Wirth and Schneider, 2016; Wolf and Eilers, 2020). Synthetic lethal screens in particular have identified core pathways that MYC-driven tumors selectively depend upon. These include among others chromatin and

transcriptional processes, DNA repair, cell cycle checkpoints, biosynthesis and cellular metabolism (Cermelli et al., 2014; Thng et al., 2021).

1.6 Aims of this work

PDAC is the third leading cause of cancer-related deaths in the Western world and has the worst prognosis of all major cancers with a 5-year survival rate of 10% (Siegel et al., 2021). Cytotoxic chemotherapeutic regimen remain standard of care, whereas targeted therapies for pancreatic cancer have largely failed in the clinic. While polychemotherapies like FOLFIRINOX have greatly improved survival, overall response rates are around 30% and are especially low in the undifferentiated basal-like subtype that is largely chemotherapy-resistant (Aung et al., 2018; Chan-Seng-Yue et al., 2020). This underscores the need to identify therapeutic targets and to develop novel therapeutic strategies. Mutant KRAS is the major oncogenic driver of PDAC and the transcription factors MYC and FRA1 are important downstream integrators of KRAS signaling.

Based on our previous work (Diersch et al., 2016), we detected strong enrichment of the AP-1 family gene network and in particular of the AP-1 transcription factor FRA1 upon the induction of oncogenic KRAS in pancreatic ductal epithelial cells. The aim of the first part of this thesis was therefore to further characterize the role of FRA1 in pancreatic cancer, especially for PDAC maintenance and drug resistance. Therefore, various isogenic gain- and loss-of-function models were generated and characterized. To decipher its function in mediating therapeutic resistance, an unbiased drug screen was performed. This revealed a role in mediating resistance to MAPK inhibition, which was studied in more detail.

The aim of the second part of this thesis was to study the role MYC and its connection to the SUMOylation machinery. Therefore, SUMOylation and MYC expression were analyzed in large datasets as well as a panel of human PDAC cell lines. Genetic gain-of-function models were generated to study the connection of MYC and SUMOylation in more detail. Furthermore, large panels of murine and human PDAC cells were screened with a SUMOylation inhibitor to determine whether SUMOylation is a druggable vulnerability of MYC-dependent PDAC.

2 Materials

2.1 Devices

Table 2-1: Devices

Product	Manufacturer
96-pin replicator pin tool	V&P Scientific, San Diego, California, USA
Analytical balance A 120 S	Sartorius AG, Göttingen
Analytical balance BP 610	Sartorius AG, Göttingen
Autoclave 2540 EL	Tuttnauer Europe B.V:, Breda, Netherlands
Axiovert 25 Inverse Microscope	Carl Zeiss, Jena
Bag sealer Folio FS 3602	Severin Elektrogeräte GmbH, Sundern
Biometra Compact L/XL Gel Electrophoresis	Biometra GmbH, Göttingen
Centrifuge 5451R	Eppendorf, Hamburg
Centrifuge Rotina 46R	Andreas Hettich GmbH & Co. KG, Tuttlingen
Clariostar Microplate Reader	BMG Labtech, Ortenberg
Consort EV243 power supply	Consort, Turnhout, Belgium
CyAn ADP Lx Flow Cytometer	Beckman Coulter GmbH, Krefeld, Germany
EPS601 power supply	GE Healthcare Life Science, Freiburg
FACSAria	BD Biosciences, Heidelberg
Fluostar Optima Microplate Reader	BMG Labtech, Ortenberg
Gallios Flow Cytometer	Beckman Coulter GmbH, Krefeld, Germany
GFL 1003 Water Bath	GFL Gesellschaft für Labortechnik mbH, Burgwedel
Heracell VIOS 250i CO_2 incubator	Thermo Fisher Scientific, Darmstadt
Horizontal gel electrophoresis system	Biozym Scientific GmbH, Hessisch Oldenburg
Laminar flow HERAsafe	Heraeus Holding GmbH, Hanau
Magnetic stirrer, Ikamag® RCT	IKA® Werke GmbH & Co. KG, Staufen
Maxwell 16 Instrument	Promega, Walldorf
Microcentrifuge 5415 D	Eppendorf AG, Hamburg
Microcentrifuge 5417 R	Eppendorf AG, Hamburg
Microplate reader Multiskan RC	Thermo Labsystems, Schwerte
Microwave	Siemens AG, Munich
Mini centrifuge MCF-2360	LMS Consult GmbH & Co, KG, Brigachtal
Mini Trans-Blot® Cell	Bio-Rad Laboratories GmbH, München

Mini-PROTEAN Tetra Cell Casting Stand & Clamps	Bio-Rad Laboratories GmbH, München
Mini-PROTEAN® Comb, 10-well, 1.5 mm	Bio-Rad Laboratories GmbH, München
Mini-PROTEAN® Spacer Plates	Bio-Rad Laboratories GmbH, München
Mini-PROTEAN® Tetra Vertical Electrophoresis Cell	Bio-Rad Laboratories GmbH, München
Multipette® stream	Eppendorf AG, Hamburg
Neubauer hemocytometer	LO - Laboroptik, Lancing, United Kingdom
Odyssey® FC imaging system	LI-COR Biotechnology, Bad Homburg
OPTIMAX X-Ray Film Processor	PROTEC, Oberstenfeld
pH meter 521	WTW Wissenschaftlich-Technische Werkstätten GmbH, Weilheim
Pipettes Reference®, Research®	Eppendorf AG, Hamburg
Pipetus®	Hirschmann Laborgeräte GmbH & Co. KG, Eberstadt
PowerPac™ Basic Power Supply	Bio-Rad Laboratories GmbH, München
Real time PCR system StepOnePlus™	Applied Biosystems, Inc., Carlsbad, CA, USA
Rocking platform Biometra WT 18	Biometra GmbH, Göttingen
Scanner Epson Perfection 1200 Photo	SEIKO Epson CORPORATION, Japan
Spectrophotometer NanoDrop 1000	Peqlab Biotechnologie GmbH
Thermocycler T- Personal	Biometra GmbH, Göttingen
Thermocycler T100	Bio-Rad Laboratories GmbH, München
Thermomixer Compact	Eppendorf AG, Hamburg
UV solo TS2 Imaging System	Analytik Jena, Jena
Vortex Genius 3	IKA® Werke GmbH & Co. KG, Staufen

2.2 Disposables

Table 2-2: Disposables

Disposables	Manufacturer
Amersham Protran 0.2 NC Nitrocellulose blotting membrane	GE Healthcare Life Sciences, Freiburg
Axygen 96-well Polypropylene PCR Microplate	Corning, Kaiserslautern
Axygen CyclerSeal sealing film	Corning, Kaiserslautern
Cell culture dishes	Corning, Kaiserslautern
Cell culture flasks	Greiner Bio-One, Frickenhausen
Cell scrapers	Sarstedt AG & Co., Nümbrecht
CL-Xposure Film	ThermoFisher Scientific, Darmstadt
ClearLine Filter tips	Kisker Biotech GmbH & Co. KG, Steinfurt
Combitips BioPur	Eppendorf AG, Hamburg
Conical tubes (15 mL, 50 mL)	Greiner Bio-One, Frickenhausen
CryoPure tubes	Sarstedt AG & Co., Nümbrecht
Disposable Scalpels	Feather Safety Razor Co., Osaka, Japan
Filtropur (S 0.2; S 0.45)	Sarstedt AG & Co., Nümbrecht
Immobilon transfer membrane, PVDF	Merck Millipore, Darmstadt
Inoculation spreader, sterile	Sarstedt AG & Co., Nümbrecht
Multiwell Plates (6-well, 12-well, 24-well, 96-well)	Corning, Kaiserslautern
Parafilm M	Brand GmbH & Co. KG, Wertheim
Pasteur pipettes	Hirschmann Laborgeräte GmbH & Co. KG, Eberstadt
PCR reaction tubes	Eppendorf AG, Hamburg
Petri dishes	Sarstedt AG & Co., Nümbrecht
Pipette tips	Sarstedt AG & Co., Nümbrecht
Reaction tubes (0.5 ml, 1.5 ml and 2 ml)	Eppendorf AG, Hamburg
Whatmann paper 3 mm chr	GE Healthcare Life Sciences, Freiburg

2.3 Chemicals and Reagents

Table 2-3: Cell Culture Media and Reagents

Reagent	Manufacturer
3-(4,5-dimethylthiazol-2-yl)-2,5-diphenyltetrazolium bromide (MTT)	Sigma-Aldrich, Taufkirchen
4-Hydroxytamoxifen (4-OHT)	Sigma-Aldrich, Taufkirchen
Blasticidin	Carl Roth, Karlsruhe
CellTiter-Glo® Luminescent Cell Viability Assay	Promega, Walldorf
Collagenase Type 2	Worthington Biochemical Corporation, Lakewood, New Jersey, USA
Dimethylsulfoxide (DMSO), cell culture grade	AppliChem GmbH, Darmstadt
Doxycycline	Cayman Chemical, Ann Arbor, Michigan, USA
Dulbecco's phosphate buffered saline (PBS)	Sigma-Aldrich, Taufkirchen
Dulbecco's Modified Eagle's Medium (DMEM) - high glucose	Sigma-Aldrich, Taufkirchen
Fetal Bovine Serum (FBS) Superior	Sigma-Aldrich, Taufkirchen
Geneticin	ThermoFisher Scientific, Darmstadt
Opti-MEM I Reduced Serum Media	Gibco, Schwerte
Penicillin-Streptomycin (Pen Strep)	Gibco, Schwerte
Polybrene	Merck Millipore, Darmstadt
Puromycin	Santa Cruz Biotechnology, Heidelberg
Roswell Park Memorial Institute (RPMI) 1640 Medium	Gibco, Schwerte
Trypsin-EDTA Solution 10X	Sigma-Aldrich, Taufkirchen

Table 2-4: Inhibitors and Compounds

Compound	Source
Cherry Pick Library	Selleckchem, Houston, Texas, USA
dTAG-13	Tocris/Bio-Techne GmbH, Wiesbaden
MK-2206	Selleckchem, Houston, Texas, USA
ML-792	Takeda Pharmaceuticals International Co, Cambridge, MA, USA
ML-93	Takeda Pharmaceuticals International Co, Cambridge, MA, USA

RO5126766	Selleckchem, Houston, Texas, USA
Trametinib	Selleckchem, Houston, Texas, USA
Ulixertinib	Selleckchem, Houston, Texas, USA

Table 2-5: Chemicals, Enzymes and other Reagents

Product	Manufacturer
1 kb plus DNA Ladder	New England Biolabs, Frankfurt
2-Mercaptoethanol	Carl Roth, Karlsruhe
2-Propanol (Isopropanol)	Merck, Darmstadt
4′,6-Diamidino-2-phenylindole dihydrochloride (DAPI)	Thermo Fisher Scientific, Darmstadt
Agarose	Sigma-Aldrich, Taufkirchen
Albumin Bovine Fraction V (BSA)	Serva, Heidelberg
Ammonium Persulfate (APS)	Sigma-Aldrich, Taufkirchen
Ammonium sulfate	Sigma-Aldrich, Taufkirchen
Ampicillin	Carl Roth, Karlsruhe
APC Annexin-V	Biolegend, San Diego, CA, USA
Bradford Reagent, 5x concentrate	Serva, Heidelberg
Bromophenol blue	Sigma-Aldrich, Taufkirchen
Calcium chloride	Sigma-Aldrich, Taufkirchen
Crystal violet	Sigma-Aldrich, Taufkirchen
Dimethyl Sulfoxide (DMSO)	PanReac AppliChem, Darmstadt
Disodium Phosphate	Merck, Darmstadt
DNase I Kit	Sigma-Aldrich, Taufkirchen
dNTP 10mM	Sigma-Aldrich, Taufkirchen
Dulbecco's Phosphate Buffered Saline	Sigma-Aldrich, Taufkirchen
Ethanol Absolut	Merck, Darmstadt
Ethidium Bromide	Applichem, Darmstadt
Ethylenediaminetetraacetic acid (EDTA)	Sigma-Aldrich, Taufkirchen
Gateway® LR Clonase® II	Thermo Fisher Scientific, Darmstadt
GeneRuler 100 bp DNA Ladder	Thermo Fisher Scientific, Darmstadt
Glycerol	Carl Roth, Karlsruhe
Glycine	Carl Roth, Karlsruhe
Hydrochloric acid (37 %)	Merck, Darmstadt
Kanamycin	Carl Roth, Karlsruhe

LB medium (Luria/Miller)	Carl Roth, Karlsruhe
LB-Agar (Luria/Miller)	Carl Roth, Karlsruhe
Lipofectamine 2000	Thermo Fisher Scientific, Darmstadt
Magnesium Chloride	Sigma-Aldrich, Taufkirchen
Methanol	Carl Roth, Karlsruhe
Multiscribe reverse Transcriptase (50 U/µl)	Applied Biosystems, Darmstadt
NEBuilder® HiFi DNA Assembly Master Mix	New England Biolabs, Frankfurt
NEM (N-ethylmaleimide)	Sigma-Aldrich, Taufkirchen
PageRuler Prestained Protein Ladder	Thermo Fisher Scientific, Darmstadt
Phosphatase-Inhibitor-Mix	Serva, Heidelberg
Phosphate buffered saline (PBS) powder	Sigma-Aldrich, Taufkirchen
Potassium chloride	Merck, Darmstadt
Propidium Iodide	Sigma-Aldrich, Taufkirchen
Protease inhibitor cocktail tablets	Roche Diagnostics, Mannheim
Proteinase K	Sigma-Aldrich, Taufkirchen
Q5® High-Fidelity DNA Polymerase	New England Biolabs, Frankfurt
REDTaq® ReadyMix™ PCR reaction mix	Sigma-Aldrich, Taufkirchen
Restriction Enzymes	New England Biolabs, Frankfurt
RLT-Buffer	Qiagen, Hilden
RNase A	Qiagen, Hilden
ROTIPHORESE®Gel 30	Carl Roth, Karlsruhe
Skim Milk Powder	Carl Roth, Karlsruhe
Sodium Chloride	Serva, Heidelberg
Sodium deoxycholate	Sigma-Aldrich, Taufkirchen
Sodium Dodecyl Sulfate (SDS)	Serva, Heidelberg
SuperSignal™ West	Thermo Fisher Scientific, Darmstadt
SYBR™ Green PCR Master Mix	Thermo Fisher Scientific, Darmstadt
TaqMan® Reverse Transcription Reagents	Thermo Fisher Scientific, Darmstadt
Tetramethylethylenediamine (TEMED)	Carl Roth, Karlsruhe
TransIT-LT1 Transfection Reagent	Mirus Bio, Madison, WI, USA
TRIS	Carl Roth, Karlsruhe
TRIS Hydrochlorid (TRIS-HCl)	Carl Roth, Karlsruhe
TritonX-100	Sigma-Aldrich, Taufkirchen
Tween 20	Carl Roth, Karlsruhe

2.4 Cell Lines

Table 2-6: Cells Lines.

Cell Line Name	Research Resource Identifiers (RRIDs)
AsPC-1	CVCL_0152
BxPC-3	CVCL_0186
DAN-G	CVCL_0243
HEK293-FT	CVCL_6911
HPAC	CVCL_3517
HPAF-II	CVCL_0313
HuP-T3	CVCL_1299
HuP-T4	CVCL_1300
IMIM-PC1	CVCL_4061
MIA PaCa-2	CVCL_0428
MZ1-PC	CVCL_1434
Panc 02.03	CVCL_1633
Panc 05.04	CVCL_1637
PANC-1	CVCL_0480
PaTu 8988t	CVCL_1847
PaTu-8988S	CVCL_1846
Phoenix-Eco	CVCL_H717
PSN1	CVCL_1644
SU.86.86	CVCL_3881
SW1990	CVCL_1723

2.5 Plasmids

Table 2-7: Plasmids

Plasmid	Source / RRID
MSCV Myc IRES GFP	Addgene_18770
MSCV-IRES-GFP	Addgene_27490
MSCV-MYC^{ER}-IRES-GFP	(Franke et al., 2015)
MSCV-rtTA-IRES-EcoReceptor-PGK-puro	(Hoellein et al., 2014)
pBabepuro-myc-ER	Addgene_19128
pENTR1A no ccDB (w48-1)	Addgene_17398
pInducer20	Addgene_44012
pInducer20-iCre	kind gift of Prof. Dr. Marc Schmidt-Supprian, TU Munich
pInducer20-Blast	Addgene_109334
pLenti PGK Puro DEST	Addgene_19068
pLEX_305-N-dTAG	Addgene_91797
pMD2.G	Addgene_12259
psPAX2	Addgene_12260

2.6 Antibodies

Table 2-8: Antibodies.

Primary Antibodies			
Antibody	Manufacturer	RRID	Dilution
Akt (#9272)	Cell Signaling Technology, Frankfurt	AB_329827	1:1000
alpha-Tubulin	Sigma-Aldrich, Taufkirchen	AB_477583	1:10000
beta-Actin (#A5316)	Sigma-Aldrich, Taufkirchen	AB_476743	1:10000
GAPDH (ACR001P)	Acris GmbH, Herford,	AB_1616730	1:10000
GFP Antibody (A-11122)	ThermoFisher Scientific, Darmstadt	AB_221569	1:1000

HA-Tag (C29F4)	Cell Signaling Technology, Frankfurt	AB_1549585	1:1000
Myc (#9402)	Cell Signaling Technology, Frankfurt	AB_2151827	1:1000
p44/42 MAPK (Erk1/2) (#4695)	Cell Signaling Technology, Frankfurt	AB_390779	1:1000
Phospho-Akt (Ser473) (#4060)	Cell Signaling Technology, Frankfurt	AB_2315049	1:1000
Phospho-FRA1 (Ser265)	Cell Signaling Technology, Frankfurt	AB_2106922	1:1000
Phospho-p44/42 MAPK (Erk1/2) (Thr202/Tyr204) (#4370)	Cell Signaling Technology, Frankfurt	AB_2315112	1:2000
SUMO-1	DSHB, Iowa City, Iowa, USA	AB_2198257	1:1000
SUMO-2/3	DSHB, Iowa City, Iowa, USA	AB_2198421	1:1000

Secondary Antibodies

Antibody	Manufacturer	RRID	Dilution
Anti-rabbit IgG (H+L) (Dylight® 680 Conjugate) #5366	Cell Signaling Technology, Frankfurt	AB_10693812	1:15000
Anti-rabbit IgG (H+L) (Dylight® 800 Conjugate) #5151	Cell Signaling Technology, Frankfurt	AB_10697505	1:15000
Anti-mouse IgG (H+L) (Dylight® 680 Conjugate) #5470	Cell Signaling Technology, Frankfurt	AB_10696895	1:15000
Anti-mouse IgG (H+L) (Dylight® 800 Conjugate) #5257	Cell Signaling Technology, Frankfurt	AB_10693543	1:15000
Anti-Mouse IgG - Horseradish Peroxidase antibody (#NA931)	GE Healthcare; Freiburg	AB_772210	1:10000
Anti-Rabbit IgG, Whole Ab ECL Antibody, HRP Conjugated	GE Healthcare; Freiburg	AB_772206	1:10000

2.7 Primers

All primers were synthesized by Eurofins Genomics (Ebersberg, Germany) and diluted in H_2O to a concentration of 10 µM.

Table 2-9: Genotyping Primers

Target	Primer Name	Sequence (5'-3')
Ptf1a^{Cre}	p48-Cre-GT-LP-URP	CCTCGAAGGCGTCGTTGATGGACTGCA
	p48-Cre-GT-wt-UP	CCACGGATCACTCACAAAGCGT
	p48-Cre-GT-mut-UP-neu	GCCACCAGCCAGCTATCAA
LSL-Kras^{G12D}	Kras-WT-UP1	CACCAGCTTCGGCTTCCTATT
	Kras-URP-LP1	AGCTAATGGCTCTCAAAGGAATGTA
	Kras^{G12D}-mut-UP	CCATGGCTTGAGTAAGTCTGC
Fra1^{lox}	Fra1-P1	GAAATGGCTCCGTGGGTAAAGGTA
	Fra1-P2	GACAGGGTTCATCTTCATAGTTCT
	Fra1-P3	TGTACCGGACGCTTGTCATCTCAT
Pdx1-Flp	Pdx5utr scUP	AGAGAGAAAATTGAAACAAGTGCAGGT
	Flpopt-scLP	CGTTGTAAGGGATGATGGTGAACT
FSF-Kras^{G12D}	Kras-WT-UP1	CACCAGCTTCGGCTTCCTATT
	Kras-URP-LP1	AGCTAATGGCTCTCAAAGGAATGTA
	R26-Tva-SA-mut-LP	GCGAAGAGTTTGTCCTCAACC
R26^{CreERT2}	Cre-ER-T2-sc-UP3	GAATGTGCCTGGCTAGAGATC
	Cre-ER-T2-sc-LP1	GCAGATTCATCATGCGGA
p53^{FRT}	p53-frt forward	CAAGAGAACTGTGCCTAAGAG
	p53-frt reverse	CTTTCTAACAGCAAAGGCAAGC

Table 2-10: qPCR primers.

Gene	Primer	Sequence (5'-3')
Fra1 (Exon 1-2)	Forward	CGCAAGCTCAGGCACAGA
	Reverse	AATGAGGCTGCACCATCCA
Fra1 (Exon 2-4)	Forward	CGGCCAGGAGTCATACGAG
	Reverse	CTTCCAGCACCAGCTCAAG
cyclophilin A	Forward	ATGGTCAACCCCACCGTGT
	Reverse	TTCTGCTGTCTTTGGAACTTTGTC

Myc	Forward	TTCCTTTGGGCGTTGGAAAC
	Reverse	GCTGTACGGAGTCGTAGTCG
Cad	Forward	CTGCCCGGATTGATTGATGTC
	Reverse	GGTATTAGGCATAGCACAAACCA
Odc1	Forward	ACATCCAAAGGCAAAGTTGG
	Reverse	AGCCTGCTGGTTTTGAGTGT
Gapdh	Forward	GGGTTCCTATAAATACGGACTGC
	Reverse	TACGGCCAAATCCGTTCACA
Sae1	Forward	GCCCTGTAAAAGAGGCGCTA
	Reverse	TGATGCCCAGGGAGTCAAAC
Sae2	Forward	CGCAAGAGGAAACCTCCAGT
	Reverse	TCTCCGCTAAATGGACTCG

Human qPCR Primers

ODC1	Forward	TCCTGGAGAGTTGCCTTTGTGAGA
	Reverse	TCGAGGAAGTGGCAGTCAAACTCT
CAD	Forward	TAGTCCTTGGCTCTGGCGTCTA
	Reverse	TAGTCGGTGCTGACTGTCTCTG
GAPDH	Forward	AATCCCATCACCATCTTCCA
	Reverse	TGGACTCCACGACGTACTCA
SUMO1	Forward	TTCAACTGAGGACTTGGGGG
	Reverse	TGGAACACCCTGTCTTTGAC
SUMO2	Forward	GCCGACGAAAAGCCCAAGG
	Reverse	TGACAATCCCTGTCGTTCACAA
MYC	Forward	TCAGAGTCTGGATCACCTTCTGCT
	Reverse	TGCGTAGTTGTGCTGATGTGTGGA

HSPE1	Forward	CATCATGTTGATGCCATTTCA
	Reverse	TGGAGGCACCAAAGTAGTTCT
SAE1	Forward	ACTGGAGCAGTGAGAAAGCA
	Reverse	GCAGGTCAGGACTAATACCCA
SAE2	Forward	AACCTCCAGTTCCGTTGGAC
	Reverse	TCCTGAGGTTTGCAGCAGAG
UBE2I	Forward	CCCATTTGGTTTCGTGGCTG
	Reverse	ACATTTTGGTGGCGAAGATGG
SUMO3	Forward	CCCAAGGAGGGTGTGAAGAC
	Reverse	ATTGACAAGCCCTGCCTCTC

Table 2-11: Primers for Mycoplasma detection test.

Primer	Sequence (5'-3')
Forward Primer Mix	CGC CTG AGT AGT ACG TTC GC
	CGC CTG AGT AGT ACG TAC GC
	TGC CTG GGT AGT ACA TTC GC
	TGC CTG AGT AGT ACA TTC GC
	CGC CTG AGT AGT ATG CTC GC
	CAC CTG AGT AGT ATG CTC GC
	CGC CTG GGT AGT ACA TTC GC
Reverse Primer Mix	GCG GTG TGT ACA AGA CCC GA
	GCG GTG TGT ACA AAA CCC GA
	GCG GTG TGT ACA AAC CCC GA

Table 2-12 Primers for Cloning of Fra1 and Sequencing

Primer	Sequence (5'-3')
muFosl1_fwd	tgtacaaaaaagcaggctttATGTACCGAGACTACGGG
muFosl1_rev	tttgtacaagaaagctgggtTCACAAAGCCAGGAGTGTAG
pENTR-F	CTACAAACTCTTCCTGTTAGTTAG
pENTR-R	ATGGCTCATAACACCCCTTG
pInducer-fwd	CCATAGAAGACACCGGGACC
HA-R	TCTGGGACGTCGTATGGGTA

hPGK-fwd	TGTTCCGCATTCTGCAAGCCTC
WPRE-R	CATAGCGTAAAAGGAGCAACA

2.8 Kits

Table 2-13. Kits.

Kit	Manufacturer
Maxwell® 16 LEV simplyRNA Purification Kit	Promega, Walldorf
NucleoBond Xtra Midi EF	Macherey-Nagel, Düren
NucleoSpin Gel and PCR Clean-up	Macherey-Nagel, Düren
NucleoSpin Plasmid	Macherey-Nagel, Düren
NucleoSpin Plasmid Transfection-grade, Mini kit	Macherey-Nagel, Düren
QIAshredder	Qiagen GmbH, Hilden
RNeasy Mini Kit	Qiagen GmbH, Hilden

2.9 Software and Online Tools

Table 2-14. Software and Online Tools.

Software	Company	RRID
AxioVision 4.9	Carl Zeiss, Jena	SCR_002677
FlowJo™ 10.4 software	FlowJo, LLC, Ashland, OR, USA	SCR_008520
GraphPad Prism 5/9	GraphPad Software, San Diego, CA, USA	SCR_002798
GSEA software v.3.0/v.4.1	UC San Diego and Broad Institute	SCR_003199
Image Studio Lite version 5.2.5	LI-COR, Inc., Lincoln, NE, USA	SCR_013715
RStudio	RStudio, Boston, MA, USA	SCR_000432
StepOne™ Software	Applied Biosystems, Inc., Carlsbad, CA, USA	SCR_014281

Online Tools

Tool	Link
GeneTrail2 1.6 (SCR_006250)	https://genetrail.bioinf.uni-sb.de/
NEBuilder Assembly Tool	https://nebuilder.neb.com
OncoLnc	http://www.oncolnc.org/
Primer Blast (RRID:SCR_003095)	https://www.ncbi.nlm.nih.gov/tools/primer-blast/
Project Score / Cancer Dependency Map (Wellcome Sanger Institute)	https://score.depmap.sanger.ac.uk/

2.10 Media/Buffers/Solutions

Table 2-15. Media, Buffers and Solutions

Buffers for DNA analyis	
Medium/Buffer/Solution	**Composition**
10x Gitschier's buffer	670 mM Tris, pH 8.8 166 mM $(NH_4)_2SO_4$ 67 mM $MgCl_2$
DNA Lysis Buffer	0.5% Triton X-100 1% 2-Mercaptoethanol 1x Gitschier's buffer 400 µg/ml Proteinase K (added prior to use)
50x Tris acetate EDTA (TAE) buffer, pH 8.5	2 M Tris 50 mM EDTA 5.71% Acetic acid
5x KCM Buffer	500 mM KCl 150 mM $CaCl_2$ 250 mM $MgCl_2$

Cell Culture Media and Solutions	
Medium/Buffer/Solution	**Composition**
Crystal violet dye solution	2% EtOH 0.2 % Crystal violet in dH_2O
Freezing medium	Dulbecco's Modified Eagle's Medium, high glucose 20 % (v/v) Fetal Bovine Serum (FBS) 10 % (v/v) DMSO
Buffers for Protein Analysis	
Medium/Buffer/Solution	Composition
Protein Loading Buffer Laemmli (5x) pH 6.8	10% (w/v) SDS 50% (v/v) Glycerol 228 mM Tris-HCl 0,75 mM bromophenol blue 5% (v/v) 2-Mercaptoethanol
Running buffer (1x)	25 mM Tris 192 mM Glycine 0.1% (w/v) SDS
Wet Blot Transfer buffer (1x)	192 mM Glycine 25 mM TRIS 20 %(v/v) Methanol
RIPA buffer (pH 7.5)	50 mM TRIS-HCl 150 mM NaCl 2 mM EDTA 1 % Triton X100 1 % Sodium deoxycholate 0.1 % SDS
Stacking Gel Buffer (pH 6.8)	0.5 M Tris-HCl
Resolving Gel Buffer (pH 8.8)	1.5 M Tris-HCl
Blocking Buffer	5% skim milk powder in PBS
Washing Buffer (PBS-T)	0.1% Tween-20 in PBS

3 Methods

3.1 Mouse Experiments

All animal studies were conducted in compliance with European guidelines for the care and use of laboratory animals and were approved by the Institutional Animal Care and Use Committees (IACUC) of Technische Universität München and Regierung von Oberbayern.

3.1.1 Mouse strains

Animals were on a mixed *C57Bl/6;129S6/SvEv* genetic background. The Cre-*loxP* and Flp-*frt* systems were used in this work for tissue-specific recombination. For Cre-mediated recombination, tissue-specific Cre strains were crossed with mice that harbored alleles flanked by *loxP* sites. For Flp-mediated recombination, Flp-recombinase carrying mice strains were crossed with mice having conditional alleles flanked by *frt*-sites.

Ptf1a/p48-Cre (Nakhai et al., 2007)

This knock-in mouse line was kindly provided by Dr. Hassan Nakhai and Prof. Roland Schmid (Klinikum rechts der Isar, Munich). *Ptf1a-Cre* mice express a Cre recombinase under control of the endogenous promoter for the pancreas specific transcription factor 1a (*Ptf1a*), which plays a critical role in the development of the exocrine and endocrine pancreas in mice. In addition to the developing pancreas, Ptf1a^{Cre} is also active in the neural tube, cerebellum and retina.

***LSL-Kras*^{G12D}** (Hingorani et al., 2003; Jackson et al., 2001)

The *LSL-Kras*^{G12D} mouse strain was kindly provided by Prof. Tyler Jacks (Massachusetts Institute of Technology, Cambridge, MA, USA). *Kras*$^{LSL-G12D}$ mice carry a G12D point mutation in the *Kras* gene, whose expression is blocked by an upstream *loxP*-flanked STOP element. Upon Cre-mediated recombination, the STOP codon is excised and the oncogenic KRAS^{G12D} protein expressed.

fra1^{lox} (Eferl et al., 2004)

The *fra1^{lox}* mouse strain carrying conditionally floxed alleles of *Fra1* was kindly provided by Prof. Erwin Wagner (CNIO, Madrid, Spain). In the *Fra1^{lox}* mice, exons 3 and 4 of Fra1, which contain the dimerization and DNA-binding domains, are flanked by *loxP* sites. Upon Cre-mediated recombination, the *loxP*-flanked exons are deleted thus rendering *Fra1* inactive. In addition, a GFP reporter gene is spliced to the residual N-terminal part of *Fra1* upon recombination, which results in expression of a FRA1-GFP fusion protein (43 kDa).

Pdx1-Flp (Schönhuber et al., 2014)

The transgenic *Pdx1-Flp* mouse strain was generated in the laboratory of Prof. Dieter Saur (Klinikum rechts der Isar, Munich). In this strain, a codon optimized flippase (Flp) recombinase is placed under the control of the Pdx1 promoter, which is active in pancreatic islets, ducts and acini.

FSF-Kras^{G12D} (Schönhuber et al., 2014)

This knock-in mouse line was kindly provided by Prof. Dieter Saur (Klinikum rechts der Isar, Munich). These mice carry a codon 12 aspartic acid mutation in exon 2 of *Kras,* which is silenced by a *FRT-stop-FRT (FSF)* cassette. Expression of oncogenic Kras^{G12D} in this lineage is activated upon Flp recombinase-mediated excision of the *FRT*-flanked Stop cassette.

FSF-CAG-R26^{CreERT2} (Schönhuber et al., 2014)

This knock-in mouse was kindly provided by Prof. Dieter Saur (Klinikum rechts der Isar, Munich). In this mouse strain, expression of the Tamoxifen-inducible Cre^{ERT2}-recombinase is silenced by a *frt*-flanked STOP cassette. Upon Flp-mediated recombination, the STOP

cassette is excised and Cre[ERT2] expressed but sequestered in the cytoplasm. Cre[ERT2] can then be activated by Tamoxifen administration.

p53[frt] (Lee et al., 2012)

In the *p53[frt]* mouse strain, exons 2-6, which encode for the DNA binding domain of the transformation related protein 53 gene (*Trp53*) are flanked by *FRT*-sites. Upon Flp-mediated recombination, the flanked exons are deleted and the gene function disrupted.

3.1.2 Genotyping

At the age of 2-3 weeks, an approximately 2 mm long piece of the tail tip was cut from an anesthetized mouse using a sterile scalpel, which was subsequently used for extraction of genomic DNA for genotyping PCR analysis. Mice were labelled with earmarks for identification of the animals.

3.1.3 Dissection of Mice

Mice were euthanized by isoflurane inhalation and subsequent cervical dislocation. For dissection, mice were fixed and sterilized with 70% ethanol. Mice were dissected with sterilized surgical instruments. Pancreatic tissue samples were taken for DNA, RNA and protein isolation and stored at -80°C until further use. Isolation of pancreatic cancer cells from tumor tissue is described in section 3.2.1. Organs were washed in PBS and fixed in 4% Paraformaldehyde (PFA).

3.2 Cell culture

Cell lines were cultivated in a CO_2-incubator at 37°C and 5% CO_2. Murine primary pancreatic tumor cell lines were cultured in Dulbecco's Modified Eagle's Medium (DMEM) supplemented with 10% (v/v) fetal bovine serum (FBS) and 1% (v/v) Penicillin-Streptomycin.

The human pancreatic cancer cell lines MIA PaCa-2 and PaTu-8988T were grown in DMEM with 10% (v/v) FBS and 1% (v/v) Penicillin-Streptomycin. All other conventional established human PDAC cells were cultivated in Roswell Park Memorial Institute 1640 Medium (RPMI 1640) supplemented with 10% (v/v) FBS and 1% (v/v) Penicillin-Streptomycin.

Identity of the murine PDAC cell lines was verified by genotyping PCR as described in Section 3.3.1. Human cell lines were authenticated by Multiplexion GmbH (Heidelberg, Germany) via Single Nucleotide Polymorphism (SNP)-Profiling or by Mycrosynth (Balgach, Switzerland) via short tandem repeat (STR) profiling.

Primary-dispersed human PDAC cells (HuPDAC3, HuPDAC7, HuPDAC17) – all three harboring a $KRAS^{G12D}$ mutation – were previously isolated and established as described by Conradt et al. (2011) from surgically-resected (HuPDAC3, HuPDAC17) or PdX-derived (HuPDAC7) human PDAC. Human primary-dispersed cell lines were established and analyzed in accordance with the declaration of Helsinki, were approved by the local ethical committee and written informed consent from the patients for research use was obtained prior to the investigation. They were cultured in RPMI 1640 Medium supplemented with 20% FBS and 1% Penicillin-Streptomycin and used within passage 10-20.

3.2.1 Isolation and Establishment of pancreatic tumor cells

During dissection of the mouse, pancreatic tumor samples were taken and placed in sterile PBS in a cell culture dish. The PDAC sample was minced into smaller pieces with a scalpel under sterile conditions in a tissue culture hood and then incubated in DMEM with Collagenase Type 2 (200 U/mL) for 24 hours in a water bath at 37°C. The following day, the cell suspension was centrifuged at 200 x g for 5 minutes, the supernatant aspirated, the cell pellet resuspended in 5 mL DMEM medium with 10% FBS and 1% Penicillin-Streptomycin and transferred to a T25 cell culture flask.

3.2.2 Cultivation and Cryopreservation of pancreatic tumor cell lines

Cell lines were cultivated in their respective growth medium, which was replaced with fresh, pre-warmed growth every 2 - 3 days. Upon reaching approximately 80% confluence, the cells

were passaged. Therefore, the medium was removed, the cells washed with phosphate buffered saline (PBS) and detached by enzymatic dissociation with 1 x Trypsin-EDTA for 5 minutes at 37°C. The detached cells were then resuspended in fresh medium. For seeding of defined number of cells, the cells were counted in a Neubauer hemocytometer. For regular cell culture, cells were split – depending on the growth of the cell line at a ratio of 1:3 to 1:10 – and transferred to a new flask with fresh medium. For long-term cryopreservation, the cells were resuspended in fresh medium upon trypsinization and centrifuged for 5 minutes at 200 x g. The supernatant was then discarded, the cells resuspended in ice-cold freezing medium and transferred to -80°C for 24 hours before long-term storage in liquid nitrogen.

3.2.3 Mycoplasma Contamination Detection

Cell lines were tested for Mycoplasma contamination by a PCR-based method (Uphoff and Drexler, 2011). Therefore, the cells were grown in 6-well-plates in 3 mL regular growth medium without antibiotics for 10 days. Afterwards, the medium was collected and centrifuged at 250 x g for 2 minutes. The supernatant was taken off and centrifuged again for 10 minutes at 16,000 x g. The pellet was resuspended in 50 µL PBS and boiled at 95°C for 5 minutes. From each sample, 2 µL were used as template for the following Mycoplasma Detection PCR (Table 3-1). Mycoplasma Detection Primers are listed in Table 2-11. Positive and negative controls were used for each PCR. Only cell lines that tested negative were used in further experiments.

Table 3-1 Mycoplasma Detection PCR

PCR Reaction Mix	Temperature	Time	
	95°C	5 min	
15 µl REDTaq Ready mix			
2 µL forward Primer Mix (10 µM each)	94°C	1 min	
2 µL reverse Primer Mix (10µM each)	60°C	1 min	40x
9 µ H_2O	72°C	1 min	
2 µL DNA template			
	72°C	10 min	

3.2.4 Flow Cytometry

Annexin V/propidium iodide (PI) or Annexin V/4',6-Diamidino-2-phenylindole dihydrochloride (DAPI) flow cytometric analysis were used to assess induction of apoptosis. Annexin V is an intracellular protein that can bind to the phospholipid phosphatidylserine (PS), which is found on the cytosolic leaflet of the plasma membrane in viable cells. During apoptosis, however, PS is translocated to the extracellular leaflet, where it can be detected by fluorochrome-labeled Annexin V. To minimize spectral overlap, apoptosis induction in cell lines expressing a GFP reporter gene was assessed by staining with APC Annexin-V and DAPI, while APC Annexin-V / PI was used for cell lines without a fluorescent reporter according to the manufacturer's instructions. Cells were treated with an inhibitor or the respective vehicle control for the indicated time points, then detached by trypsinization and resuspended in Annexin V binding buffer ($1x10^6$ cells/mL). The cells were stained by adding 5 µL Annexin V to 100 µL of the cell suspension and 10 µL PI solution or DAPI, incubated for 15 minutes at room temperature in the dark, adjusted with 400 µL Annexin V binding buffer and analyzed by flow cytometry. Annexin V-positive / PI (or DAPI) – negative cells were considered as apoptotic cells, while PI or DAPI-positive cells were deemed necrotic.

The cell cycle profile of the cells upon inhibitor treatment was determined by staining the DNA with PI and quantitation of the DNA content by flow cytometry analysis. The cells were harvested at the indicated time points and fixed for 1 hour in ice-cold 70% ethanol. After fixation, the cells were centrifuged at 800 x g for 5 minutes and the pellet resuspended in 1 mL PBS. To ensure that only DNA is stained, the samples were treated with RNase A (50 µg/mL) for 1 hour at 37°C in the dark and then stained with propidium iodide (50 µg/mL). Samples were passed through a 30 µm cell filter and analyzed by flow cytometry to determine the proportion of cells in each phase of the cell cycle. Results were analyzed with FlowJo™ Software.

3.2.5 Clonogenic Assays

To assess clonogenic growth of the KCF cells transduced with the pLenti RFP and pLenti FRA1 constructs, 1000 cells per well were cells were seeded in triplicates in 2 mL DMEM growth medium in 6-well plates and cultured for 10 days until visible colonies had formed.

For inhibitor treatments, cells were seeded in multiwell plates at the density and in the volume indicated in Table 3-2 and allowed to attach overnight. The number of cells seeded was adjusted according to the growth of the cells. Inhibitors were added at the indicated concentrations.

Table 3-2: Clonogenic Assay Conditions

Well-Plate	Cells/Well	Growth Medium	0.2% Crystal Violet	1% SDS
24-well plate	500 - 2000	500 µL	200 µL	500 µL
12-well plate	1000 – 4000	1 mL	500 µL	1 mL
6-well plate	1000	2 mL	1 mL	1.5 mL

The cells were cultured for another 5 – 10 days depending on the growth of the cell lines until the cells in the DMSO treated control well were nearly confluent.

For staining of the colonies, the medium was carefully aspirated, the cells washed with PBS and then stained with 0.2% crystal violet solution for 20 minutes on an orbital shaker at room temperature. Next, the plates were washed 2 - 3 times with water to remove the background staining, then dried overnight and scanned on a flatbed scanner the following day for visualization.

For quantification, the crystal violet dye was dissolved with 1% (w/v) SDS overnight on an orbital shaker at room temperature and the absorbance at 570 nm was measured with a microplate reader (CLARIOstar, BMG Labtech, Ortenberg Germany). Absorbance values were normalized to DMSO treated controls or – in case of the clonogenic growth of the KCF pLenti RFP and pLenti FRA1 cells – normalized to the pLenti RFP control cell line and are depicted as relative values.

3.2.6 Cell Viability Assays

Cell Viability was determined by CellTiter-Glo® (Promega) or MTT assay (Sigma). The CellTiter-Glo® assay is a luminescent cell viability assay that allows for the quantitation of cellular ATP as a readout for the number of viable, metabolically active cells in the culture. After 72 hours of treatment, the ATP content of the cells was assessed with CellTiter-Glo as a readout for the cell viability. Therefore, the plates were adjusted to room temperature for 30 minutes and then 25 µL of CellTiter-Glo were added to each well. After gentle shaking and 15 minutes incubation, the luminescence was measured on a FLUOstar OPTIMA microplate reader (BMG Labtech).

The MTT assay is a colorimetric assay that measures metabolic activity and thus functions as a readout for cell viability. The yellow tetrazolium salt MTT (3-(4,5-dimethylthiazol-2-yl)-2,5-diphenyltetrazolium bromide) is reduced by oxidoreductases in viable, metabolically active cells to purple formazan crystals, which can then be dissolved and the absorbance of the resulting colorimetric solution measured in a microplate reader.

For the MTT assays, 1,000 cells per well were seeded out in 100 µL growth medium in 96-well plates. In case of inhibitor treatments, the cells were treated the following day with the respective drugs in seven-point dilutions. After 72 hours treatment, 10 µL MTT (5 mg/mL dissolved in PBS) was added to each well and incubated for another 4 hours at 37°C. The medium was then removed and the formazan crystals dissolved in 200 µL DMSO:EtOH (1:1) solubilization solution for 15 minutes on a shaker at room temperature. The absorbance of the resulting purple-colored solution was then measured at 595 nm in a Multiskan RC Microplate photometer (Thermo Scientific).

3.2.7 Growth Curve

The MTT assay was also used to measure cell growth by seeding out 1,000 cells per well in 100 μL growth medium in 96-well plates. One plate was seeded out for each day of measurement. In case of doxycycline treatment of the pInducer-transduced cells to induce FRA1 expression or dTAG13 treatment to degrade FRA1-dTAG fusion protein, the cells were treated the next day with 100 ng/mL doxycycline or 1 μM dTAG13 respectively. Viability of the cells was then measured by MTT assay – as described above (section 3.2.6) – at day 1, 2, 3 and 4 after seeding. Absorbance values were normalized to measurements at day 1 after seeding and are depicted as relative growth.

3.2.8 Drug Screen

The drug library consisting of 99 inhibitors targeting various relevant cancer pathways in PDAC was purchased from Selleckchem. The two SUMO inhibitors ML-93 and TAK-981 were from Takeda and later added to the library. Serial seven-point 1:3 dilutions of the drugs – ranging from 10 mM to ~10 μM (with the exception of A-1210477 (2 mM starting concentration) and APX2009 (100 mM starting concentration) – were prepared in DMSO, pipetted into 384-well plates and stored at -80°C.

For the drug screen, the two FRA1-deficient KCF cell lines SDF287 and SDF716 transduced either with the control vector pLenti RFP or reconstituted with pLenti FRA1 were seeded out in white 96-well plates at a density of 1000 cells per well in 100 μL DMEM growth medium. The following day, the drug library was transferred with a 96-pin replicator pin tool (V&P Scientific) from the drug plates to the cells (0.1 μL/well) giving a final concentration dose range from ~10 nM to 10 μM (with the exception of A-1210477 and APX2009 as mentioned above). Each drug was analyzed in technical duplicates. After each transfer step, the pins were cleaned in DMSO/EtOH (1:1), dried on blot paper for 15 seconds and then cleaned in isopropanol twice (15 seconds drying after the first wash and 30 seconds drying on blot paper after the last wash to avoid contamination and spillovers). After 72 hours of treatment, the cell viability was

measured with CellTiter-Glo reagent. Therefore, the plates were adjusted to room temperature for 30 minutes and then 25 µL of CellTiter-Glo added to each well. After gentle shaking and 15 minutes incubation, the luminescence was measured on a FLUOstar OPTIMA microplate reader (BMG Labtech). Area-under-the-Curve (AUC) and half-maximal growth inhibitory concentration (GI_{50}) values from the results were calculated with the RStudio software tool using a script based on the GRmetrics methodology (Clark et al., 2017).

3.3 Molecular methods

3.3.1 Polymerase Chain Reaction (PCR)

Polymerase Chain Reaction was mainly used for genotyping of the transgenic mouse strains and murine pancreatic tumor cells. For extraction of genomic DNA, mouse tail ends (1 mm) or cell pellets were lysed in 50 µL DNA lysis buffer at 55°C for 90 minutes followed by 15 minutes at 95°C to inactivate the Proteinase K. The lysates were then centrifuged at 16,000 x g for 10 minutes and the supernatant containing the DNA was transferred to a new tube. The crude DNA lysate was subsequently used as DNA template for the genotyping and recombination PCR analysis. PCR reaction was performed with 1.5 µL DNA template using REDTaq ReadyMix according to the PCR conditions shown in Table 3-3. Annealing Temperatures for the respective genotyping PCR and the expected size of the PCR products are depicted in Table 3-4. PCR products were subsequently analyzed by agarose gel electrophoresis.

Table 3-3 Genotyping PCR

PCR Reaction Mix	PCR conditions		
	Temperature	Time	Cycles
12.5 µL REDTaq Ready Mix	95°C	3 minutes	1x
0.25 – 1 µL Forward Primer	95°C	45 seconds	
0.25 – 1 µL Reverse Primer	55 – 62 °C	60 seconds	40x
1.5 µL DNA template	72°C	90 seconds	
ad 25 µL dH$_2$O	72°C	5 minutes	1x

Table 3-4 Annealing Temperatures and PCR Product Sizes

PCR	Annealing Temperature	PCR Product Size
Ptf1a^{Cre}	60°C	400 bp (mut) 600 bp (wt)
LSL-Kras^{G12D}	55°C	170 bp (mut) 270 bp (wt) 300 bp (del)
Fra1^{lox}	59°C	354 bp (mut) 308 bp (wt) 408 bp (del)
Pdx1-Flp	55°C	620 bp (mut)
FSF-Kras ^{G12D}	55°C	351 bp (mut) 270 bp (wt)
R26-Cre^{ERT2}	55°C	190 bp (mut)
p53^{frt}	57 °C	292 bp (mut) 258 bp (wt)

wt=wild type allele; mut=mutant allele; del=deleted/recombined allele; bp=base pairs

3.3.2 Agarose Gel Electrophoresis

PCR products were analyzed on 1 - 2% agarose gels by electrophoresis. Agarose gels were prepared with 1x TAE buffer. Ethidium Bromide (0.5 µg/mL) was added to the agarose gel for visualization of the DNA. In general, 10 µL per sample were loaded onto the gel. Depending on the size of the PCR product, GeneRuler 100 bp DNA Ladder or 1 kb Plus DNA Ladder were used as reference marker. The gel electrophoresis was run in 1x TAE Buffer for approximately 1 hour until the bands were sufficiently separated. Results were analyzed with the UVsolo TS gel documentation system.

3.3.3 Bacterial Transformation

For bacterial transformation, 10 - 50 ng plasmid DNA or cloning reaction mix were mixed with 20 µL 5x KCM buffer, adjusted to 100 µL with dH$_2$O and added to 100 µL of One Shot™ Stbl3™ chemically competent *E. coli* (Thermo Fisher). The mixture was incubated for 20 minutes on ice, 10 minutes at room temperature and then adjusted with 1 mL LB Medium. The bacteria were then transferred to a shaker for 1 hour at 37°C, pelleted by centrifugation, resuspended in fresh LB Medium and streaked onto LB Agar plates with the respective selection antibiotic (100 µg/mL Ampicillin or 50 µg/mL Kanamycin).

3.3.4 Plasmid Preparation

For plasmid preparation, bacterial clones were incubated in LB-Medium with the corresponding selection antibiotic with constant shaking overnight at 37°C. Plasmid DNA was isolated on the following day with a plasmid DNA purification kit (NucleoSpin Plasmid or NucleoBond Xtra Midi Plus EF, Macherey-Nagel) according to the manufacturer's instructions. DNA concentrations were determined using the spectrophotometer NanoDrop® 1000. Plasmids were sequenced by Sanger Sequencing (Eurofins).

3.3.5 Cloning Strategies

Cloning of *Fra1* was done in a two-step process. First, the coding sequence of *Fra1* was cloned into the entry vector pENTR using the NEBuilder HiFi DNA Assembly (NEB) kit, which allows for high-fidelity assembly of DNA fragments in an isothermal reaction. In the second step, *Fra1* was shuttled to the destination vectors via Gateway Cloning, which is a recombination based cloning method that allows for shuttling of DNA from a donor to a destination vector. The GFP-dTAG plasmid used in this study was generated in our lab analogous to the methods described here for FRA1 and was kindly gifted by Lukas Krauß. All plasmids generated in this study were submitted to Addgene (Addgene ID 188665, 188742 and 192267).

3.3.6 DNA Hifi Assembly Cloning

In the first step, *Fra1*-specific primers for the coding sequence with specific overhangs corresponding to the pENTR vector were designed with the web tool NEBuilder (NEB). *Fra1* cDNA from murine primary pancreatic tumor cells (Ptf1a$^{Cre/+}$, Kras$^{G12D/+}$) was used as a template for the PCR amplification with NEB Q5 polymerase according to the conditions in Table 3-5 and Table 3-6.

Table 3-5: Q5 polymerase PCR reaction mix

Component	50 µl Reaction	Final concentration
5x Q5 Reaction Buffer	10 µl	1X
10 mM dNTPs	1 µl	200 µM
10 µM Forward Primer	2.5 µl	0.5 µM
10 µM Reverse Primer	2.5 µl	0.5 µM
Template DNA	variable	20 - 100 ng
Q5 High-Fidelity DNA Polymerase	1.25 µl	2.5 µl
Nuclease-Free Water	to 50 µl	

Table 3-6: Q5 Polymerase PCR conditions

Step	Temperature	Time
Initial Denaturation	98°C	30 seconds
30 cycles	98°C	10 seconds
	64°C	30 seconds
	72°C	30 seconds
Final extension	72°C	2 minutes

The PCR product was purified according to the manufacturer's instructions with the NucleoSpin Gel and PCR Clean-up kit (Macherey-Nagel) and analyzed on an agarose gel.

The pENTR vector was linearized by restriction digest with XbaI and DraI (New England Biolabs) according to the manufacturer's instructions. Briefly, 1 µg pENTR plasmid DNA was mixed with 5 µL 10x CutSmart Buffer (NEB), 1 µL XbaI, 1 µL DraI in a 50 µL reaction volume adjusted with H_2O and incubated at 37°C for 1 hour.

Next, the *Fra1* PCR product was assembled into the linearized pENTR vector using the NEBuilder HiFi DNA Assembly kit (NEB) according to the manufacturer's instructions.

Briefly, 100 ng of linearized vector were mixed with 2-fold molar excess of the insert, adjusted with dH_2O to 10 µL and added to 10 µL NEBuilder HiFi DNA Assembly Master Mix. The samples were then incubated in a thermocycler at 50°C for 15 minutes and the assembled product subsequently used for bacterial transformation (section 3.3.3). Correct assembly of the *Fra1* insert into the pENTR vector was verified by Sanger Sequencing (Eurofins).

3.3.7 Gateway Cloning

After assembly of *Fra1* into the pENTR entry vector, the *Fra1* insert was shuttled into the destination vectors pInducer20-BLAST, pLenti and pLEX-N-dTAG via Gateway Cloning using the Gateway® LR Clonase® II enzyme mix (Thermo Fisher) according to the manufacturer's instructions. Therefore, 100 ng of the pENTR-vector with the *Fra1* insert sequence were mixed with 100 ng of the respective destination vector and adjusted with H_2O to a volume of 8 µL. Next, 2 µL of LR Clonase enzyme were added and incubated at 25°C for 2 hours. Afterwards, 5 µL of the reaction were used for bacterial transformation (see Bacterial Transformation 3.3.3). Successful shuttling of the *Fra1* insert into the respective destination vectors was verified by Sanger Sequencing (Eurofins).

3.3.8 Retroviral transduction

The pBabe-Puro Myc^{ER} plasmid (Addgene #19128) was used to generate murine MYC^{ER} – expressing cells. The empty pBabe-Puro backbone vector served as control. For generation of retroviral particles, the "Phoenix Eco" retroviral packaging cell line was seeded into 10 cm cell culture dishes. The following day, 2 µg of the plasmid was mixed with 18 µL TransIT-LT1 or Lipofectamine 2000 transfection reagent in Opti-MEM I Reduced Serum Media, incubated for 20 minutes to allow the complex to form and then carefully added to the cells. The medium was replaced with 5 mL fresh DMEM growth medium on the next day. After another 24 hours, the medium was collected in a tube and replaced with 5 mL fresh medium, which was again collected the following day. The collected medium from both days was filtrated through a 0.2 µm filter and either used freshly for transduction or stored at -80°C.

For the retroviral transduction, murine PDAC cells were seeded in 6-well plates at a density of 50,000 cells per well in 2 mL DMEM. The following day, the medium was aspirated and 1 mL of the retroviral particles from the previous step was added to the cells together with 8 µg/mL Polybrene. The medium was replaced with fresh medium after 24 hours and the cells were selected with 3 µg/mL Puromycin 48 hours post-transduction for 3-7 days until all cells in the non-transfected control well had died. MYC^{ER} protein expression was confirmed by immunoblotting.

Upon retroviral transduction of the murine PDAC cell lines PPT-5671 and PPT-53631 with the MSCV-MYC-IRES-GFP or the MSCV-IRES-GFP empty vector, cells were FACS-sorted for GFP expression (FACSAria, Becton Dickinson). MYC and GFP protein expression was confirmed by immunoblotting.

The human PDAC cell line IMIM-PC1 was first transfected with MSCV-rtTA-IRES-EcoReceptor-PGK-puro using Lipofectamine 2000 and selected for stable expression of the ectropic receptor with puromycin. The IMIM-PC1 cells expressing the ectropic receptor were then retrovirally transduced with the MSCV MYC^{ER}-IRES-GFP plasmid and FACS-sorted for GFP expression (FACSAria, Becton Dickinson).

3.3.9 Lentivirus Production Protocol

For production of lentiviral particles, HEK293FT cells were seeded in 10 cm dishes in 10 mL DMEM growth medium. The next day, plasmid mix consisting of 1.25 µg psPax2 packaging plasmid, 0.75 µg pMD2 VSV-G envelope expressing plasmid and 2 µg lentiviral vector expressing the gene of interest was prepared and gently mixed with 270 µL Opti-MEM I Reduced Serum Media. Next, 18 µL TransIT-LT1 were carefully added, gently mixed by pipetting and incubated for 20 – 30 minutes at room temperature to allow the transfection complex formation. Afterwards, the mixture was carefully added dropwise to the HEK293FT cells and incubated overnight at 37°C. On day 1 post-transfection, the medium was aspirated and changed to 4 mL DMEM with 30% FBS. On day 2, Lentivirus supernatant was collected and stored in a reaction tube at 4°C overnight. Fresh medium was again added to the HEK293FT and collected the next day (day 3). Lentivirus harvests from both days were pooled, filtered through a 0.2 µm filter and stored at -80°C until further use.

For lentiviral transduction, cells were seeded at a density of 50,000 cells per well in 6-well plates. The next day, the medium was aspirated and 1 mL lentiviral supernatant with 8 µg/mL Polybrene was added to the cells and incubated overnight at 37°C. The following day, the lentiviral supernatant was aspirated and fresh DMEM growth medium added to the cells. Selection with antibiotic selection marker was started 48 hours post-transduction and lasted for 3-7 days for Puromycin (3-4 µg/mL) and 7 – 10 days for Geneticin (500 µg/mL) and Blasticidin (10 µg/mL) with medium change every 3 days until all cells in the control well had died.

3.3.10 RNA isolation and reverse transcription

RNA was extracted from pancreatic cancer cell lines at the indicated time points after treatment or when cells reached approximately 80% confluency in a 10 cm cell culture dish. Cells were washed with ice-cold PBS and collected in 600 µL RLT-Buffer with 1% (v/v) 2-Mercaptoethanol. Samples were frozen at -80°C until further use. Total RNA was isolated

using the RNeasy kit (Qiagen) or the Maxwell® 16 LEV simplyRNA Purification Kit (Promega) according to the manufacturer's instructions. RNA concentration was measured using the NanoDrop 1000 spectrophotometer. Isolated RNA was stored at -80°C until further use. For reverse transcription of the isolated RNA samples into cDNA, 2 µg of RNA was used in a total reaction volume of 100 µL with TaqMan reverse transcription reagents (Thermo Fisher) in a thermal cycler according to the conditions in Table 3-7. The obtained cDNA was diluted 1:5 in H_2O and stored at -20°C until further use.

Table 3-7: Reverse Transcription

Component	Final concentration	Reaction Conditions
10 x TaqMan RT Buffer	1 x	
25 mM MgCl2	5.5 mM	
10 mM dNTP mix	500 µM each	25°C 10 minutes
50 µM Random hexamers	2.5 µM	48°C 60 minutes
RNase Inhibitor (20 U/µL)	0.4 U/µl	95°C 5 minutes
Multiscribe RT (50 U/µl)	1.25 U/µl	
RNA	2 µg	
RNase free water	ad 100 µl	

3.3.11 Real-Time quantitative PCR

Primers for real-time quantitative PCR (qPCR) were designed using the Primer-BLAST online tool from the National Center for Biotechnology Information (NCBI). Primers were synthesized by Eurofins and dissolved in H_2O to a final concentration of 10 µM. Real time quantitative PCR analysis was performed with 100 nM of each primer and SYBR Green qPCR Master Mix using the StepOnePlus™ real time PCR system and software. Samples were analyzed in technical triplicates and normalized to expression of the housekeeping genes *Cyclophilin* or *GAPDH*. The delta-delta Ct ($2^{-\Delta\Delta CT}$) method (Livak and Schmittgen, 2001) was used for relative quantification of gene expression based on the Ct (cycle threshold) values:

ΔCt = Ct (gene of interest) – Ct (housekeeping gene)

$\Delta\Delta Ct$ = ΔCt (treated sample) – ΔCt (reference sample)

Relative fold gene expression = $2^{-\Delta\Delta Ct}$

3.3.12 RNA-seq and Gene Set Enrichment Analysis

The samples for the RNA-seq of the 4-OHT treated IMIM-PC1 MYC^{ER} was prepared using an Illumina TruSeq Stranded RNA Library Prep Kit and analyzed on an Illumina HiSeq2000 system (DKFZ Heidelberg, NGS core facility). Resulting Fastq files (approximately 25M reads/sample (single-end reads)) were processed and analyzed using the Galaxy Project platform (Afgan et al., 2018). TrimGalore! (Galaxy version 0.4.3.1) was used to remove adapters from Fastq files and Bowtie2 (Galaxy version 2.3.2.2) (Langmead and Salzberg, 2012) to map the sequencing-reads to the human reference genome hg19 (GRCh37). Sequencing-reads were annotated with the hg19 GTF annotation file from the UCSC genome browser database (Casper et al., 2018). Differential expression of count data (htseq-count 0.6.1galaxy3) was determined by DESeq2 (Galaxy version 2.11.39)(Anders et al., 2015; Love et al., 2014).

The murine 53631PPT cells – retrovirally transduced with a MYC-IRES-GFP expression vector or the respective control – and the pLenti-FRA1/pLenti RFP or dTAG-FRA1 transduced cells were analyzed by bulk 3'-sequencing of poly(A)-RNA at the Sequencing Core Unit at the TranslaTUM of the Technical University Munich. The library was prepared as previously described (Parekh et al., 2016). Briefly, barcoded cDNA of each sample was generated with Maxima RT polymerase (Thermo Fisher) using oligo-dT primer containing barcodes, unique molecular identifiers (UMIs) and an adaptor. A template switch oligo (TSO) was used to extend the cDNA 5' ends. Full-length cDNA was amplified by using primers that bind to the TSO-site and adapter. The Nextera XT kit (Illumina) was used for tagmentation of the cDNA and 3'-end-fragments amplified using primers with Illumina P5 and P7 overhangs. To achieve a better cluster recognition, the P5 and P7 sites were exchanged compared to Parekh et al. (2016) to allow for sequencing of the cDNA in read1 and barcodes and UMI in read2. Sequencing of the library was performed on NextSeq 500 (Illumina) with 75 cycles for the cDNA in read1 and 16 cycles for the barcodes and UMIs in read2. To generate sample- and gene-wise UMI tables,

the data were processed using the Drop-seq pipeline (v1.0) and aligned to the reference genomes (GRCm38, murine; GRCh37, human). ENSEMBL annotation release 75 was used for transcript and gene definitions. Accession numbers: GSE119423, PRJNA489233 and PRJEB34637.

For RNA-seq analysis of the FRA1-cells, transcript and gene definitions were used according to the GENCODE Version M25. RNAseq analysis was performed with R-Studio (R version 4.0.2 (2020-06-22), open source license) and DEseq2. Genes with sum (read counts) < n (n=number of Samples) were removed and remaining counts were normalized and transformed using regularized log transformation (rlog) implemented in the DEseq2 package.

Additionally, publicly available mRNA expression datasets were accessed and utilized for this work: A recently published RNA-seq dataset of 38 murine PDAC cancer cell lines (Mueller et al., 2018), which were used in this study, was accessed via ENA: PRJEB23787. The expression profiles of conventional human PDAC cell lines from the Cancer Cell Line Encyclopedia (Barretina et al., 2012) were downloaded via the cBioPortal platform (http://www.cbioportal.org) (Cerami et al., 2012).

The gene expression profiling of pancreatic ductal epithelial cells upon conditional activation of oncogenic $Kras^{G12D}$ was done in our lab by Sandra Diersch and has been previously described (Diersch et al., 2016). The corresponding microarrays can be accessed via EMBL-EBI ArrayExpress (Accession number: E-MTAB-2592).

TCGA PAAD mRNA expression data and clinical data sets were accessed via UCSC cancer genomics browser (Cline et al., 2013).

For gene set enrichment analysis (GSEA), the GeneTrail2 1.6 web tool (Stöckel et al., 2016) and GSEA software from the Broad Institute (Subramanian et al., 2005) were used. Statistical values (nominal p-value, FDR q-value) were calculated and are indicated in the respective figures.

3.3.13 Protein Extraction

For protein sample preparation, cells were seeded out in 10 cm cell culture dishes. If left untreated to determine basal protein expression, cells were harvested for protein extraction, when they reached 80% confluency. Otherwise cells were treated with the respective compound 24 hours after seeding and harvested at the indicated time points.

For whole cell protein extraction, the cells were washed with PBS and lysed with 100 - 200 µL of RIPA Buffer supplemented with Protease and Phosphatase Inhibitors. For analysis of SUMO-conjugated proteins, the SUMO protease inhibitor N-ethylmaleimide (NEM, 20 mM) was added freshly to the protein lysis buffer. The lysate was collected using a cell scraper and stored at -80°C until further use.

3.3.14 Bradford Assay

Protein concentrations were determined using the Bradford Assay. Therefore, the whole cell protein extractions were thawed on ice, centrifuged at 16,000 x g for 20 minutes in a pre-cooled centrifuge at 4°C and the supernatant transferred to a fresh tube. The 5x Bradford Reagent (Serva) was diluted with distilled water to a 1x working concentration and 300 µL per well of the 1 x Bradford Solution were added to a 96-well plate.

One microliter of protein sample was added per well and three wells per sample were analyzed. Bovine Serum Albumin (BSA) (0, 0.5, 1, 2, 4, 8 µL of a 1 µg/µL stock solution) was used for setting up the standard curve.

Protein concentrations were then determined by measuring the absorbance in a microplate reader at 570 nm. Samples were adjusted to equal protein concentrations with RIPA Buffer, mixed with 5x Laemmli protein loading buffer, boiled at 95°C for 5 minutes and then stored until further use at -20°C.

3.3.15 Immunoblotting

SDS-PAGE (sodium dodecyl sulphate–polyacrylamide gel electrophoresis) was used to electrophoretically fraction the proteins according to their molecular mass. Depending on the

protein size, 7.5% - 15% resolving gels were prepared according to Table 3-8, poured into the gel chambers and covered with Isopropanol.

Table 3-8: Composition of Stacking and Resolving Gels

Component	Stacking Gel (4%)	Resolving Gel		
		7.5%	10%	15%
dH$_2$O	1.5 mL	2.45 mL	2 mL	1.25 mL
Stacking Gel Buffer	0.65 mL	-	-	-
Resolving Gel Buffer	-	1.3 mL	1.3 mL	1.3 mL
30% Acrylamide	375 µL	1.25 mL	1.65 mL	2.5 mL
10% SDS	25 µL	50 µL	50 µL	50 µL
10% APS	12.5 µL	25 µL	25 µL	25 µL
TEMED	7.5 µL	7.5 µL	7.5 µL	7.5 µL

After polymerization, the isopropanol was carefully discarded, the stacking gel poured on top of the separating gel and a comb inserted between the glass plates to create the pockets for the samples. The comb was removed after the polymerization of the stacking gel and the gel transferred to the electrophoresis chamber with Running Buffer. Samples were loaded into the wells of the gel together with a protein ladder. A voltage of 80 V was applied until the samples had migrated to the separation gel. Thereafter, the samples were separated at a voltage of 100 - 120 Volt for 1 - 2 hours until the bromophenol blue dye front had run out of the gel.

To immobilize the proteins on a membrane, the proteins were transferred to a PVDF or nitrocellulose membrane by wet tank electroblotting in an electrophoresis chamber with Wet Blot Buffer for 2 hours at 300 mA or overnight at 90 mA.

Afterwards, to prevent unspecific binding of the antibodies, the membranes were blocked in 5% skim milk in PBS for 30 minutes. After blocking, the membranes were incubated overnight with gentle shaking at 4°C in primary antibody dilution.

The next day, the membranes were washed three times in PBS with 0.1% Tween (PBS-T) for 5 minutes on a shaker at room temperature and then incubated with secondary antibody for 1 hour at room temperature with gentle shaking. The membranes were again washed three times with PBS-T and then imaged in a Li-Cor Odyssey FC at 700 nm or 800 nm wavelength. Alternatively, for chemiluminescent Western detection, Western blots were incubated with horseradish peroxidase (HRP) labelled secondary antibodies. After washing, membranes were incubated for 5 minutes with SuperSignal™ West HRP-substrate working solution and visualized on CL-Xposure Film using the OPTIMAXX X-Ray Film Processor.

3.4 Statistical Analysis

GraphPad Prism was used to generate graphs and perform statistical analysis. Data are from at least three independent experiments unless noted otherwise and are presented as mean +/- standard deviation (SD). Statistical significance was tested using ANOVA or two-sided t-test. Bonferroni and Sidak tests were used to correct for multiple comparisons. Statistical methods are indicated in the figure legends. P-Values are indicated in the respective figure and represented by: * $P \leq 0.05$; **$P \leq 0.01$; ***P ≤ 0.001; **** $P \leq 0.0001$

4 Results

4.1 The role of FRA1 in pancreatic cancer

4.1.1 Establishment of FRA1-deficient PDAC cell lines

In previous work, our group established primary pancreatic ductal epithelial cells (PDECs) from $R26^{CreERT2}$;LSL-$Kras^{G12D/+}$ mice that allow for temporally controlled expression of oncogenic $Kras^{G12D}$ from the endogenous promoter to decipher the early signaling network activated by mutant KRAS in the pancreas (Diersch et al., 2016; Schneeweis et al., 2018). In this system, activation of the Cre^{ERT2} recombinase by 4-Hydroxytamoxifen (4-OHT) induces recombination of the *Lox-Stop-Lox (LSL)* silenced *Kras* locus and subsequent expression of oncogenic $KRAS^{G12D}$ from the endogenous promoter (Figure 1 A). In addition to the previously described induction of EGFR-MYC cross signaling (Diersch et al., 2016; Schneeweis et al., 2018), a strong activation of the AP-1 (activator protein 1) gene network upon activation of mutant KRAS was observed in the PDECs (Figure 1 B). AP-1 is a family of transcription factors that contains members of the JUN, FOS, ATF and MAF protein families and which has been implicated in various oncogenic processes such as cell proliferation, differentiation, apoptosis and tumor invasion (Eferl and Wagner, 2003). Out of the various AP-1 family member, *Fosl1* (*Fra1*) was the most highly enriched factor upon activation of oncogenic KRAS (Figure 1 C). High expression of *FRA1* has been linked to a worse survival in PDAC patients and a cross-species, cross-tumor meta-analysis has unveiled FRA1 to be a critical downstream dependency of mutant KRAS in lung and pancreatic cancer (Vallejo et al., 2017a).

Therefore, to further study the role of FRA1 in pancreatic cancer in more detail, *Fra1*-floxed mice (Eferl et al., 2004) were crossed with $Ptf1a^{Cre/+}$; LSL-$Kras^{G12D/+}$ *(KC)* and *Pdx1-Flp; FSF-*$Kras^{G12D/+}$, $p53^{frt/+}$ mice. In these *Fra1*-floxed mice, exons 3 and 4 coding for the dimerization and the DNA-binding domains of *Fra1* are flanked by *loxP* sites (Figure 1 D). Upon Cre-mediated recombination, FRA1 function is thus rendered inactive and a GFP reporter gene is spliced to the N-terminal residue of FRA1 (Eferl et al., 2004). FRA1-deficient cell lines were established from $Ptf1a^{Cre/+}$; LSL-$Kras^{G12D/+}$; $Fra1^{lox/lox}$ (KCF) mice. The isolated murine PDAC

cells from the KCF mice showed complete recombination of the *Fra1* locus (Figure 1 E) and expression of the FRA1-GFP reporter fusion protein (Figure 1 F). A *Fra1* qPCR specific for the floxed exons 3 and 4 showed complete loss in expression of these transcripts in KCF cells compared to their proficient KC controls – indicating a successful knockout – whereas expression of exons 1 and 2 was still detectable and even upregulated in KCF cells (Figure 1 G).
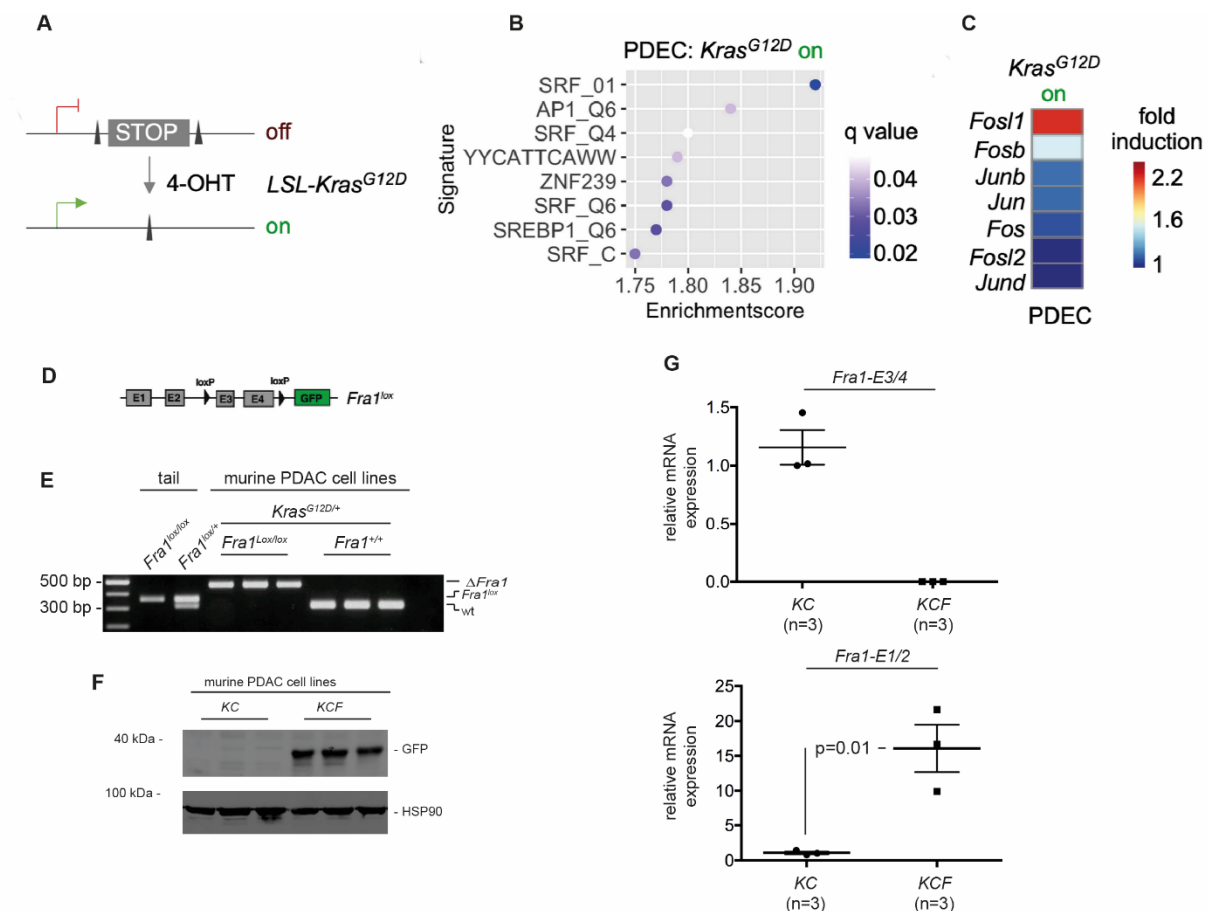

Figure 1: Establishment of FRA1-deficient cell lines

(A) Schematic description of the genetic strategy to activate oncogenic KRAS in pancreatic ductal epithelial cells (PDECs). Expression of Kras[G12D] in *R26[CreERT2];LSL-Kras[G12D/+]* PDECs is induced by addition of 4-Hydroxytamoxifen, which activates the Cre[ERT2] recombinase and subsequent recombination of the *lox-stop-lox* silenced *Kras* locus.

(B) Enrichment of oncogenic transcriptional signatures upon activation of KRAS[G12D] in PDEC. Enrichment plots of transcriptional signatures induced by Kras[G12D] from microarrays of 4-OHT (200 nM, 3 days) treated PDECs

(C) Expression of AP-1 family transcription factors is induced in Kras[G12D]-activated PDEC. Relative fold induction of AP-1 transcription factors from microarrays of 4-OHT treated PDECs ("Kras on").

(D) Genetic strategy for the conditional knockout in *Fra1[lox]* mice. In *Fra1[lox]* mice (Eferl et al., 2004), exons 3 and 4 that code for the dimerization and the DNA-binding domains of *Fra1* are flanked by *loxP* sites. Upon Cre-mediated recombination in the pancreas, *Fra1* function is ablated and a GFP reporter gene is spliced to the N-terminus of FRA1.

(E) *Fra1* genotyping PCR. Genotyping of three PDAC cell lines derived from *Ptf1a^{Cre/+};LSL-Kras^{G12D/+} Fra1^{lox/lox}* (KCF) PDAC shows complete recombination of *Fra1*. Three PDAC cell lines from *Ptf1a^{Cre/+};LSL-Kras^{G12D/+}* (KC) mice and DNA from the tail of homozygous *Fra1^{lox/lox}* and heterozygous *Fra1^{lox/+}* served as controls. One experiment analyzed.

(F) GFP western blot in KC and KCF PDAC cells. Recombination and Deletion of *Fra1* in the pancreas of *Ptf1a^{Cre/+};LSL-Kras^{G12D/+} Fra1^{lox/lox}* (KCF) mice generates a fusion protein between the residual N-terminal part of FRA1 and GFP (43 kDa), which can be detected by Western blot in KCF PDAC cells using an anti-GFP antibody. HSP90 served as loading control. One lysate was analyzed.

(G) *Fra1* mRNA expression in KC and KCF PDAC cell lines. Relative *Fra1* mRNA expression was determined by qPCR in three KC and three KCF PDAC cell lines using the delta-delta Ct method with cyclophilin A mRNA expression as reference. *Fra1* mRNA expression in one KC PDAC cell line was arbitrarily set to 1. Upper graph: Exon 3 and 4 specific qPCR. Lower graph: Exon 1 and 2 specific qPCR. Results are from one mRNA preparation per cell line analyzed in technical triplicates.

4.1.2 The role of FRA1 in PDAC maintenance

To study the role of FRA1 in tumor maintenance *in vitro*, isogenic gain- and loss-of-function models were established. An epithelial (SDF287) and a mesenchymal (SDF716) FRA1-deficient KCF cell line were chosen and transduced with a lentiviral construct to constitutively express FRA1 (pLenti FRA1) or a RFP-fluorescent control (pLenti RFP) (Figure 2 A, B). The FRA1-specific antibodies that were tested all target the N-terminus and recognized both FRA1 as well as the GFP fusion protein, and since both have similar sizes, it was not possible to differentiate between FRA1-proficient and -deficient cells by immunoblotting. However, phosphorylation of FRA1 on Ser265 stabilizes the FRA1 protein, and a phospho-FRA1 (Ser265) specific antibody was able to differentiate between FRA1-deficient and FRA1-reconstituted cells (Figure 2 B). Reconstitution of FRA1 accelerated cell growth compared to the FRA1-deficient parental or RFP-control vector transduced cell lines (Figure 2 C, D). In long-term clonogenic assays, FRA1-reconstituted cells demonstrated higher clonogenic growth capabilities than the RFP mock-transduced cells (Figure 2 E, F, G). However, while growth upon FRA1-reconstitution was significantly higher in SDF287 cells, only a trend towards higher growth was observed in the SDF716 cell line (Figure 2 C - G), indicating that there might be a heterogeneity between cells in their dependency on FRA1 for growth. In contrast to the constitutive expression of FRA1, acute activation of FRA1 did not affect cell growth in KCF cells transduced with pInducer-FRA1, which allows for temporally controlled expression of FRA1 upon induction with doxycycline (Figure 2 H, I, J, K).
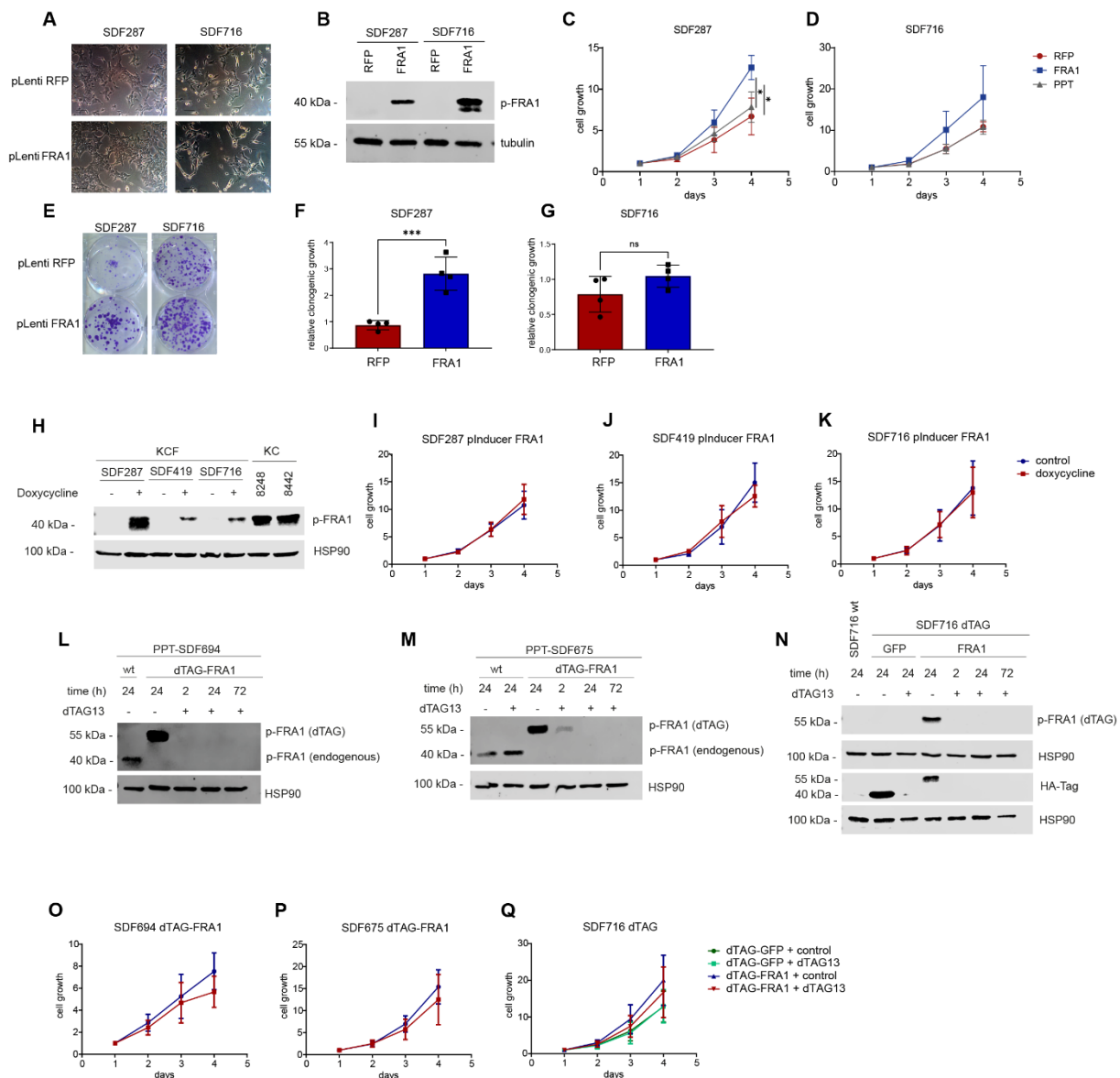
Figure 2: FRA1 promotes growth in PDAC cells.

(A) Phase-contrast microscopy images of KCF cell lines reconstituted with FRA1 vector or RFP control. A more mesenchymal (SDF716) and a more epithelial KCF (SDF287) PDAC cell line was transduced either with a pLenti RFP fluorescent control or pLenti-FRA1 construct. Scale Bar: 100 μM

(B) Reconstitution of FRA1 expression in KCF PDAC cells. Western Blot with anti-phospho-FRA1 (Ser265) antibody of KCF cell lines transduced either with pLenti-RFP or pLenti-FRA1 vector. Tubulin served as loading control. Representative Western Blot from two independent experiments.

(C) and **(D) Growth curves of FRA1-reconstituted PDAC cells.** To determine the cell growth, FRA1-reconstitued, RFP-mock transduced and parental cells from the KCF PDAC cells SDF287 **(C)** and SDF716 **(D)** were seeded out triplicates in 96-well plates (1000 cells/well) and cell viability was assessed by MTT on days 1, 2, 3 and 4 after seeding. Displayed is the relative growth normalized to day 1 after seeding. * P value from 2way ANOVA with multiple comparisons. * P ≤ 0.05.

(E) Clonogenic Growth of FRA1-proficient and -deficient cells. FRA1-proficient (pLenti-FRA1) and -deficient (pLenti-RFP) cells from the SDF287 and SDF716 KCF cell lines were seeded out in triplicates in 12-well plates (1000 cells/well) and stained with crystal violet after 10 days. A representative clonogenic assay from four independent biological replicates is displayed.

(F) and **(G) Quantification of Clonogenic Growth**. The clonogenic assays from **(E)** were solubilized with 1% SDS and absorbance was measured as a readout of the clonogenic growth. Results are displayed as relative clonogenic growth from four independent biological replicates. *** P-value of an unpaired t-test ≤ 0.001. ns: non-significant. Each dot represents the mean from one independent experiment.

(H) Conditional induction of FRA1 expression in KCF PDAC cells. Western Blot with anti-phospho-FRA1 (Ser265) antibody of KCF cell lines transduced with pInducer-FRA1 construct. Cells were treated with 100 ng/mL Doxycycline for 24 hours to induce FRA1 expression or left untreated as control. The FRA1-proficient KC cell lines 8442 and 8248 served as control for FRA1 expression. HSP90 served as loading control. Representative Western Blot from two independent experiments

(I); **(J)** and **(K) Growth curves of PDAC cells upon conditional expression of FRA1**. To determine the cell growth upon conditional induction of FRA1 expression, KCF PDAC cell lines **(I)** SDF287 **(J)** SDF419 and **(K)** SDF716 were transduced with a pInducer-FRA1 construct for conditional expression of FRA1, seeded out in triplicates in 96-well plates (1000 cells/well) and treated on the following day with 100 ng/mL Doxycycline to induce expression of FRA1 or left untreated as control. Cell viability was assessed by MTT on days 1, 2, 3 and 4 after seeding. Displayed is the relative growth normalized to day 1.

(L) and **(M) Selective degradation of dTAG-FRA1 fusion protein**. Western Blot with anti-phospho-FRA1 (Ser265) antibody of the *Pdx1-Flp;FSF-Kras$^{G12D/+}$, p53$^{frt/+}$; Fra1$^{lox/lox}$* cell lines **(L)** SDF675 and **(M)** SDF694 transduced with an inducible Cre recombinase (pInducer-iCre) and a FKBP12^{F36V}-FRA1 (dTAG-FRA1) construct. After treatment for 8 days with 100 ng/mL Doxycycline to induce the Cre-Recombinase and subsequent recombination of the endogenous floxed *Fra1*, cells were seeded out and treated on the following day with 0.5 µM of the small-molecule degrader dTAG13 for the indicated time points to induce selective degradation of the dTAG-FRA1 fusion protein. The parental wild-type (wt) cell line served as a control for expression of endogenous FRA1. HSP90 was used as a loading control. Representative Western Blots from two independent experiments

(N) Selective degradation of dTAG-FRA1 and dTAG-GFP fusion proteins. Western Blot with anti-phospho-FRA1 (Ser265) and anti-HA-Tag antibodies of the KCF PDAC cell line SDF716 either transduced with a FKBP12^{F36V}-FRA1 (dTAG-FRA1) or with a fluorescent control FKBP12^{F36V}-GFP (dTAG-GFP) construct. Cells were seeded out and treated on the following day with 0.5 µM of the small-molecule degrader dTAG13 for the indicated time points to induce selective degradation of the dTAG-GFP or dTAG-FRA1 fusion proteins. The dTAG-fusion proteins contain an HA-Tag (Nabet et al., 2018), which allowed for immunodetection with an anti-HA-Tag antibody. The FRA1-deficient SDF716 parental wild-type (wt) cell line served as a control. HSP90 was used as a loading control. Representative Western Blot from two independent experiments

(O), (P) and **(Q) Cell Growth upon small molecule mediated degradation of FRA1**. To determine the cell growth upon degradation of dTAG-FRA1, the dTAG-FRA1 transduced cell lines (O) SDF694, (P) SDF675 and (Q) SDF716 were seeded out triplicates in 96-well plates (1000 cells/well). In (Q), SDF716 dTAG-GFP was used as a mock-transduced control. Cells were treated with 1 µM dTAG13 or DMSO as control one day after seeding. Cell viability was assessed by MTT on days 1, 2, 3 and 4 after seeding. Displayed is the relative growth normalized to day 1.

To study the effect that a loss-of-function of FRA1 has on tumor maintenance, the dTAG-System – which allows for the selective small-molecule mediated degradation of FKBP12^{F36V} fusion proteins – was utilized (Nabet et al., 2018). Therefore, two *Pdx1-Flp;FSF-Kras$^{G12D/+}$, p53$^{frt/+}$; Fra1$^{lox/lox}$* cell lines (SDF675 and SDF694) were transduced with a construct to ectopically express the FKBP12^{F36V}-FRA1 (dTAG-Fra1) fusion protein and a pInducer-iCre vector for the doxycycline-inducible expression of an iCre recombinase. The SDF675 and SDF694 cells were treated with 100 ng/mL doxycycline for 8 days to induce expression of the Cre recombinase and recombination of endogenous, floxed *Fra1*. The *Fra1*-recombined cells

were then treated with 0.5 µM dTAG13, which induced rapid degradation of the dTAG-FRA1 fusion protein within two hours (Figure 2 L, M). As a control, no degradation of the endogenous FRA1 was observed upon dTAG13 treatment in the parental wild-type (wt) cell line SDF675 (Figure 2 M). In all further experiments with these two dTAG-FRA1 lines, only cells with completely recombined endogenous *Fra1* as seen in Figure 2 L and M were used. In addition, the FRA1-knockout KCF cell line SDF716 was reconstituted with either the dTAG-FRA1 fusion protein or a control dTAG-GFP construct. Also in this cell line, degradation of the fusion protein (dTAG-FRA1 or dTAG-GFP) was observed on the western blot upon treatment with dTAG13 (Figure 2 N). Depletion of FRA1 induced a slight but non-significant decrease in growth in the SDF675 and SDF694 dTAG-FRA1 cell lines (Figure 2 O, P). In the SDF716 cell line, reconstitution with dTAG-FRA1 slightly increased cell growth compared with the dTAG-GFP cell line (Figure 2 Q). Degradation of the dTAG-GFP fusion protein upon treatment with dTAG13 did not have an effect on cell growth, whereas depletion of dTAG-FRA1 slightly, but non-significantly decreased cell growth (Figure 2 Q).

In conclusion, FRA1-deficient PDAC cells are viable, but FRA1-proficient cells tend to display increased cell growth, indicating that – whereas FRA1 is not essential for tumor maintenance – it does seem to play a role in promotion of cellular growth in PDAC cells.

4.1.3 Identification of druggable vulnerabilities of FRA1-deficient cell lines

As loss of FRA1 by itself was not sufficient to induce substantial antitumor activity, an unbiased drug screen with a library containing 102 compounds was performed in the SDF287 and SDF716 pLenti-RFP and pLenti-FRA1 reconstituted cell lines to find druggable targets, whose loss might synergize with knockout of *Fra1*. Cell viability was assessed after 72 hours of treatment by Cell Titer-Glo (Promega). Area-under-the-curve (AUC) and half-maximal growth inhibitory concentration (GI_{50}) values were calculated by the GR-Metrics package (Clark et al., 2017) in RStudio software. The delta AUC (AUC pLenti-FRA1 - pLenti-RFP) and the ratio of GI_{50}-values (pLenti-FRA1/p-Lenti-RFP) were calculated for each drug. Overall, reconstitution of FRA1 rendered the cell more resistant (delta $AUC_{FRA1-RFP} > 0$) to a majority of the drugs in both cell lines (Figure 3 A, B). A Venn diagram analysis identified an overlap of 12 drugs, to which both FRA1-reconstituted cell lines were more resistant to compared with the FRA1-depleted controls (ratio of GI_{50}-Values pLenti-FRA1/pLenti-RFP > 1.5) (Figure 3 C). Among them were an inhibitor of SUMOylation (COH000), a TRK/ROS1/ALK inhibitor (Entrectinib), an EGFR/ErbB2 inhibitor (Lapatinib), an HSP90 inhibitor (Luminespib), two Histone Methyltransferase inhibitors (MI-463 and UNC-1999), a MDM2 inhibitor (NVP-CGM097) and an AKT-Inhibitor (MK-2206) (Figure 3 D). Intriguingly, out of the 12 drugs, four were targeted against the MAPK pathway: i) the dual MEK/Aurora Kinase inhibitor BI-847325, ii) the MEK inhibitor Trametinib, iii) the RAF-MEK inhibitor RO5126766 and iv) the ERK inhibitor Ulixertinib, thus indicating that the entire MAPK pathway might be a druggable vulnerability in FRA1-deficient cells.
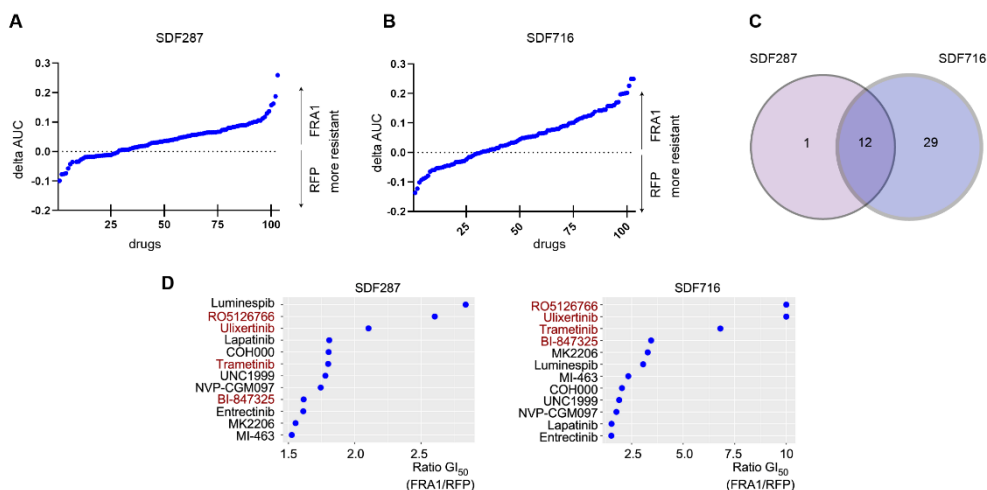
Figure 3: Unbiased Drug Screen identifies the MAPK pathway as a therapeutic vulnerability of FRA1-deficient PDAC cells.

(A) and (B) **Delta AUC of Drug Screen from FRA1-proficient and -deficient cells.** A drug screen with a library containing 102 compounds was performed in FRA1-reconstituted (pLenti-FRA1) and FRA1-deficient (pLenti-RFP) KCF PDAC cell lines (A) SDF287 and (B) SDF716. Viability was assessed by CellTiter-Glo after 72 hours of drug treatment and AUC and GI_{50} scores were calculated according to the GRMetrics method (Clark et al., 2017). To determine differential sensitivity, delta-AUC scores (AUC_{FRA1}-AUC_{RFP}) were calculated. Positive delta-AUC (delta AUC > 0) scores indicates that FRA1-proficient (pLenti-FRA1) cells are more resistant to the drug, while delta scores < 0 indicate that the FRA1-deficient pLenti-RFP cells are more resistant.

(C) **Identification of common hits.** Venn diagram analysis to identify drugs to which FRA1-deficient cells are more sensitive in both cell lines SDF287 and SDF716. A GI_{50}-ratio (GI_{50} FRA1 / GI_{50} RFP) > 1.5 was chosen as threshold.

(D) **Ratio of GI_{50} values.** The Ratio of GI_{50} Values (FRA1/RFP) for the twelve drugs identified in (C) to which the FRA1-deficient cells are more sensitive to both in SDF287 and SDF716 cell lines. Inhibitors of the MAPK pathway are marked in red. Ratios >10 were arbitrarily set to 10.

4.1.4 The MAPK pathway as a therapeutic vulnerability in FRA1-deficient PDAC

The RAF-MEK-ERK inhibitors were therefore chosen for further analysis. First, the results for the MAPK inhibitors Trametinib, RO5126766 and Ulixertinib were validated by MTT viability assay for the SDF287 (Figure 4 A, B, C) and SDF716 (Figure 4 D, E, F) cell line. In each case, a right-shift in the dose response was observed in the FRA1-reconstituted (pLenti-FRA1) cells. This translated to an approximately 3 - 7 fold increase in GI_{50} values in the FRA1-reconstituted cells for Ulixertinib (Figure 4 B, E) and Trametinib (Figure 4 C, F) and a more than 10-fold increase in RO5126766 GI_{50} values (Figure 4 A, D) compared with the FRA1-deficient controls. Additionally, FRA1-reconstituted cells in both cell lines were more resistant to the MEK inhibitor Trametinib in long-term clonogenic growth assays (Figure 4 G, H, I).

In MTT assays, the FRA1-reconstituted cell lines were not only more resistant to the MAPK inhibitors, but also – with an around threefold increase in GI_{50} – to the AKT inhibitor MK2206 as was identified in the screen (Figure 4 J, K), indicating that FRA1-proficiency might mediate resistance to the inhibition of both major KRAS downstream effector pathways.
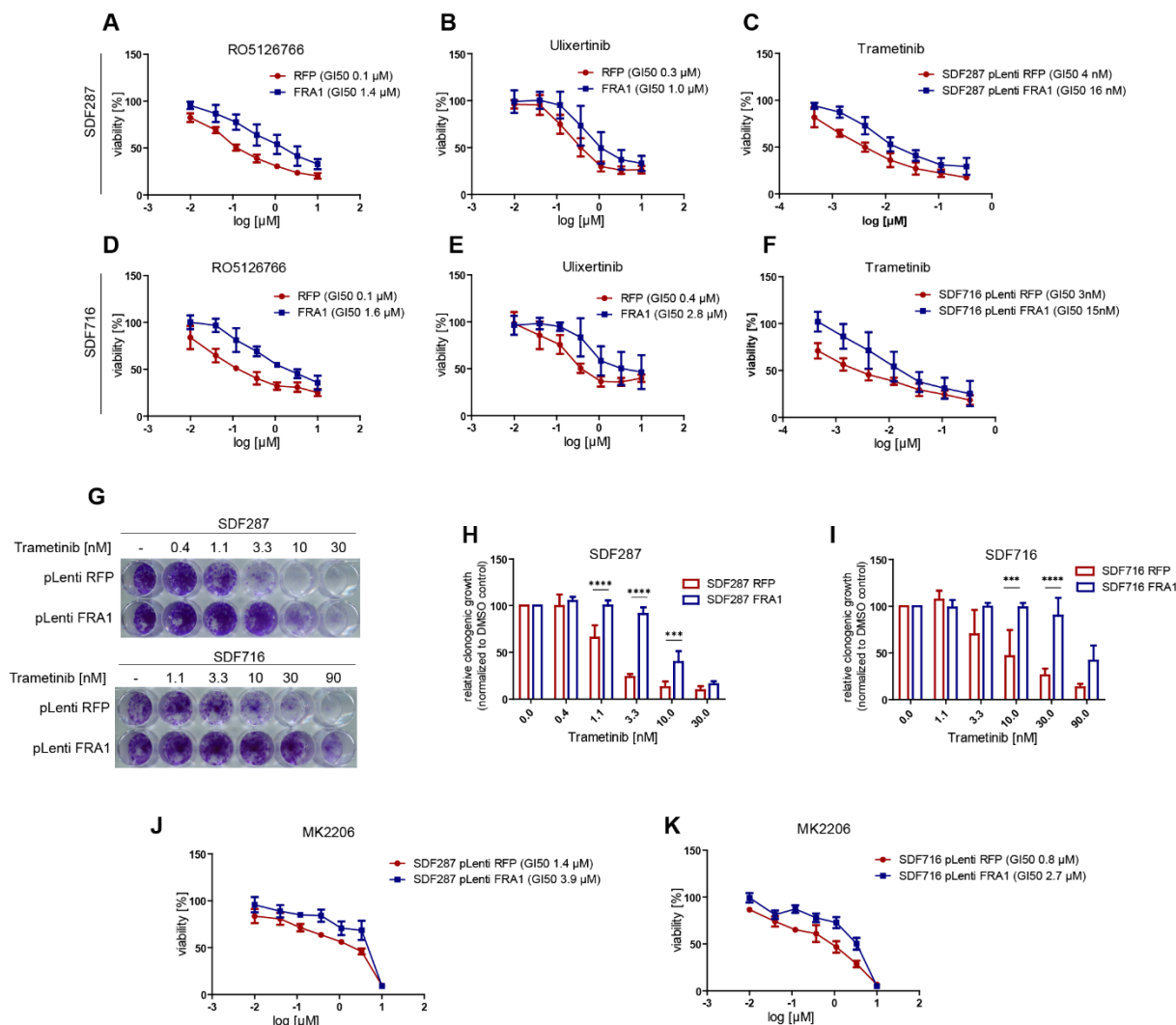

Figure 4: FRA1-deficient PDAC cells are sensitive to MAPK inhibition

(A) - **(F) Drug Response Curves of inhibitors of the RAF-MEK-ERK pathway.** FRA1-proficient (pLenti-FRA1) and -deficient cells (pLenti-RFP) from the cell lines SDF287 (A-C) and SDF716 (D-F) were treated with 7-point, 3-fold dilutions of the dual RAF/MEK inhibitor RO5126766 (A and D), the ERK1/2 inhibitor Ulixertinib (B and E) and the MEK1/2 inhibitor Trametinib (C and F). Viability was assessed by MTT assay after 72 hours of treatment and is displayed as normalized values [%] relative to DMSO treated controls.

(G) Clonogenic Assays of Trametinib-treated FRA1-proficient and -deficient cells. FRA1-proficient (pLenti-FRA1) and -deficient cells (pLenti-RFP) from the cell lines SDF287 (upper panel) and SDF716 (lower) were seeded out (1000 cells/well) in technical duplicates in 24-well plates and treated the following day with the indicated doses of the MEK inhibitor Trametinib. One representative clonogenic assay out of three independent biological replicates is displayed.

(H) and (I) Quantification of the clonogenic assays. The crystal violet staining from the clonogenic assays in **(G)** was solubilized with 1% SDS and the absorbance measured. Absorbance values were normalized to DMSO-treated controls and are displayed as relative clonogenic growth. The mean +/- SD from three

independent biological replicates is displayed. P values from 2way ANOVA with multiple comparisons. ***
P ≤ 0.001. **** P ≤ 0.0001.

(J) and (K) Drug Response Curves of the AKT Inhibitor MK2206. FRA1-proficient (pLenti-FRA1) and -deficient cells (pLenti-RFP) from the cell lines SDF287 **(J)** and SDF716 **(K)** were treated with 7-point, 3-fold dilutions of the AKT inhibitor MK2206. Viability was assessed by MTT assay after 72 hours of treatment and is displayed as normalized values [%] relative to DMSO treated controls.

4.1.5 Small molecule-mediated degradation of FRA1 synergizes with MAPK inhibition

Acute expression of FRA1 by doxycycline treatment in the FRA1-deficient KCF cell line SDF419 pInducer-FRA1 rendered the cells more resistant to the MAPK inhibitors, with an 10-20 fold increase in GI_{50} values upon doxycycline treatment (Figure 5 A,B,C). This indicates that even short-term expression of FRA1 expression can increase resistance to MAPK inhibition.

The transcription factor FRA1 is currently not a "druggable" target. To mimic the effects that acute small-molecule mediated depletion of FRA1 would have in conjunction with MAPK pathway inhibition, the dTAG-FRA1 system was utilized, which allows for selective degradation of the dTAG-FRA1 fusion protein upon treatment with the small molecule degrader dTAG13 (Nabet et al., 2018). In the FRA1-deficient KCF cell line SDF716, reconstitution of FRA1 with dTAG-FRA1 rendered the cells more resistant to the tested MAPK inhibitors RO5126766, Ulixertinib and Trametinib compared to the control-transduced dTAG-GFP cells as indicated by the right-shift in the dose-response curve and the increased GI_{50} values (Figure 5 D, E, F). Treatment of the dTAG-GFP cell line with dTAG13 did not have a substantial effect on the response to MAPK inhibition. In contrast, degradation of the dTAG-FRA1 fusion protein by dTAG13 sensitized the dTAG-FRA1 cells to MAPK inhibition with a 3-4 fold decrease in GI_{50} values (Figure 5 D,E,F), thus underscoring both the selectivity of the system as well as the role of FRA1 in the resistance to MAPK inhibitors.

However, not all cell lines were sensitized to MAPK inhibition by dTAG-FRA1 degradation, which underscores the heterogeneity in drug response in PDAC cell lines. While there was a slight left-shift in the dose-response to MEK inhibition (~1.5 fold decrease in GI_{50}) upon dTAG13-mediated degradation of FRA1 in the MTT assays (Figure 5 G) and a more substantial

sensitization to Trametinib in the long-term clonogenic assays (Figure 5 H, I) in the SDF675 dTAG-FRA1 cell line at least in the higher dose range, no such sensitization was observed in the SDF694 dTAG-FRA1 cell line (Figure 5 J, K, L).
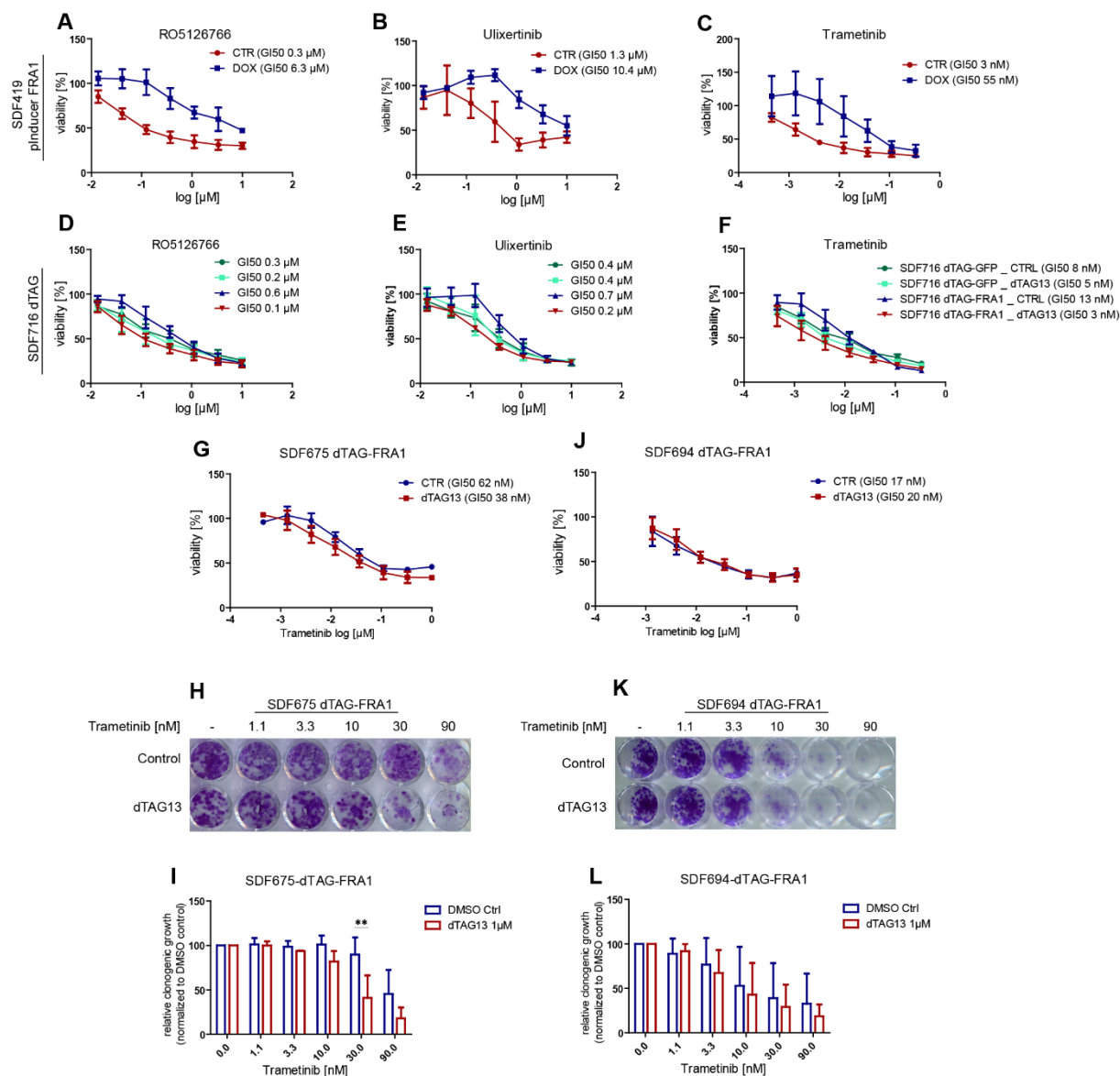

Figure 5: Acute small-molecule mediated degradation of FRA1 degradation sensitizes PDAC cells to MEK inhibition

(A) ,(B) and (C) Drug Response Curves of RAF-MEK-ERK pathway inhibitors upon conditional expression of FRA1. The FRA1-deficient KCF cell line SDF419 was transduced with a pInducer-FRA1 vector for conditional expression of FRA1 upon Doxycycline addition. Cells (1000/well) were seeded out in 96-well plates in medium containing 100 ng/mL Doxycycline to induce FRA1 expression or left untreated. On the following days, cells were treated in triplicates with 7-point, 3-fold dilutions of the dual RAF/MEK inhibitor RO5126766 (A), the ERK1/2 inhibitor Ulixertinib (B) and the MEK1/2 inhibitor Trametinib (C). Viability was assessed by MTT assay after 72 hours of treatment and is displayed as normalized values [%] relative to DMSO treated controls.

(D) ,(E) and (F) Drug Response Curves of RAF-MEK-ERK pathway inhibitors upon acute degradation of FRA1. The FRA1-deficient KCF cell line SDF716 was transduced either with a dTAG-FRA1 or a control

dTAG-GFP construct. SDF716 dTAG-FRA1 and dTAG-GFP Cells (1000/well) were seeded out in 96-well plates in medium containing 1 µM dTAG13 to induce degradation of the dTAG-fusion protein or DMSO as control. On the following days, cells were treated in triplicates with 7-point, 3-fold dilutions of the dual RAF/MEK inhibitor RO5126766 **(D)**, the ERK1/2 inhibitor Ulixertinib **(E)** and the MEK1/2 inhibitor Trametinib **(F)**. Viability was assessed by MTT assay after 72 hours of treatment and is displayed as normalized values [%] relative to DMSO treated controls.

(G) **and (J) Drug Response Curves of MEKi Trametinib upon acute degradation of FRA1.** The *Pdx1-Flp;FSF-Kras$^{G12D/+}$, p53$^{frt/+}$; Fra1$^{lox/lox}$* PDAC cell lines SDF675 and SDF694 were transduced with an inducible Cre recombinase (pInducer-iCre) and a dTAG-FRA1 construct and then treated for 8 days with Doxycycline (100 ng/mL) until complete recombination of the endogenous floxed *Fra1*. SDF675 dTAG-FRA1 **(G)** and SDF694 dTAG-FRA1 **(J)** cells with completely recombined endogenous *Fra1* were seeded (1000/well) in 96-well plates in medium containing 1 µM dTAG13 to induce degradation of the dTAG-fusion protein or DMSO as control. On the following days, cells were treated in triplicates with 7-point, 3-fold dilutions of the MEK1/2 inhibitor Trametinib. Viability was assessed by MTT assay after 72 hours of treatment and is displayed as normalized values [%] relative to DMSO treated controls.

(H) **and (K) Clonogenic Assays of Trametinib-treated PDAC cells upon acute degradation of FRA1.** The *Pdx1-Flp;FSF-Kras$^{G12D/+}$, p53$^{frt/+}$; Fra1$^{lox/lox}$* PDAC cell lines SDF675 and SDF694 were transduced with an inducible Cre recombinase (pInducer-iCre) and a dTAG-FRA1 construct and then treated for 8 days with Doxycycline (100 ng/mL) until complete recombination of the endogenous floxed *Fra1*. SDF675 dTAG-FRA1 **(H)** and SDF694 dTAG-FRA1 **(K)** cells with completely recombined endogenous *FRA1* were seeded (1000/well) in 24-well plates in technical duplicates in medium containing 1 µM dTAG13 to induce degradation of the dTAG-fusion protein or DMSO as control. On the following day, cells were treated with the indicated doses of the MEK inhibitor Trametinib. One representative clonogenic assay out of three independent biological replicates is displayed.

(I) **and (L) Quantification of clonogenic assays.** The crystal violet staining from the clonogenic assays in **(H)** and **(K)** were solubilized with 1% SDS and the absorbance measured. Absorbance values were normalized to DMSO-treated control (-) and are displayed as relative clonogenic growth. The mean +/- SD from three independent biological replicates is displayed. P values from 2way ANOVA with multiple comparisons. ** P ≤ 0.01

4.1.6 Increased MAPK pathway activation in FRA1-deficient cell lines

To identify the molecular mechanisms that might explain the increased sensitivity of FRA1-deficient cells to MAPK inhibitors, phospho-ERK and phospho-AKT were analyzed by immunoblot (Figure 6 A,B). ERK phosphorylation in the SDF287 and SDF716 cell lines was decreased upon treatment with the MEKi after 24 (Figure 6 A, C, D) and 72 hours (Figure 6 B, E,F) in both the FRA1-proficient as well as -deficient cells, indicating effective MAPK pathway inhibition in both settings. AKT phosphorylation was slightly increased in response to Trametinib treatment, but again no difference was observed between FRA1-proficient and -deficient cells (Figure 6 A, B and G-J). At the basal level without Trametinib treatment, however, FRA1-reconstituted cells tended to show decreased – yet not significantly – phosphorylation of ERK (Figure 6 A,B and C-F) and AKT (Figure 6 A,B and G-J) compared to FRA1-deficient cells.

This was also observed at the transcriptomic level, as Gene Set Enrichment Analysis (GSEA) of RNA-seq profiles from isogenic FRA1-proficient and -deficient cell lines demonstrated enrichment of ERK1/2 gene signatures in the FRA1-deficient pLenti-RFP cells compared to the FRA1-reconstituted cells (Figure 6 K). Enrichment of the ERK1/2 gene signature was also observed upon acute degradation (24 hours) of FRA1 in the dTAG-FRA1 transduced cell lines (Figure 6 L). In addition, ERK phosphorylation was increased upon acute degradation of FRA1 after 24 and 72 hours in the SDF675 dTAG-FRA1 cell line (Figure 6 M, N). In contrast to the constitutively FRA1-deficient cell lines, which showed a trend towards increased AKT phosphorylation, no such change was observed upon acute degradation of FRA1 (Figure 6 M, O).

In conclusion, upon Trametinib treatment, phospho-ERK tended to be decreased and phospho-AKT increased in both FRA1-proficient and -deficient cell lines. At the basal level, however, FRA1-deficent cells displayed enrichment of ERK1/2 gene signatures and increased levels of phosphorylated ERK, which was further supported by the observation that phospho-ERK is increased upon acute loss of FRA1 in the dTAG-FRA1 system.
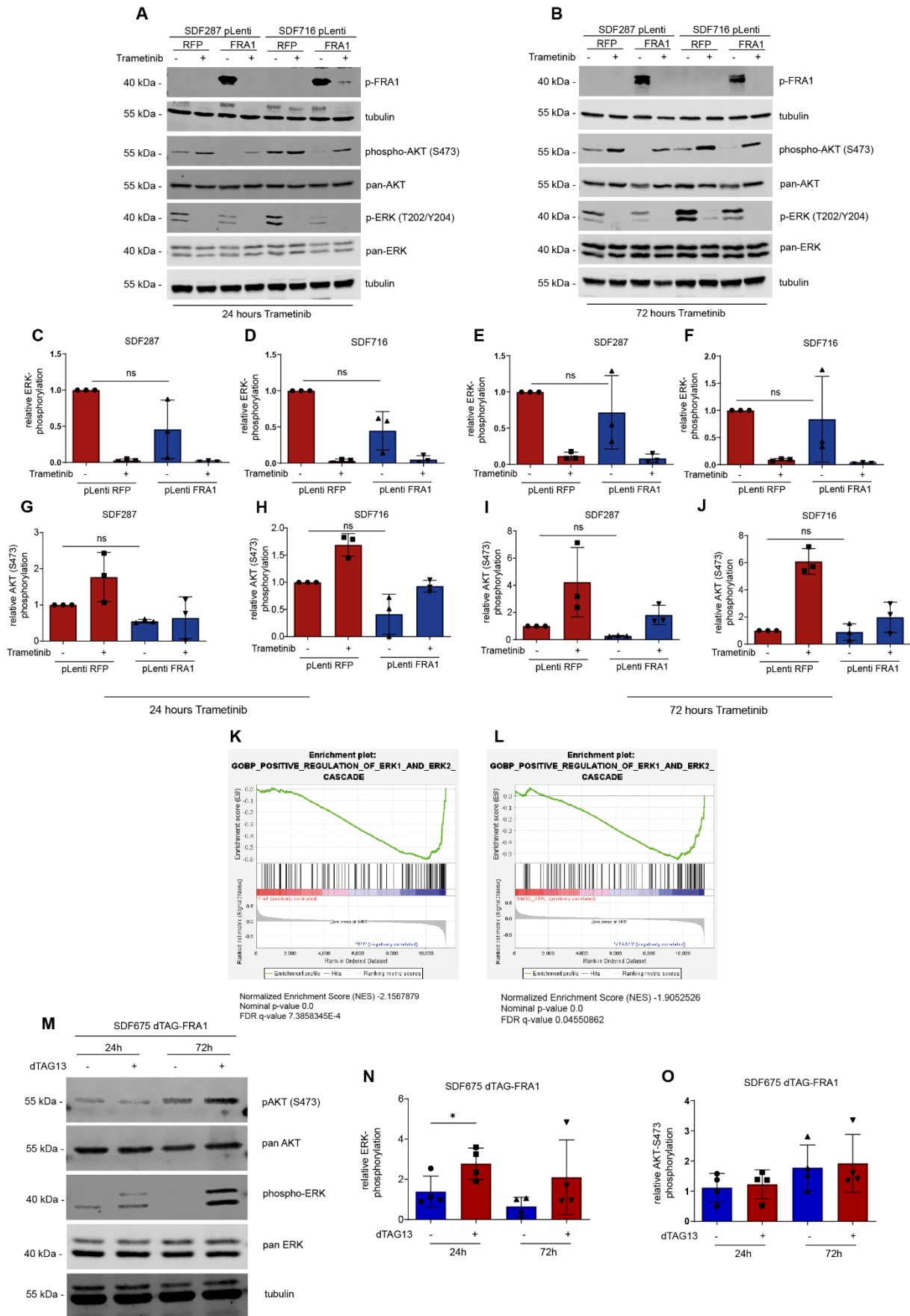
Figure 6: Increased MAPK pathway activity upon loss of FRA1

(A) **and (B) Western Blot of FRA1-proficient and -deficient cells upon MEK inhibition.** The KCF PDAC cell lines SDF287 and SDF716 mock-transduced with pLenti RFP or reconstituted with pLenti-FRA1 were treated with 25 nM Trametinib for **(A)** 24 and **(B)** 72 hours. Western blot of phospho-AKT (Ser473), pan-AKT, phospho-FRA1 (Ser265), phospho-ERK (Thr202/Tyr204) and pan-ERK. Same protein extracts were blotted to different membranes and loading was controlled by tubulin. Representative image of one out of three independent biological replicates.

(C) **– (F) Quantification of ERK phosphorylation.** Relative phosphorylation of ERK (Thr202/Tyr 204) from three independent biological replicates of the blots depicted in **(A)** and **(B)** was quantified by densitometric analysis with Licor Image Studio Quantification Software. Depicted is the ratio of the phospho-protein to the pan-protein. Values are normalized to untreated pLenti-RFP samples (arbitrarily set to 1). **(C)** and **(D)**: Relative ERK phosphorylation after 24 hours of trametinib treatment in **(C)** SDF287 and **(D)** SDF716 cell lines. **(E)** and **(F)**: Relative ERK phosphorylation after 72 hours of Trametinib treatment in **(E)** SDF287 and **(F)** SDF716 cell lines. ns: non-significant from ANOVA with multiple comparisons performed on non-normalized results.

(G) **– (J) Quantification of AKT phosphorylation**. Relative phosphorylation of AKT (Ser473) from three independent biological replicates of the blots depicted in **(A)** and **(B)** was quantified by densitometric analysis with Licor Image Studio Quantification Software. Depicted is the ratio of the phospho-protein to the pan-protein. Values are normalized to untreated pLenti-RFP samples (arbitrarily set to 1). **(G)** and **(H)**: Relative AKT phosphorylation after 24 hours of trametinib treatment in **(G)** SDF287 and **(H)** SDF716 cell lines. **(I)** and **(J)**: Relative AKT phosphorylation after 72 hours of Trametinib treatment in **(I)** SDF287 and **(J)** SDF716 cell lines. ns: non-significant from ANOVA with multiple comparisons performed on non-normalized results.

(K) **Gene Set Enrichment of ERK1/2 signatures in FRA1-deficient cell lines.** RNA-seq mRNA expression profiles from four independent biological replicates of pLenti-RFP and pLenti-FRA1 transduced KCF cell lines SDF287 and SDF716 were analyzed by Gene Set Enrichment Analysis (GSEA) of the Gene Ontology Biological Processes (GO-BP) gene set. The normalized enrichment score (NES), nominal P-value and FDR q-value are indicated.

(L) **Gene Set Enrichment of ERK1/2 signatures upon acute loss of FRA1.** RNA-seq mRNA expression profiles from four independent biological replicates of dTAG-FRA1 transduced cell lines SDF287, SDF675 and SDF694 upon treatment for 24 hours with 1 µM dTAG13 (or DMSO control) were analyzed by Gene Set Enrichment Analysis (GSEA) of the Gene Ontology Biological Processes (GO-BP) gene set. The normalized enrichment score (NES), nominal P-value and FDR q-value are indicated.

(M) **Immunoblot of phosphorylated ERK and AKT upon acute depletion of FRA1.** The SDF675 dTAG-FRA1 cell line was treated with 1 µM dTAG13 for 24 and 72 hours to induce degradation of the FRA1-fusion protein. Same protein extracts were blotted to different membranes and phospho-AKT (Ser473), pan-AKT, phospho-ERK (Thr202/Tyr204) and pan-ERK expression determined. Loading was controlled by tubulin. Representative image of one out of four independent biological replicates.

(N) **And (O) Quantification of ERK and AKT phosphorylation.** Relative phosphorylation of **(N)** ERK (Thr202/Tyr 204) and **(O)** AKT (Ser473) from four independent biological replicates of the blots depicted in **(M)** was quantified by densitometric analysis with Licor Image Studio Quantification Software. Depicted is the ratio of the phospho-protein to the pan-protein. Values are normalized to one DMSO-treated control (arbitrarily set to 1).   *P-value of an unpaired t test <0.05.

4.2 The role of MYC and SUMOylation in PDAC

4.2.1 SUMOylation is connected to MYC expression in PDAC

MYC is the sole oncogene in PDAC whose amplification is linked to a worse survival (Witkiewicz et al., 2015). MYC is a central regulator of cell growth and metabolism, and therefore represents an interesting therapeutic target (Dang, 2012). However, so far MYC is still considered to be undruggable (Dang et al., 2017). Various approaches to target MYC have been tested and employed (Wirth et al., 2016; Wolf and Eilers, 2020). One of them is the concept of synthetic lethality (Cermelli et al., 2014; Thng et al., 2021). SUMOylation has been shown to by synthetic lethal with MYC overexpression in various tumor entities (Hoellein et al., 2014; Kessler et al., 2012; Liu et al., 2015). However, little is known so far about the role of SUMOylation in PDAC and its connection to MYC. Analysis of the TCGA-PAAD dataset showed that PDAC patients with MYC amplifications had a worse survival than patients without MYC amplification (Figure 7A). Concomitantly, HALLMARK gene signatures for MYC target gene expression were upregulated together with REACTOME signatures for SUMOylation as well as core SUMO pathway signatures in MYC-amplified tumors (Figure 7 B,C,D).
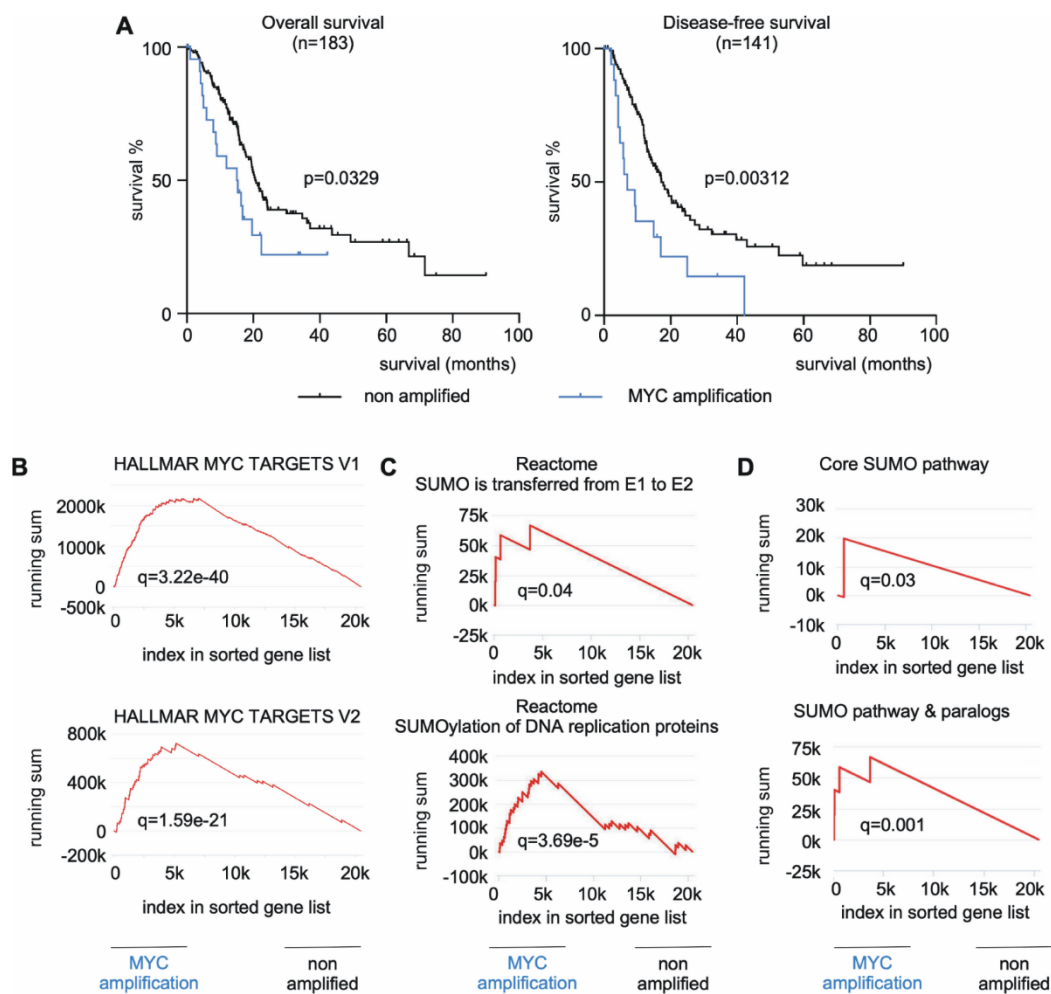
Figure 7: Connection of MYC and SUMOylation in PDAC

(A) PDAC patients with MYC amplification (23/183 cases, 12%) show reduced overall survival (OS) (median OS 15.11 vs 20.83 months; n=183; p=0.033) and disease-free survival (median DFS 7 vs 17.28 months; n=141; p=0.003) (data retrieved from the TCGA-PAAD dataset).

(B) Enrichment of HALLMARK MYC target gene signatures in MYC-amplified PDACs. Data from unweighted GSEA with GeneTrail2 1.6. q values are indicated.

(C) and **(D)** Gene Signatures connected to the SUMOylation machinery are significantly enriched in MYC-amplified PDAC. **(C)** GSEA of Reactome gene set. **(D)** GSEA using manually curated SUMOylation pathway gene sets. Core SUMO pathway: SAE1, UBA2, UBE2I. SUMO pathway and paralogs: SAE1, UBA2, UBE2I, SUMO1, SUMO2, SUMO3. Data from unweighted GSEA with GeneTrail2 1.6. q values are indicated.

4.2.2 The SUMOylation machinery is induced upon MYC expression

To gain a better understanding about the role of MYC and SUMOylation in PDAC, ten human PDAC cell lines were analyzed in more detail. Immunoblotting showed that a subset of human PDAC cell lines had an increased MYC protein expression (Figure 8 A,B). These cells also showed a trend towards higher SUMOylation as demonstrated by immunoblots for SUMO1 as well as SUMO2/3 (Figure 8 C).

To gain a more mechanistic insight, the IMIM-PC1 cell line, which has a rather low MYC expression (Figure 8 A,B), was transduced with a retroviral MYC estrogen receptor fusion (MYC^{ER}) construct that allows for ectopic expression of MYC by addition of 4-Hydroxytamoxifen (Figure 8 D). MYC target genes such as *ODC1* and *CAD* were upregulated upon addition of 4-OHT (Figure 8 E). This genetic model was then used to perform RNA-seq to gain insight into the pathways that are controlled by MYC in an unbiased manner. GSEA analysis revealed upregulation of MYC target genes (Figure 8 F) together with an increase in SUMOylation signatures (Figure 8 G), thus underscoring the direct connection of MYC expression to SUMOylation. In addition, murine PDAC cell lines were transduced with a retroviral MYC-IRES-GFP construct for constitutive expression of MYC protein. Immunoblots showed a twofold increase in MYC expression in these cell lines compared to parental or GFP-controls (Figure 8 H, I). Concomitantly, MYC as well as SUMOylation signatures were upregulated in the GSEA of the RNA-seq (Figure 8 J, K). Furthermore, at the protein level, MYC-IRES-GFP-transduced cells tended to show higher SUMOylation of SUMO1 as well as SUMO2/3 in the immunoblots (Figure 8 L).
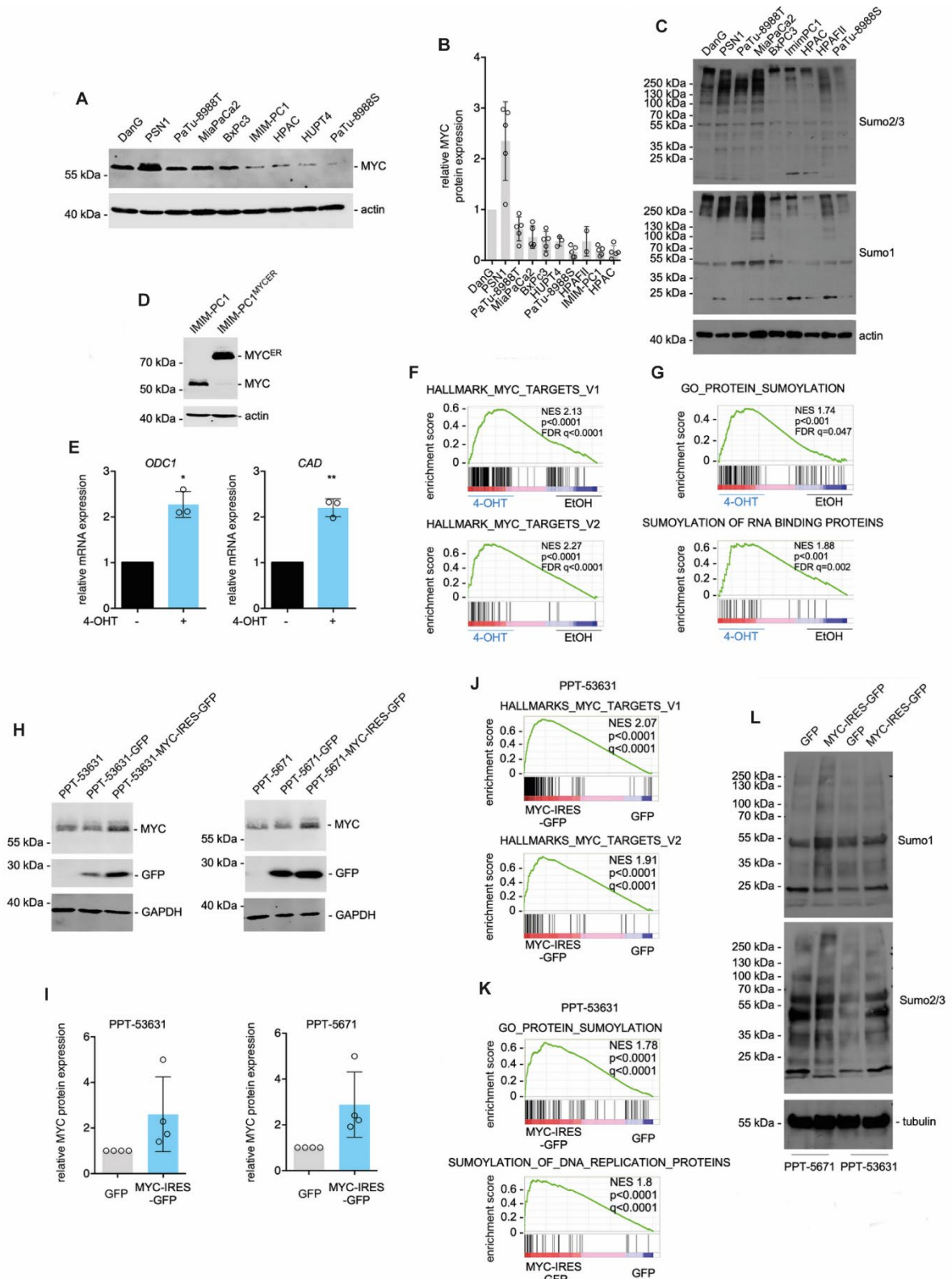
Figure 8: Activation of the SUMOylation machinery upon MYC induction in PDAC.

(A) and **(B)** MYC protein expression in human PDAC cell lines. Loading was controlled by actin. **(A)** Representative image of a MYC immunoblot **(B)** MYC protein quantification of the MYC Western blots in **(A)**. Relative MYC expression is depicted (normalized to DanG cells, arbitrarily set to 1). Depicted is the mean ± SD from at least three independent biological replicates (indicated by dots). HPAF-II cells are not included in the representative Western blot of **(A)**.

(C) Immunoblot of SUMO1 and SUMO2/3 in human PDAC cell lines. Actin was used as loading control

(D) MYC Western blot of IMIM-PC1^{MYC-ER} and IMIM-PC1 cells. Actin: loading control.

(E) Induction of MYC target genes upon MYC^{ER} activation. qPCR of MYC downstream targets ODC1 and CAD in IMIM-PC1^{MYC-ER} cells upon treatment with 4-OHT (500 nM) for 24 hours. Quantification from three independent biological replicates performed in technical duplicates. P value of a paired t-test.

(F) and **(G)** Enrichment of MYC and SUMOylation gene signature upon activation of MYC^{ER}. RNA-Seq data of IMIM-PC1^{MYC-ER} upon treatment with 4-OHT for 24 hours were analyzed by GSEA demonstrating that **(F)** MYC target gene signatures as well as **(G)** SUMOylation pathway gene signatures are enriched upon activation of MYC^{ER} compared with vehicle treated controls. Normalized Enrichment Scores (NES), nominal p and FDR q values are indicated.

(H) and **(I)** MYC protein expression in murine PDAC cell lines transduced with a GFP or an MYC-IRES-GFP vector. **(H)** Representative MYC and GFP Western blots of murine PDAC cell lines PPT-5671 and PPT-53631 in wild-type parental, GFP-transduced and MYC-IRES-GFP-transduced cells. GAPDH served as loading control. **(I)** Quantification of MYC protein expression in MYC-IRES-GFP and GFP-mock transduced cells from Western blots depicted in **(H)**. Four independent biological replicates were quantified (depicted as dots).

(J) and **(K)** Enrichment of MYC and SUMOylation gene signature in MYC-overexpressing murine PDAC cells. RNA-Seq data of GFP-transduced and MYC-IRES-GFP-transduced PPT-53631 cells was analyzed by GSEA demonstrating enrichment of **(J)** HALLMARK MYC target gene signatures and **(K)** SUMOylation pathway gene signatures in MYC-IRES-GFP cells. Normalized Enrichment scores (NES), nominal p and FDR q-values are indicated.

(L) Representative SUMO1 and SUMO2/3 Western blots of the GFP-transduced and MYC-IRES-GFP-transduced murine PDAC PPT-5671 and PPT-53631 cell lines. Tubulin served as loading control.

4.2.3 SUMOylation inhibitors target a MYC-high PDAC subtype

While the importance of SUMOylation in cancer has already been demonstrated for other tumor entities such as hematological cancers (Hoellein et al., 2014), little is known so far about the role of SUMOylation in PDAC. It was therefore the aim of this project to investigate the role of SUMO in PDAC. To gain a better understanding about the relevance of SUMO for cancer maintenance and as a therapeutic target in PDAC, a well-characterized panel of 48 *Kras^{G12D}*- and *PI3K/p110^{H1047R}-driven* murine PDAC cells (Eser et al., 2013; Mueller et al., 2018) was screened with the two SUMO inhibitors ML-792 and ML-93 (Figure 9 A).

While the GI$_{50}$ values of the two SUMO inhibitors ML792 and ML-93 showed a high correlation (Pearson r=0.88), ML-93 showed a higher potency with GI$_{50}$ values largely in the nanomolar range, whereas ML792 GI$_{50}$ values tended more toward the micromolar range (Figure 9 A). To investigate the connection between MYC expression and SUMOi sensitivity, MYC protein expression of the most ML-93 resistant cell lines (marked as red dots in Figure 9 A) was compared to the most ML-93 sensitive cells (marked as blue dots) by immunoblot (Figure 9 B,C). Cell lines that were sensitive to ML-93 showed a significantly higher MYC expression

than ML-93 resistant cells (Figure 9 C). In addition, gene set enrichment analysis of the cell lines that were most sensitive to both SUMO inhibitors showed an enrichment of MYC signatures (Figure 9 D) thus underscoring the critical relevance of the SUMO machinery for MYC^{high} PDAC cells.

To investigate the relevance of these findings also for the human context, GI$_{50}$ values for ML-93 were determined in a panel of 17 human PDAC cell lines, revealing a marked heterogeneity in sensitivity (Figure 9 E). Human PDAC cell lines with high MYC protein expression had significantly lower GI$_{50}$ values than MYC^{low} cell lines (Figure 9 F), indicating that the connection of higher MYC expression to an increased SUMO inhibitor sensitivity is applicable across species.

A comparison of loss-of-fitness scores from the Project Score database (https://score.depmap.sanger.ac.uk/), which are based on large-scale, genome-wide CRISPR-Cas9 dropout screens (Behan et al., 2019), shows a correlation between the sensitivity to MYC knockout and loss of UBE2I across 23 human PDAC cells and thus further reinforces the notion of a co-addiction of both pathways (Figure 9 G).

To determine whether these findings are also applicable to more clinically relevant disease models, primary-dispersed human PDAC cells (HuPDAC3, HuPDAC7 and HuPDAC17) were further investigated. Immunoblot analysis showed that HuPDAC7 had the highest MYC protein expression, while HuPDAC3 had the lowest MYC expression (Figure 9 H,I). *MYC* mRNA expression was also strongly reduced in HuPDAC3 compared to HuPDAC7 (Figure 9 J). Concomitantly, expression of MYC target genes such as *CAD*, *ODC1* and *HSPE1* was also reduced together with the SUMO components *SAE1, SAE2 and UBE2I* (Figure 9 J). SUMOylation was also decreased in HuPDAC3 as shown by immunoblotting for SUMO2/3- and SUMO1-conjugated proteins (Figure 9 K), thus underscoring the connection between MYC expression and SUMOylation also in primary patient-derived PDAC cells.

In line with the previous findings, the MYC/SUMO^{high} cell line HuPDAC7 had the highest sensitivity to ML-93 and ML-792, while the MYC/SUMO^{low} HuPDAC3 cell line was the most

resistant, with HuPDAC17 showing an intermediate response (Figure 9 L,M,N). HuPDAC7 also

showed the highest reduction in clonogenic growth (Figure 9 O,P) and an increased induction
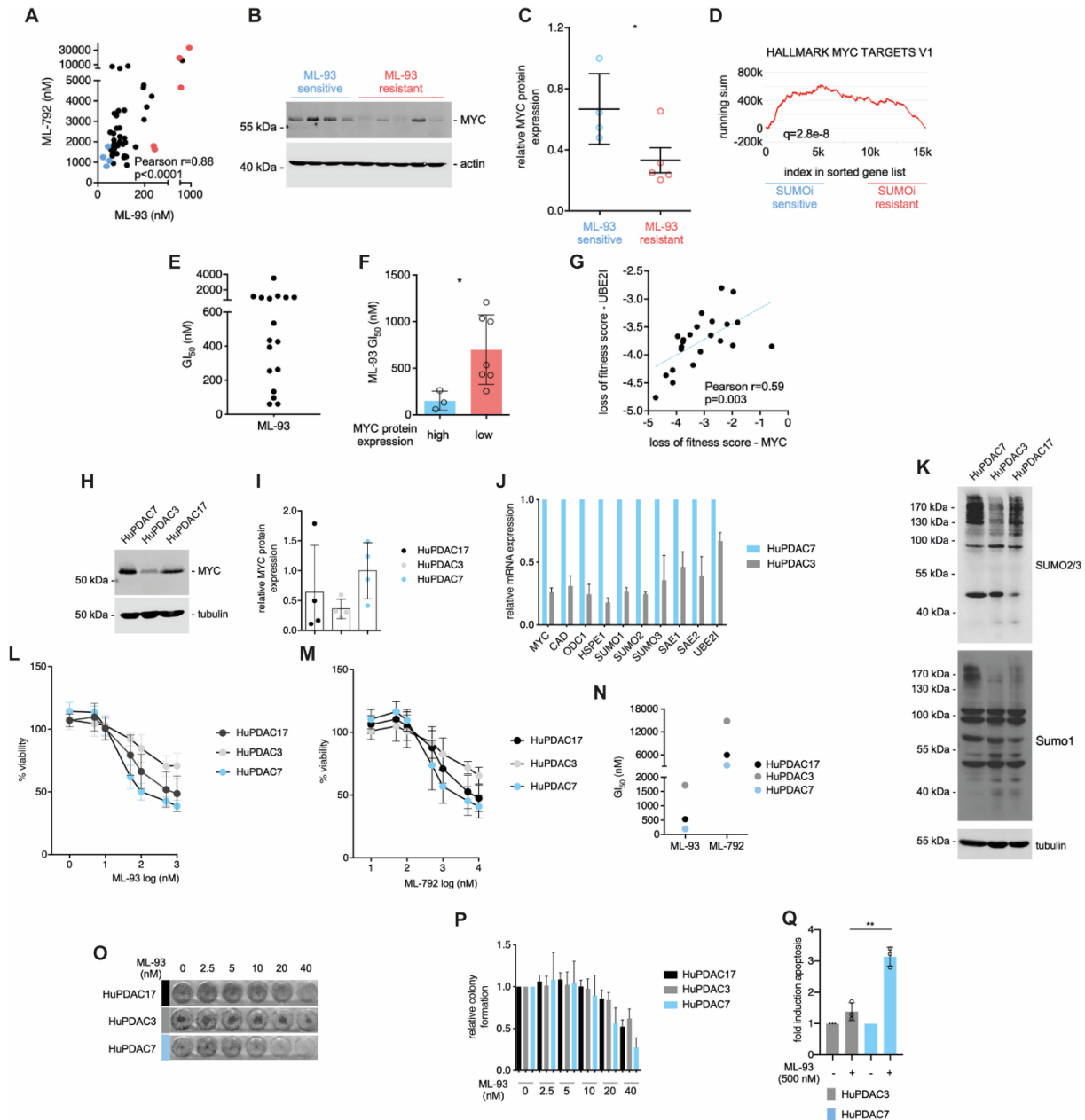
of apoptosis (Figure 9 Q) compared to HuPDAC3.

Figure 9: SUMOylation as a therapeutic target in MYC^{high} PDAC

(A) Growth Inhibitory Concentrations 50% (GI$_{50}$) for ML-93 and ML-792 in 48 murine PDAC cell lines. Dose response curves of 7-point dilutions of SUMO inhibitors ML-93 (0–1000 nM) and ML-792 (0–5000 nM) in technical triplicates were determined by MTT after 72h hours of drug treatment. GI$_{50}$ were determined from at least three independent biological replicates in GraphPad Prism using non-linear regression of log-transformed concentrations. GI$_{50}$ values >1000 nM for ML-93 and >5000 nM for ML-792 represent extrapolated values from the fitted curve. Pearson correlation coefficient between ML-93 and ML-792 as well as the p values are indicated. Blue dots: ML-93 sensitive lines; red dots: ML-93 resistant lines.

(B) and **(C) MYC Western blot of the ML-93 sensitive and the ML-93 resistant murine PDAC cell lines**. Actin: loading control. **(C)** MYC expression in the Western Blots depicted in **(B)** was quantified. Mean MYC protein expression (normalized to Actin expression) from three independent biological replicates of each cell line is depicted (marked by dot). *P value of an unpaired t-test <0.05

(D) Enrichment of MYC target gene signature in SUMO inhibitor sensitive PDAC. RNA-seq data from the most ML-93/ML-792 sensitive quartile (common cell lines with ML-93 and the ML-792 GI50 values <25th percentile) and most ML-93/ML-792 resistant quartile (ML-93 and the ML-792 GI_{50} values were >75th percentile) of PDAC cells was analyzed by unweighted GSEA using the GeneTrail2 platform. Q-value is indicated.

(E) GI_{50} values for SUMO inhibitor ML-93 in human PDAC cell lines. Dose response curves of 7-point dilutions of the SUMO inhibitor ML-93 (0–1000 nM) in technical triplicates were determined by CellTiter-Glo assay after 72h hours of drug treatment in 17 human PDAC cell lines. GI_{50} were determined from at least three independent biological replicates in GraphPad Prism using non-linear regression of log-transformed concentrations. GI_{50} values >1000 nM represent extrapolated values from the fitted curve.

(F) GI_{50} values for SUMO inhibitor ML-93 in MYC^{high} and MYC^{low} human PDAC cell lines. Comparison of GI_{50} from **(E)** between MYC^{high} (> 66th percentile) and MYC^{low} (<66th percentile) human PDAC cell lines as determined in Figure 8 A and B. *P value of an unpaired t-test <0.05.

(G) Correlation of Loss-of-fitness scores for MYC and UBE2I across 23 human PDAC cells. Scores were retrieved from the project score database (https://score.depmap.sanger.ac.uk/). Pearson correlation coefficient and the p value are depicted.

(H) and **(I) MYC expression in primary human PDAC cell lines. (H)** MYC protein expression in primary-dispersed human PDAC cell lines HuPDAC3, HuPDAC7 and HuPDAC17 was analyzed by immunoblotting. Tubulin served as loading control. Representative western blot is shown. **(I)** Quantification of MYC protein expression from Western Blots in **(H)**. Relative MYC protein expression normalized to loading control from four independent biological replicates (each depicted as dot) is shown.

(J) Downregulation of MYC and SUMO pathway genes mRNA expression in MYC^{low} HuPDAC3. Expression of MYC, CAD, ODC1, HSPE1 (MYC pathway) and SUMO1, SUMO2, SUMO3, SAE1, SAE2, UBE2I (SUMO pathway) mRNA was analyzed in technical triplicates by qPCR in primary-dispersed human PDAC cells HuPDAC3 and HuPDAC7. Depicted is the mean mRNA expression (normalized to GAPDH) +/- SD from three independent biological replicates relative to expression in HuPDAC7 (arbitrarily set to 1).

(K) SUMO1 and SUMO2/3 Western blots of the primary dispersed human PDAC cell lines HuPDAC3, HuPDAC7 and HuPDAC17. Tubulin served as loading control.

(L) and **(M)** Drug Response Curves for the SUMO inhibitors ML-93 **(L)** and ML-792 **(M)** were determined by CellTiter-Glo assay by treatment for 72 hours with a 7-point dilution of the inhibitors.

(N) GI_{50} values were determined from the drug response curves in **(L)** and **(M)** by non-linear regressions in GraphPad Prism. GI_{50} values >1000 nM for ML-93 and >5000 nM for ML-792 are extrapolations from the fitted curve.

(O) and **(P) Clonogenic growth of HuPDAC3, HuPDAC7, HuPDAC17 upon treatment with SUMO inhibitor ML-93**. Representative image (O) and quantification (P) of the clonogenic assay are depicted. Shown is the mean±SD of at least three biological replicates performed as duplicates.

(Q) Induction of Apoptosis upon treatment with ML-93. Apoptosis was determined by Annexin V/PI flow cytometric analysis after 72 hours of treatment with ML-93. Relative increase in apoptotic fraction versus DMSO control is indicated. Results from three biological replicates are shown, with each circle representing an independent experiment. ** P value of an unpaired t-test <0.01.

4.2.4 Overexpression of MYC sensitizes PDAC cells to SUMOylation inhibitors

To investigate the connection between MYC and SUMO in more detail, various genetic models to overexpress MYC were generated. Constitutive overexpression of MYC in the two murine PDAC cell lines PPT-53631 and PPT-5671 that were transduced with a retroviral MYC-IRES-GFP (Figure 8 H,I) construct sensitized the cells to SUMO inhibition as demonstrated by increased apoptosis (Figure 10 A) and reduced clonogenic growth (Figure 10 B) after treatment with ML-93 compared to the mock-transduced or parental cell lines.

To study the effects of acute overexpression of MYC on SUMOi sensitivity, several murine PDAC cell lines were transduced with a retroviral MYC^{ER} construct (Figure 10 C), which allows for activation of MYC by addition of 4-Hydroxytamoxifen (4-OHT) as indicated by increased expression of MYC target genes such as *Odc1* in the qPCR (Figure 10 D). Activation of MYC induced an increased sensitivity to the SUMO inhibitors ML-93, as shown by the left shift in the dose response curve in Figure 10 E after addition of 4-OHT, which was also observed in the human IMIM-PC1^{MYCER} PDAC cell line (Figure 10 F). To rule out of off-target effects by Tamoxifen treatment itself, the PDAC cell line PPT-53631 was transduced with an empty backbone construct (Figure 10 C). No shift in the dose response curve was observed in the mock-transduced cells (Figure 10 E), thus showing that the increased sensitivity in the MYC^{ER}-transduced cells is indeed due to the MYC activation itself. The increased sensitivity to SUMO inhibition upon MYC activation was also corroborated by long-term clonogenic assays, which demonstrated reduced clonogenic growth upon MYC induction by 4-OHT (Figure 10 G).
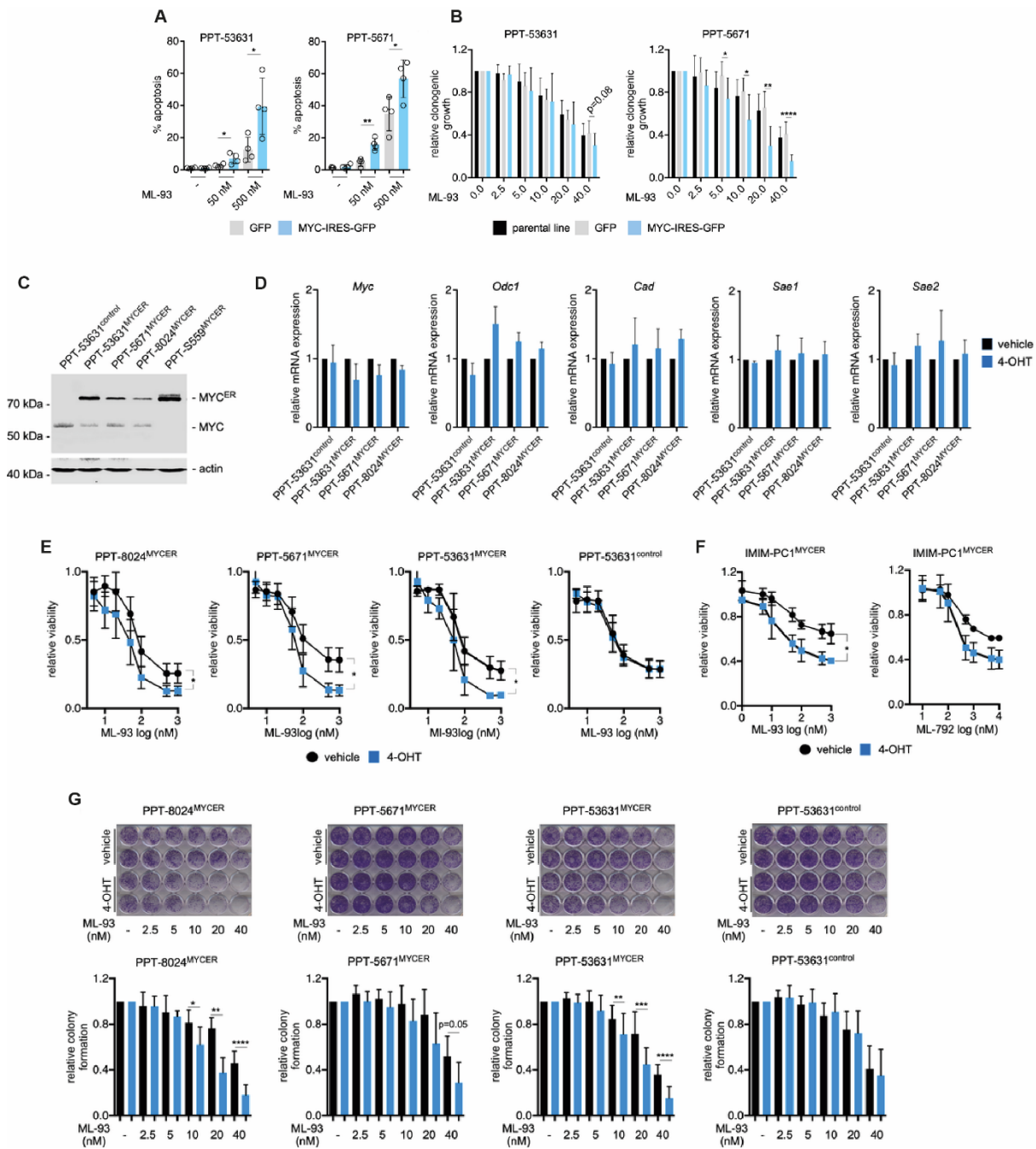
Figure 10: MYC overexpression sensitizes PDAC cells to SUMO inhibition

(A) **Apoptosis induction upon treatment with ML-93.** Apoptosis in murine PPT-53631 or PPT-5671 PDAC cells, transduced with GFP or MYC-IRES-GFP vectors, was determined by Annexin V/DAPI flow cytometric analysis after 72 hours of treatment with 50 and 500 nM ML-93. Relative increase in apoptotic fraction versus DMSO control is indicated. Results from three biological replicates are shown, with each circle representing an independent experiment. ** P value of an unpaired t-test <0.01.

(B) Clonogenic Growth in murine PPT-53631 and PPT-5671 PDAC cell lines, transduced with GFP or MYC-IRES-GFP and parental controls, were treated with ML-93. Depicted is the quantification of clonogenic growth from at least three biological replicates performed in technical duplicates. P value of an unpaired t-test: *<0.05, **<0.01, ****<0.0001.

(C) **MYC Western Blot of murine PDAC cell lines transduced with MYC^ER or empty backbone control**. Endogenous MYC and MYC^ER are indicated. Actin served as loading control.

(D) **qPCR of MYC and SUMO pathway members upon activation of MYC^ER**. The mRNA expression of MYC, Odc1, Cad, Sae1, and Uba2/Sae2 upon activation of MYC^ER with 600 nM 4-OHT for 8 hours was assessed by qPCR. *Gapdh* mRNA expression was used as reference for normalization. *Gapdh* mRNA

was used for normalization. Experiments were performed in technical triplicates and the mean +/- SD from three independent experiments is depicted.

(E) Dose Response to SUMO Inhibitor ML-93 in murine PDAC cells upon activation of MYC[ER]. The indicated murine PDAC cell lines – either transduced with MYC[ER] or with empty backbone control vector (PPT-53631[control]) – were treated with 600 nM 4-OHT or vehicle control and 7-fold dilutions of ML-93. Viability was assessed by MTT assay after 72 hours of drug treatment. The mean +/- SD from at least three independent biological experiments (performed in technical triplicates) is indicated. * p value of a t-test <0.05

(F) Dose Response to SUMO Inhibitors ML-93 and ML-792 in human PDAC cell line IMIM-PC1[MYC-ER] **upon activation of MYC**[ER]. IMIM-PC1 cells, transduced either with MYC[ER], were treated with 500 nM 4-OHT or vehicle control and 7-fold dilutions of ML-93 and ML-792 as indicated. Viability was assessed by MTT assay after 72 hours of drug treatment. The mean +/- SD from n=4 (ML-93) and n=2 (ML-792) experiments (performed in technical triplicates) is indicated. * p value of a t-test <0.05

(G) Clonogenic Growth in murine PDAC cells upon activation of MYC[ER]**.** Clonogenic Assays from murine PDAC cells from **(C)**, **(D)**, **(E)** treated with 600 nM 4-OHT or vehicle control and the indicated doses of ML-93. Upper Panel: Representative Clonogenic Assays. Lower Panel: Corresponding Quantification from at least three independent biological replicates performed in technical duplicates. Shown is the mean +/- SD. t-test *p<0.05, **p<0.01, ***p<0.001, ****p<0.0001.

4.2.5 SUMOylation inhibition leads to mitotic disruption and apoptosis

Mechanistically, SUMO inhibition induced apoptosis in a time- and dose-dependent manner as shown by annexin V/PI flow cytometric analysis, with the MYC-amplified cell line PSN1 showing a stronger response than MiaPaCa2 (Figure 11A). In addition to an apoptotic response upon ML-93 treatment, PI cell cycle flow cytometric analysis further revealed a distinct accumulation of cells in the G2/M phase of the cell cycle as well as a significant increase in polyploidy (Figure 11 B), pointing to the critical role of the SUMO machinery especially during mitosis.

In summary, MYC activation induces increased expression of the SUMO pathway. MYC-high cells critically depend on SUMOylation especially at the G2-M phase of the cell cycle, which fits to the described critical role of MYC and SUMOylation during mitosis (Figure 11 C). SUMOylation therefore presents an exploitable vulnerability to indirectly target MYC in PDAC.
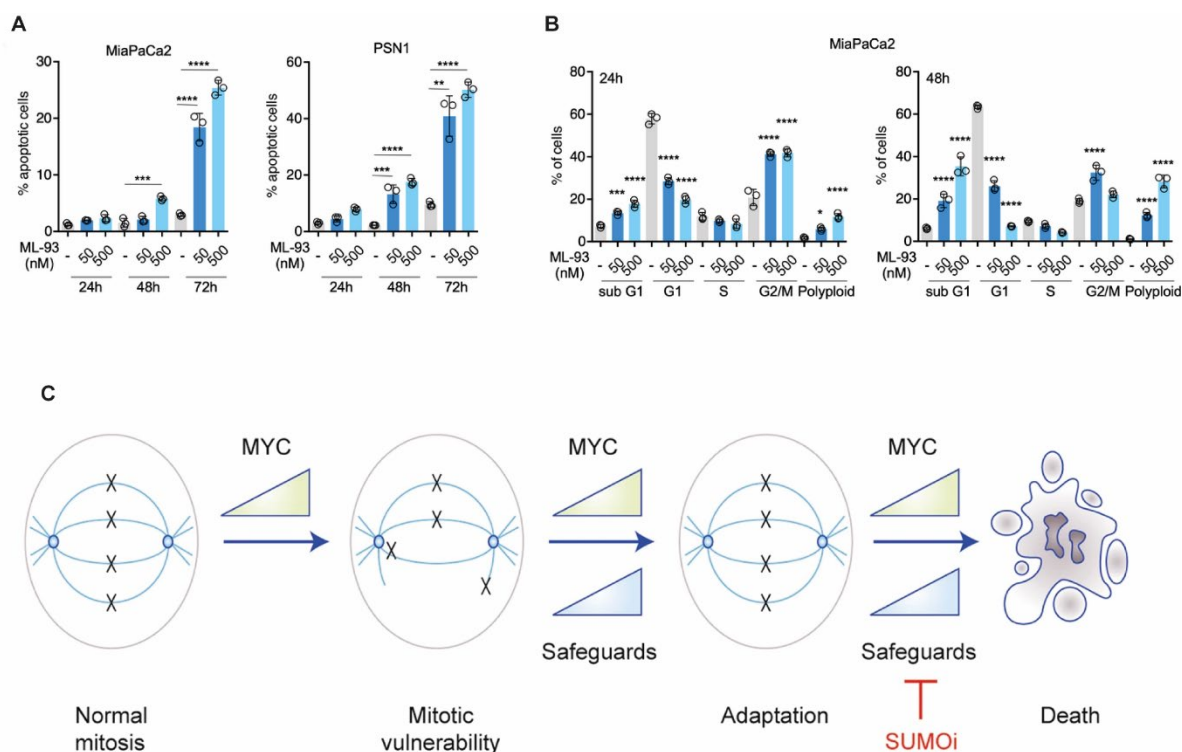
Figure 11: SUMO inhibition induces apoptosis, mitotic arrest and polyploidization

(A) **Apoptosis induction upon SUMO inhibition**. Apoptosis in human PDAC cells MiaPaCa2 and PSN1 upon treatment with 50 and 500 nM ML-93 for 24, 48 and 72 hours was determined by Annexin V/PI flow cytometric analysis. Results from three independent replicates performed as technical triplicates are shown. ANOVA **p<0.01, ***p<0.001, ****p<0.0001.

(B) **PI cell cycle flow cytometric analysis of human MiaPaCa2 PDAC cell line upon treatment with ML-93 for 24 (left panel) and 48 hours (right panel).** Proportions of cells in the sub-G1, G1, S and G2/M phases from three independent experiments (performed in technical triplicates) are shown. ANOVA: **p<0.01, ***p<0.001, ****p<0.0001.

(C) **Schematic concept of SUMO inhibitor sensitivity in MYC^high PDAC cells**. Overexpression of MYC causes mitotic vulnerabilities and generates dependencies of MYC^high cells on safeguard mechanisms to adapt and cope with the increased mitotic stress. Among others, the SUMOylation machinery, is critical for mitotic spindle function, and therefore presents a therapeutically targetable mitotic vulnerability in MYC^high cancers, as SUMO pathway inhibition induces G2/M phase cell cycle arrest, polyploidy, and apoptotic cell death.

5 Discussion

5.1 The role of FRA1 in pancreatic cancer

FRA1 has recently been identified as a central downstream integration node of oncogenic mutant KRAS signaling (Vallejo et al., 2017a; Vallejo et al., 2017b). This thesis further supports these findings by showing that already at the level of non-transformed pancreatic ductal cells, activation of oncogenic KRAS induces an AP1-directed gene network. Among the AP1 family, *Fra1* was one of the main upregulated genes upon activation of KRAS. While it was possible to establish FRA1-knockout PDAC cells from KCF mice, FRA1-deficient cells showed a reduced cell growth *in vitro*. Constitutive reconstitution of FRA1 increased growth in KCF cells and therefore demonstrates that FRA1 plays an important but not essential role in cell growth in PDAC. This is supported by work from Vallejo et al. demonstrating that loss of FRA1 reduces growth in KRAS-mutant lung and PDAC cells (Vallejo et al., 2017a). In addition, large-scale CRISPR-Cas9 drop out screens have shown that FRA1 plays a vital role for cell growth in at least a subset of PDAC cells (Behan et al., 2019). Furthermore, a recent analysis of genome-scale CRISPR-Cas9 loss-of-function screens from over 500 cancer cell lines from the Cancer Dependency Map (https://www.depmap.org/), identified FRA1 as one of the most significant preferential dependencies of KRAS mutant compared to WT cancer cell lines (Waters et al., 2021).

However, in another study, overexpression of FRA1 did not have a significant effect on cell proliferation (Dai et al., 2021). The work in this thesis also shows that the cell-intrinsic role of FRA1 might be more complex and nuanced. Despite the reported dependencies of KRAS mutant cell lines on FRA1, cellular growth in the dTAG-FRA1 cell lines was only slightly diminished by the acute degradation of FRA1. One possible explanation might be the observed compensatory upregulation of PI3K and MAPK signaling pathways in *Fra1* depleted cell lines that might help them to cope with loss of FRA1. Upregulation of MAPK signaling – as indicated by increased phosphorylation of ERK – was already observed within 24 hours upon degradation of FRA1 in the dTAG-FRA1 model. This indicates that the increased activation of

MAPK is rather not due to clonal selection, but a rapid adaptive rewiring of signaling. Compensatory adaptive kinome reprogramming with subsequent activation of MAPK and PI3K upon downregulation of FRA1 has been described in ovarian cancer (Kurimchak et al., 2019) and melanoma cells (Obenauf et al., 2015).

These findings underscore the complex multilayered network of oncogenic signaling, where loss of one node is quickly compensated by activation of other signaling nodes (Trusolino and Bertotti, 2012). This multilayer buffering presents a major problem for targeted therapies. Our group has recently demonstrated that genetic knockout or pharmacological inhibition of mTOR leads to an adaptive rewiring of oncogenic signaling resulting in increased activation of phospho-ERK and phospho-AKT (Hassan et al., 2018). MEK inhibition, on the other hand, has been shown to induce activation of AKT signaling in PDAC cells (Collisson et al., 2012), which was also observed in this work, where treatment with the MEK inhibitor Trametinib increased phosphorylation of AKT. This upregulation of alternative signaling pathways allows the cells to cope with the target inhibition. This might at least partially explain why growth is only marginally affected upon acute FRA1 depletion in the dTAG-FRA1 cells despite its described critical role in KRAS mutant cancers (Vallejo et al., 2017a; Vallejo et al., 2017b). However, compensatory upregulation of signaling pathways upon loss of oncogenic drivers has been shown to create new dependencies and vulnerabilities that can be exploited therapeutically (Settleman et al., 2021). It was therefore the aim of the unbiased drug screen to identify druggable vulnerabilities of FRA1-depleted PDAC cells. Among the common hits of inhibitors that preferentially target FRA1-deficient cells, several MAPK inhibitors as well as an AKT inhibitor were found. This suggests that the two major downstream effectors of KRAS – the RAF-MEK-ERK and the PI3K-AKT signaling pathway – might represent therapeutically targetable acquired vulnerabilities of FRA1-deficient PDAC.

 In context of the MAPK pathway, it has already been demonstrated that vertical inhibition of two or more kinase components of the MAPK pathway (RAF, MEK, ERK) shows synergism compared to the individual inhibition alone (Fernandes Neto et al., 2020; Ozkan-Dagliyan et

al., 2020). The findings from the drug screen indicate that targeting FRA1, a transcription factor downstream of ERK, in conjunction with RAF, MEK or ERK inhibitors has synergistic effects in a subset of PDAC cells as well. A limitation of this study is the relatively small number of cell lines tested, the focus on murine cell lines only, as well as the ectopic overexpression of FRA1 in the genetic models that might not entirely reflect its endogenous function. However, recently published genome-scale loss-of-function CRISPR-Cas9 screens in the presence of a MEK1/2 inhibitor in various human KRAS-mutant pancreatic and lung cancer cell lines, have identified FRA1 to be among the genes that cooperate with MEK inhibition (Sulahian et al., 2019), thus supporting the findings in this thesis. In addition, a genome-scale CRISPR interference screen identified FRA1 as one of the genes, whose loss enhances susceptibility to $KRAS^{G12C}$ inhibition (Lou et al., 2019), therefore showing that the findings in this thesis might not only apply to inhibitors of the MAPK pathway but could also be extended to inhibition of KRAS. These large-scale CRISPR screens also underscore the heterogeneity in genetic modifiers of MEK inhibitor sensitivity across KRAS-mutant cell lines. Whereas a genome-scale CRISPR-Cas9 loss-of-function screen in two pancreatic cancer cell lines did not identify FRA1 as a modulator of Trametinib sensitivity (Wang et al., 2017), FRA1 was identified as a co-dependency in 2 out of 5 PDAC cell lines – but none of the 5 lung cancer cells – in the screen by Sulahian et al. (2019). This heterogeneity, which presents a fundamental problem for targeted therapies in PDAC, was also found in this current work, where for example no sensitization to MEK inhibition upon depletion of FRA1 was observed in the cell line SDF694. Therefore, additional research is necessary to identify the factors that determine the molecular context, in which depletion of FRA1 functions as a sensitizer to MEK inhibition. This will be necessary for proper patient selection in order to develop effective combination strategies. Intriguingly, whereas FRA1 was identified as a factor whose loss enhances susceptibility to direct $KRAS^{G12C}$ inhibition in the pancreatic cancer cell line MiaPaCa2 in the study by Lou et al. (2019), depletion of FRA1 did not sensitize to MEK inhibition in MiaPaCa2 in the CRISPR screen by (Sulahian et al., 2019). These findings point to a possible context dependency that varies not only across cell lines, but also with the targeted signaling node of the RAS-MEK-ERK cascade, allowing increased

flexibility of compensation with down-stream inhibitors. In addition, the mechanism by which FRA1 depletion sensitizes to the inhibitor treatment also seems to vary depending on the context. Lou et al. (2019) demonstrate that FRA1 is necessary to cross-activate AKT signaling to ensure cell survival and proliferation. The requirement of FRA1 for activation of AKT has also been observed in squamous cell carcinoma of the skin and head and neck (Zhang et al., 2016). In this thesis, however, FRA1 does not seem to be essential for cross-activation of AKT signaling. At the basal level, AKT signaling even tends to be increased in FRA1-deficient cells and upon Trametinib treatment, cross-activation of AKT is observed in both the FRA1-deficient as well as the FRA1-proficient cell lines.

In this work, FRA1 rather seems to confer increased independence from upstream MAPK and possibly AKT signaling input. This is supported by the observation that FRA1-proficient cells display reduced levels of phospho-ERK and phospho-AKT at the basal level despite having higher cell proliferation rates. FRA1-reconstituted cells also showed higher resistance to MAPK and AKT inhibitors, indicating that they are less dependent on these pathways than FRA1-depleted cells.

Acute depletion of FRA1 induced increased phospho-ERK signaling within 24 hours that went together with a higher sensitivity towards MEK inhibition. GSEA showed an enrichment of ERK1/2 signatures in both constitutively FRA1-deficient cells as well as upon acute depletion (24 hours) of FRA1. In melanoma cells, downregulation of FRA1 upon treatment with a RAF inhibitor drives a tumor-promoting secretome that activates the AKT pathway and confers resistance (Obenauf et al., 2015). A similar observation was made in Neurofibromin 1 (NF1)-deficient ovarian cancer cells, where FRA1 knockdown or MEKi-mediated destabilization of FRA1 resulted in induced expression of receptor tyrosine kinases that mediated resistance to MEK inhibitor treatment (Kurimchak et al., 2019). In contrast to these studies, where downregulation of FRA1 induced resistance to MAPK pathway inhibition, loss of FRA1 in the current work rather induced sensitivity to RAF-MEK-ERK inhibitors, pointing to a context dependency. If this is due to the different tumor entities, the different oncogenic drivers or other

reasons remains to be determined. AP-1 signaling can exert oncogenic as well as anti-oncogenic effects (Eferl and Wagner, 2003) and the studies by Obenauf et al. (2015) and Kurimchak et al. (2019) suggest the promotion of growth and therapy resistance upon knockdown of FRA1. To avoid unintended consequences, it will be therefore critical to define the molecular context in which FRA1 ablation synergizes with MAPK pathway inhibition.

Whether activation of the MAPK pathway in FRA1-deficient PDAC cells is also driven by a tumor secretome as the enrichment of the ERK1/2 gene signature might suggest, or whether other mechanisms contribute to it, needs to be studied in more detail. More detailed research in a larger panel of cell lines will also be necessary to determine in which context FRA1 is needed to cross-activate AKT signaling as observed in the study by (Lou et al., 2019), and in which case it tends more towards feedback reactivation of MAPK signaling. While there are currently no FRA1-specific inhibitors available, the recent successful development of PROteolysis TArgeting Chimeras (PROTACs) has opened up new opportunities to target previously "undruggable" proteins such as transcription factors like FRA1 (Samarasinghe and Crews, 2021). The proof-of-concept experiments with the dTAG system (Nabet et al., 2018) in the current study, which showed that acute proteasomal degradation of the dTAG-FRA1 fusion protein sensitized the cells to MEK inhibition, suggest at least the feasibility of using small-molecule mediated degradation of FRA1 in conjunction with MAPK inhibitors as an actionable therapeutic strategy for PDAC.

In summary, the current study suggests that targeting FRA1 by itself might not be an effective enough therapeutic strategy, due to the observed compensatory activation of MAPK and PI3K pathway activity. However, combined inhibition of FRA1 in conjunction with mutant KRAS or downstream MAPK signaling might show synergistic effects in a subset of PDAC, so that these combination strategies should be further explored and developed.

5.2 The role of MYC and SUMOylation in pancreatic cancer

This work demonstrates the strong connection between MYC and SUMOylation in pancreatic cancer. In large datasets of human pancreatic cancer, MYC amplification is correlated with increased SUMOylation and linked to a worse survival. MYC and SUMO are especially highly expressed in the basal subtype of PDAC, which has the worst prognosis and is highly resistant to current chemotherapies. New targeted therapies – especially for this particular subtype – are therefore urgently needed. The work in this thesis shows that MYC generates an exploitable dependency on SUMOylation, which can be therapeutically targeted by SUMO inhibitors.

MYC is a strong oncogene that can increase cell metabolism and growth (Dang, 2012). However, its strong effect also generates new vulnerabilities that can be therapeutically exploited (Thng et al., 2021; Wirth et al., 2016). Unbiased MYC synthetic lethal screens have already demonstrated that hyperactive MYC creates dependencies on various cellular networks such as chromatin and transcriptional processes as well as DNA repair and cell cycle checkpoints (Cermelli et al., 2014).

The dependency of high-MYC cells on the SUMOylation machinery has already been observed in human mammary epithelial cells (Kessler et al., 2012), B-cell lymphoma (Hoellein et al., 2014) and small cell lung cancer (Liu et al., 2015). This work goes on to demonstrate that these findings also apply to PDAC.

The cell cycle analysis shows that SUMO inhibition leads to an arrest in the G2-M phase of the cell cycle, increased polyploidy and apoptosis, which fits to previous data from genetic SAE2 inhibition (Kessler et al., 2012; Littler et al., 2019) as well as from SAE inhibitors (He et al., 2017). The importance of SUMOylation for mitotic progression and chromosome segregation has already been shown, as many mitotic functions such as chromosome structure, centromere/kinetochore organization and cytokinesis critically depend on proper SUMOylation (Mukhopadhyay and Dasso, 2017). MYC is a key regulator of entry and progression through the cell cycle and its critical functions especially for the G1 and S-Phase of the cell cycle are

well characterized (Bretones et al., 2015). Yet, the role of MYC in mitosis is much less understood so far. Recently, however, several studies demonstrated the critical dependency of MYC[high]-tumors on the mitotic machinery (Littler et al., 2019; Rohrberg et al., 2020; Topham et al., 2015). These studies show that overexpression of MYC causes mitotic stress, which heightens their dependency on the mitotic protein network. The study by Rohrberg et al. (2020) demonstrates that MYC-overexpressing cells upregulate mitotic genes in a MYC-dependent manner. In particular, they identified three factors, namely Survivin, EG5 and TPX2, as crucial for cellular survival of MYC^{high} cells. Intriguingly, proteomic analysis has demonstrated that these three MYC-dependent mitotic proteins all harbor SUMOylation sites (Hendriks and Vertegaal, 2016) and SUMOylation is known to be critical for proper organization of the spindle and kinetochore complexes (Abrieu and Liakopoulos, 2019). Further analysis is needed to identify in detail how mitotic progression is affected by SUMOylation and which are the crucial factors that explain the mitotic arrest and polyploidy observed after SUMO inhibition in PDAC.

A better understanding of these processes might also help to identify biomarkers beyond MYC that determine responsiveness and thus better define subgroups of patients that respond especially well to SUMO inhibitors, as not all MYC^{high} cells in this study were sensitive to the SUMO inhibitors. Given that tumor fitness in the MYC[high] tumors depend on additional co-factors that can have implications for survival and drug response (Magen et al., 2019), identification of such co-factors that determine sensitivity to SUMO inhibition in MYC[high] tumors could help in selecting patient subgroups that respond well to SUMO-targeted therapies.

The SUMO inhibitor TAK-981, which – like ML-93 – is based on the initial lead compound ML-792 (Langston et al., 2021), is currently tested in Phase 1 clinical trials in patients with lymphomas and solid tumors (NCT03648372, NCT04074330, and NCT04381650). It is well tolerated in pre-clinical models and has been demonstrated to inhibit tumor growth of syngeneic cancers in mice and increase intratumoral T cells and natural killer cells through reactivation of type 1 interferon (IFN1) signaling (Lightcap et al., 2021). Combination with immune checkpoint inhibitors further prolonged the survival of these mice. Considering the

important role that MYC plays in impeding antitumor immune response (Dhanasekaran et al., 2021; Sodir et al., 2020) – such as repression of the type 1 interferon pathway (Muthalagu et al., 2020) – SUMO inhibitors that can reactivate IFN1 signaling and anticancer immune responses might therefore be an intriguing therapeutic option especially for MYC[high] tumors that should be further tested in syngeneic tumor models of PDAC. Indeed, a recent 2022 study demonstrated that the SUMO E1 inhibitor TAK-981 activated anti-tumor immunity in a syngeneic PDAC model by inducing interferon signaling (Kumar et al., 2022), thus further underscoring the potential of SUMO inhibitors to treat PDAC.

In conclusion, the work presented here demonstrates the strong connection between MYC and SUMOylation in PDAC and indicates that SUMOylation might be a druggable vulnerability of MYC-driven PDACs that should be further developed in the future.

6 References

Abrieu, A., and Liakopoulos, D. (2019). How Does SUMO Participate in Spindle Organization? Cells *8*, 801. 10.3390/cells8080801.

Afgan, E., Baker, D., Batut, B., van den Beek, M., Bouvier, D., Cech, M., Chilton, J., Clements, D., Coraor, N., Grüning, B.A., et al. (2018). The Galaxy platform for accessible, reproducible and collaborative biomedical analyses: 2018 update. Nucleic Acids Res *46*, W537-w544. 10.1093/nar/gky379.

Aguirre, A.J., Nowak, J.A., Camarda, N.D., Moffitt, R.A., Ghazani, A.A., Hazar-Rethinam, M., Raghavan, S., Kim, J., Brais, L.K., Ragon, D., et al. (2018). Real-time Genomic Characterization of Advanced Pancreatic Cancer to Enable Precision Medicine. Cancer Discov *8*, 1096-1111. 10.1158/2159-8290.CD-18-0275.

Alagesan, B., Contino, G., Guimaraes, A.R., Corcoran, R.B., Deshpande, V., Wojtkiewicz, G.R., Hezel, A.F., Wong, K.-K., Loda, M., Weissleder, R., et al. (2015). Combined MEK and PI3K Inhibition in a Mouse Model of Pancreatic Cancer. Clinical Cancer Research *21*, 396. 10.1158/1078-0432.CCR-14-1591.

Allen-Petersen, B.L., Risom, T., Feng, Z., Wang, Z., Jenny, Z.P., Thoma, M.C., Pelz, K.R., Morton, J.P., Sansom, O.J., Lopez, C.D., et al. (2019). Activation of PP2A and Inhibition of mTOR Synergistically Reduce MYC Signaling and Decrease Tumor Growth in Pancreatic Ductal Adenocarcinoma. Cancer Res *79*, 209-219. 10.1158/0008-5472.Can-18-0717.

Anders, S., Pyl, P.T., and Huber, W. (2015). HTSeq--a Python framework to work with high-throughput sequencing data. Bioinformatics *31*, 166-169. 10.1093/bioinformatics/btu638.

Angel, P., Imagawa, M., Chiu, R., Stein, B., Imbra, R.J., Rahmsdorf, H.J., Jonat, C., Herrlich, P., and Karin, M. (1987). Phorbol ester-inducible genes contain a common cis element recognized by a TPA-modulated trans-acting factor. Cell *49*, 729-739. 10.1016/0092-8674(87)90611-8.

Appleman, V.A., Ahronian, L.G., Cai, J., Klimstra, D.S., and Lewis, B.C. (2012). KRAS(G12D)- and BRAF(V600E)-induced transformation of murine pancreatic epithelial cells requires MEK/ERK-stimulated IGF1R signaling. Mol Cancer Res *10*, 1228-1239. 10.1158/1541-7786.MCR-12-0340-T.

Ardito, C.M., Grüner, B.M., Takeuchi, K.K., Lubeseder-Martellato, C., Teichmann, N., Mazur, P.K., Delgiorno, K.E., Carpenter, E.S., Halbrook, C.J., Hall, J.C., et al. (2012). EGF receptor is required for KRAS-induced pancreatic tumorigenesis. Cancer cell *22*, 304-317. 10.1016/j.ccr.2012.07.024.

Aung, K.L., Fischer, S.E., Denroche, R.E., Jang, G.H., Dodd, A., Creighton, S., Southwood, B., Liang, S.B., Chadwick, D., Zhang, A., et al. (2018). Genomics-Driven Precision Medicine for Advanced Pancreatic Cancer: Early Results from the COMPASS Trial. Clin Cancer Res *24*, 1344-1354. 10.1158/1078-0432.CCR-17-2994.

Awad, M.M., Liu, S., Rybkin, II, Arbour, K.C., Dilly, J., Zhu, V.W., Johnson, M.L., Heist, R.S., Patil, T., Riely, G.J., et al. (2021). Acquired Resistance to KRAS(G12C) Inhibition in Cancer. N Engl J Med *384*, 2382-2393. 10.1056/NEJMoa2105281.

Bachireddy, P., Bendapudi, P.K., and Felsher, D.W. (2005). Getting at MYC through RAS. Clinical Cancer Research *11*, 4278. 10.1158/1078-0432.CCR-05-0534.

Bailey, P., Chang, D.K., Nones, K., Johns, A.L., Patch, A.M., Gingras, M.C., Miller, D.K., Christ, A.N., Bruxner, T.J., Quinn, M.C., et al. (2016). Genomic analyses identify molecular subtypes of pancreatic cancer. Nature *531*, 47-52. 10.1038/nature16965.

Barretina, J., Caponigro, G., Stransky, N., Venkatesan, K., Margolin, A.A., Kim, S., Wilson, C.J., Lehár, J., Kryukov, G.V., Sonkin, D., et al. (2012). The Cancer Cell Line Encyclopedia enables predictive modelling of anticancer drug sensitivity. Nature *483*, 603-607. 10.1038/nature11003.

Basbous, J., Chalbos, D., Hipskind, R., Jariel-Encontre, I., and Piechaczyk, M. (2007). Ubiquitin-independent proteasomal degradation of Fra-1 is antagonized by Erk1/2 pathway-mediated phosphorylation of a unique C-terminal destabilizer. Mol Cell Biol *27*, 3936-3950. 10.1128/MCB.01776-06.

Bedard, P.L., Tabernero, J., Janku, F., Wainberg, Z.A., Paz-Ares, L., Vansteenkiste, J., Van Cutsem, E., Pérez-García, J., Stathis, A., Britten, C.D., et al. (2015). A phase Ib dose-escalation study of the oral pan-PI3K inhibitor buparlisib (BKM120) in combination with the oral MEK1/2 inhibitor trametinib (GSK1120212) in patients with selected advanced solid tumors. Clin Cancer Res *21*, 730-738. 10.1158/1078-0432.Ccr-14-1814.

Behan, F.M., Iorio, F., Picco, G., Goncalves, E., Beaver, C.M., Migliardi, G., Santos, R., Rao, Y., Sassi, F., Pinnelli, M., et al. (2019). Prioritization of cancer therapeutic targets using CRISPR-Cas9 screens. Nature *568*, 511-516. 10.1038/s41586-019-1103-9.

Bejjani, F., Evanno, E., Zibara, K., Piechaczyk, M., and Jariel-Encontre, I. (2019). The AP-1 transcriptional complex: Local switch or remote command? Biochim Biophys Acta Rev Cancer *1872*, 11-23. 10.1016/j.bbcan.2019.04.003.

Bejjani, F., Tolza, C., Boulanger, M., Downes, D., Romero, R., Maqbool, Muhammad A., Zine El Aabidine, A., Andrau, J.-C., Lebre, S., Brehelin, L., et al. (2021). Fra-1 regulates its target genes via binding to remote enhancers without exerting major control on chromatin architecture in triple negative breast cancers. Nucleic Acids Research *49*, 2488-2508. 10.1093/nar/gkab053.

Beroukhim, R., Mermel, C.H., Porter, D., Wei, G., Raychaudhuri, S., Donovan, J., Barretina, J., Boehm, J.S., Dobson, J., Urashima, M., et al. (2010). The landscape of somatic copy-number alteration across human cancers. Nature *463*, 899-905. 10.1038/nature08822.

Bian, B., Bigonnet, M., Gayet, O., Loncle, C., Maignan, A., Gilabert, M., Moutardier, V., Garcia, S., Turrini, O., Delpero, J.-R., et al. (2017). Gene expression profiling of patient-derived pancreatic cancer xenografts predicts sensitivity to the BET bromodomain inhibitor JQ1: implications for individualized medicine efforts. EMBO Mol Med *9*, 482-497. 10.15252/emmm.201606975.

Biankin, A.V., Waddell, N., Kassahn, K.S., Gingras, M.C., Muthuswamy, L.B., Johns, A.L., Miller, D.K., Wilson, P.J., Patch, A.M., Wu, J., et al. (2012). Pancreatic cancer genomes reveal aberrations in axon guidance pathway genes. Nature *491*, 399-405. 10.1038/nature11547.

Blasco, M.T., Navas, C., Martín-Serrano, G., Graña-Castro, O., Lechuga, C.G., Martín-Díaz, L., Djurec, M., Li, J., Morales-Cacho, L., Esteban-Burgos, L., et al. (2019). Complete Regression of Advanced Pancreatic Ductal Adenocarcinomas upon Combined Inhibition of EGFR and C-RAF. Cancer Cell *35*, 573-587.e576. 10.1016/j.ccell.2019.03.002.

Bonacci, T., Audebert, S., Camoin, L., Baudelet, E., Bidaut, G., Garcia, M., Witzel, I.-I., Perkins, N.D., Borg, J.-P., Iovanna, J.-L., and Soubeyran, P. (2014). Identification of New Mechanisms of Cellular Response to Chemotherapy by Tracking Changes in Post-Translational Modifications by Ubiquitin and Ubiquitin-Like Proteins. Journal of Proteome Research *13*, 2478-2494. 10.1021/pr401258d.

Bretones, G., Delgado, M.D., and León, J. (2015). Myc and cell cycle control. Biochim Biophys Acta *1849*, 506-516. 10.1016/j.bbagrm.2014.03.013.

Buscail, L., Bournet, B., and Cordelier, P. (2020). Role of oncogenic KRAS in the diagnosis, prognosis and treatment of pancreatic cancer. Nat Rev Gastroenterol Hepatol *17*, 153-168. 10.1038/s41575-019-0245-4.

Canon, J., Rex, K., Saiki, A.Y., Mohr, C., Cooke, K., Bagal, D., Gaida, K., Holt, T., Knutson, C.G., Koppada, N., et al. (2019). The clinical KRAS(G12C) inhibitor AMG 510 drives anti-tumour immunity. Nature *575*, 217-223. 10.1038/s41586-019-1694-1.

Casalino, L., Bakiri, L., Talotta, F., Weitzman, J.B., Fusco, A., Yaniv, M., and Verde, P. (2007). Fra-1 promotes growth and survival in RAS-transformed thyroid cells by controlling cyclin A transcription. EMBO J *26*, 1878-1890. https://doi.org/10.1038/sj.emboj.7601617.

Casper, J., Zweig, A.S., Villarreal, C., Tyner, C., Speir, M.L., Rosenbloom, K.R., Raney, B.J., Lee, C.M., Lee, B.T., Karolchik, D., et al. (2018). The UCSC Genome Browser database: 2018 update. Nucleic Acids Res *46*, D762-d769. 10.1093/nar/gkx1020.

Castellano, E., and Downward, J. (2011). RAS Interaction with PI3K: More Than Just Another Effector Pathway. Genes Cancer *2*, 261-274. 10.1177/1947601911408079.

Cerami, E., Gao, J., Dogrusoz, U., Gross, B.E., Sumer, S.O., Aksoy, B.A., Jacobsen, A., Byrne, C.J., Heuer, M.L., Larsson, E., et al. (2012). The cBio cancer genomics portal: an open platform for exploring multidimensional cancer genomics data. Cancer Discov *2*, 401-404. 10.1158/2159-8290.Cd-12-0095.

Cermelli, S., Jang, I.S., Bernard, B., and Grandori, C. (2014). Synthetic lethal screens as a means to understand and treat MYC-driven cancers. Cold Spring Harbor perspectives in medicine *4*, a014209. 10.1101/cshperspect.a014209.

Chan-Seng-Yue, M., Kim, J.C., Wilson, G.W., Ng, K., Figueroa, E.F., O'Kane, G.M., Connor, A.A., Denroche, R.E., Grant, R.C., McLeod, J., et al. (2020). Transcription phenotypes of pancreatic cancer are driven by genomic events during tumor evolution. Nat Genet *52*, 231-240. 10.1038/s41588-019-0566-9.

Choi, B.H., Philips, M.R., Chen, Y., Lu, L., and Dai, W. (2018). K-Ras Lys-42 is crucial for its signaling, cell migration, and invasion. J Biol Chem *293*, 17574-17581. 10.1074/jbc.RA118.003723.

Clark, N.A., Hafner, M., Kouril, M., Williams, E.H., Muhlich, J.L., Pilarczyk, M., Niepel, M., Sorger, P.K., and Medvedovic, M. (2017). GRcalculator: an online tool for calculating and mining dose-response data. BMC Cancer *17*, 698. 10.1186/s12885-017-3689-3.

Cline, M.S., Craft, B., Swatloski, T., Goldman, M., Ma, S., Haussler, D., and Zhu, J. (2013). Exploring TCGA Pan-Cancer data at the UCSC Cancer Genomics Browser. Sci Rep *3*, 2652. 10.1038/srep02652.

Cohen, D.R., Ferreira, P.C., Gentz, R., Franza, B.R., Jr., and Curran, T. (1989). The product of a fos-related gene, fra-1, binds cooperatively to the AP-1 site with Jun: transcription factor AP-1 is comprised of multiple protein complexes. Genes Dev *3*, 173-184. 10.1101/gad.3.2.173.

Collisson, E.A., Bailey, P., Chang, D.K., and Biankin, A.V. (2019). Molecular subtypes of pancreatic cancer. Nat Rev Gastroenterol Hepatol *16*, 207-220. 10.1038/s41575-019-0109-y.

Collisson, E.A., Sadanandam, A., Olson, P., Gibb, W.J., Truitt, M., Gu, S., Cooc, J., Weinkle, J., Kim, G.E., Jakkula, L., et al. (2011). Subtypes of pancreatic ductal adenocarcinoma and their differing responses to therapy. Nat Med *17*, 500-503. 10.1038/nm.2344.

Collisson, E.A., Trejo, C.L., Silva, J.M., Gu, S., Korkola, J.E., Heiser, L.M., Charles, R.P., Rabinovich, B.A., Hann, B., Dankort, D., et al. (2012). A central role for RAF-->MEK-->ERK signaling in the genesis of pancreatic ductal adenocarcinoma. Cancer Discov *2*, 685-693. 10.1158/2159-8290.CD-11-0347.

Conradt, L., Godl, K., Schaab, C., Tebbe, A., Eser, S., Diersch, S., Michalski, C.W., Kleeff, J., Schnieke, A., Schmid, R.M., et al. (2011). Disclosure of erlotinib as a multikinase inhibitor in pancreatic ductal adenocarcinoma. Neoplasia *13*, 1026-1034. 10.1593/neo.111016.

Dai, C., Rennhack, J.P., Arnoff, T.E., Thaker, M., Younger, S.T., Doench, J.G., Huang, A.Y., Yang, A., Aguirre, A.J., Wang, B., et al. (2021). SMAD4 represses FOSL1 expression and pancreatic cancer metastatic colonization. Cell Rep *36*, 109443. 10.1016/j.celrep.2021.109443.

Dang, C.V. (2012). MYC on the path to cancer. Cell *149*, 22-35. 10.1016/j.cell.2012.03.003.

Dang, C.V. (2013). MYC, metabolism, cell growth, and tumorigenesis. Cold Spring Harb Perspect Med *3*. 10.1101/cshperspect.a014217.

Dang, C.V., Reddy, E.P., Shokat, K.M., and Soucek, L. (2017). Drugging the 'undruggable' cancer targets. Nat Rev Cancer *17*, 502-508. 10.1038/nrc.2017.36.

Desmet, C.J., Gallenne, T., Prieur, A., Reyal, F., Visser, N.L., Wittner, B.S., Smit, M.A., Geiger, T.R., Laoukili, J., Iskit, S., et al. (2013). Identification of a pharmacologically tractable Fra-1/ADORA2B axis promoting breast cancer metastasis. Proc Natl Acad Sci U S A *110*, 5139-5144. 10.1073/pnas.1222085110.

Dhanasekaran, R., Deutzmann, A., Mahauad-Fernandez, W.D., Hansen, A.S., Gouw, A.M., and Felsher, D.W. (2021). The MYC oncogene — the grand orchestrator of cancer growth and immune evasion. Nature Reviews Clinical Oncology. 10.1038/s41571-021-00549-2.

Dhillon, A.S., and Tulchinsky, E. (2015). FRA-1 as a driver of tumour heterogeneity: a nexus between oncogenes and embryonic signalling pathways in cancer. Oncogene *34*, 4421-4428. 10.1038/onc.2014.374.

Diersch, S., Wirth, M., Schneeweis, C., Jörs, S., Geisler, F., Siveke, J.T., Rad, R., Schmid, R.M., Saur, D., Rustgi, A.K., et al. (2016). Kras(G12D) induces EGFR-MYC cross signaling in murine primary pancreatic ductal epithelial cells. Oncogene *35*, 3880-3886. 10.1038/onc.2015.437.

Dreyer, S.B., Chang, D.K., Bailey, P., and Biankin, A.V. (2017). Pancreatic Cancer Genomes: Implications for Clinical Management and Therapeutic Development. Clin Cancer Res *23*, 1638-1646. 10.1158/1078-0432.CCR-16-2411.

Ducreux, M., Seufferlein, T., Van Laethem, J.L., Laurent-Puig, P., Smolenschi, C., Malka, D., Boige, V., Hollebecque, A., and Conroy, T. (2019). Systemic treatment of pancreatic cancer revisited. Semin Oncol *46*, 28-38. 10.1053/j.seminoncol.2018.12.003.

Duncan, James S., Whittle, Martin C., Nakamura, K., Abell, Amy N., Midland, Alicia A., Zawistowski, Jon S., Johnson, Nancy L., Granger, Deborah A., Jordan, Nicole V., Darr, David B., et al. (2012). Dynamic Reprogramming of the Kinome in Response to Targeted MEK Inhibition in Triple-Negative Breast Cancer. Cell *149*, 307-321. 10.1016/j.cell.2012.02.053.

Eferl, R., Hoebertz, A., Schilling, A.F., Rath, M., Karreth, F., Kenner, L., Amling, M., and Wagner, E.F. (2004). The Fos-related antigen Fra-1 is an activator of bone matrix formation. EMBO J *23*, 2789-2799. 10.1038/sj.emboj.7600282.

Eferl, R., and Wagner, E.F. (2003). AP-1: a double-edged sword in tumorigenesis. Nat Rev Cancer *3*, 859-868. 10.1038/nrc1209.

Eifler, K., Cuijpers, S.A.G., Willemstein, E., Raaijmakers, J.A., El Atmioui, D., Ovaa, H., Medema, R.H., and Vertegaal, A.C.O. (2018). SUMO targets the APC/C to regulate transition from metaphase to anaphase. Nat Commun *9*, 1119. 10.1038/s41467-018-03486-4.

Engelman, J.A., Chen, L., Tan, X., Crosby, K., Guimaraes, A.R., Upadhyay, R., Maira, M., McNamara, K., Perera, S.A., Song, Y., et al. (2008). Effective use of PI3K and MEK inhibitors to treat mutant Kras G12D and PIK3CA H1047R murine lung cancers. Nat Med *14*, 1351-1356. 10.1038/nm.1890.

Eser, S., Reiff, N., Messer, M., Seidler, B., Gottschalk, K., Dobler, M., Hieber, M., Arbeiter, A., Klein, S., Kong, B., et al. (2013). Selective requirement of PI3K/PDK1 signaling for Kras oncogene-driven pancreatic cell plasticity and cancer. Cancer Cell *23*, 406-420. 10.1016/j.ccr.2013.01.023.

Eser, S., Schnieke, A., Schneider, G., and Saur, D. (2014). Oncogenic KRAS signalling in pancreatic cancer. Br J Cancer *111*, 817-822. 10.1038/bjc.2014.215.

Farrell, A.S., Allen-Petersen, B., Daniel, C.J., Wang, X., Wang, Z., Rodriguez, S., Impey, S., Oddo, J., Vitek, M.P., Lopez, C., et al. (2014). Targeting inhibitors of the tumor suppressor PP2A for the treatment of pancreatic cancer. Mol Cancer Res *12*, 924-939. 10.1158/1541-7786.Mcr-13-0542.

Farrell, A.S., Joly, M.M., Allen-Petersen, B.L., Worth, P.J., Lanciault, C., Sauer, D., Link, J., Pelz, C., Heiser, L.M., Morton, J.P., et al. (2017). MYC regulates ductal-neuroendocrine lineage plasticity in pancreatic ductal adenocarcinoma associated with poor outcome and chemoresistance. Nature Communications *8*, 1728. 10.1038/s41467-017-01967-6.

FDA (2019). FDA approves olaparib for gBRCAm metastatic pancreatic adenocarcinoma. https://www.fda.gov/drugs/resources-information-approved-drugs/fda-approves-olaparib-gbrcam-metastatic-pancreatic-adenocarcinoma.

Fedele, C., Ran, H., Diskin, B., Wei, W., Jen, J., Geer, M.J., Araki, K., Ozerdem, U., Simeone, D.M., Miller, G., et al. (2018). SHP2 Inhibition Prevents Adaptive Resistance to MEK Inhibitors in Multiple Cancer Models. Cancer discovery *8*, 1237-1249. 10.1158/2159-8290.CD-18-0444.

Fernandes Neto, J.M., Nadal, E., Bosdriesz, E., Ooft, S.N., Farre, L., McLean, C., Klarenbeek, S., Jurgens, A., Hagen, H., Wang, L., et al. (2020). Multiple low dose therapy as an effective strategy to treat EGFR inhibitor-resistant NSCLC tumours. Nat Commun *11*, 3157. 10.1038/s41467-020-16952-9.

Flotho, A., and Melchior, F. (2013). Sumoylation: a regulatory protein modification in health and disease. Annu Rev Biochem *82*, 357-385. 10.1146/annurev-biochem-061909-093311.

Franke, K., Vilne, B., Prazeres da Costa, O., Rudelius, M., Peschel, C., Oostendorp, R.A., and Keller, U. (2015). In vivo hematopoietic Myc activation directs a transcriptional signature in endothelial cells within the bone marrow microenvironment. Oncotarget *6*, 21827-21839. 10.18632/oncotarget.5217.

Golan, T., Hammel, P., Reni, M., Cutsem, E.V., Macarulla, T., Hall, M.J., Park, J.O., Hochhauser, D., Arnold, D., Oh, D.-Y., et al. (2021). Overall survival from the phase 3 POLO trial: Maintenance olaparib for germline BRCA-mutated metastatic pancreatic cancer. Journal of Clinical Oncology *39*, 378-378. 10.1200/JCO.2021.39.3_suppl.378.

Golan, T., Hammel, P., Reni, M., Van Cutsem, E., Macarulla, T., Hall, M.J., Park, J.O., Hochhauser, D., Arnold, D., Oh, D.Y., et al. (2019). Maintenance Olaparib for Germline BRCA-Mutated Metastatic Pancreatic Cancer. N Engl J Med *381*, 317-327. 10.1056/NEJMoa1903387.

Grilley-Olson, J.E., Bedard, P.L., Fasolo, A., Cornfeld, M., Cartee, L., Razak, A.R., Stayner, L.A., Wu, Y., Greenwood, R., Singh, R., et al. (2016). A phase Ib dose-escalation study of the MEK inhibitor trametinib in combination with the PI3K/mTOR inhibitor GSK2126458 in patients with advanced solid tumors. Invest New Drugs *34*, 740-749. 10.1007/s10637-016-0377-0.

Guo, C., and Henley, J.M. (2014). Wrestling with stress: roles of protein SUMOylation and deSUMOylation in cell stress response. IUBMB Life *66*, 71-77. 10.1002/iub.1244.

Hallin, J., Engstrom, L.D., Hargis, L., Calinisan, A., Aranda, R., Briere, D.M., Sudhakar, N., Bowcut, V., Baer, B.R., Ballard, J.A., et al. (2020). The KRAS(G12C) Inhibitor MRTX849 Provides Insight toward Therapeutic Susceptibility of KRAS-Mutant Cancers in Mouse Models and Patients. Cancer Discov *10*, 54-71. 10.1158/2159-8290.CD-19-1167.

Hanker, A.B., Kaklamani, V., and Arteaga, C.L. (2019). Challenges for the Clinical Development of PI3K Inhibitors: Strategies to Improve Their Impact in Solid Tumors. Cancer Discov *9*, 482-491. 10.1158/2159-8290.CD-18-1175.

Hassan, Z., Schneeweis, C., Wirth, M., Veltkamp, C., Dantes, Z., Feuerecker, B., Ceyhan, G.O., Knauer, S.K., Weichert, W., Schmid, R.M., et al. (2018). MTOR inhibitor-based combination therapies for pancreatic cancer. Br J Cancer *118*, 366-377. 10.1038/bjc.2017.421.

Hayashi, A., Hong, J., and Iacobuzio-Donahue, C.A. (2021). The pancreatic cancer genome revisited. Nat Rev Gastroenterol Hepatol *18*, 469-481. 10.1038/s41575-021-00463-z.

He, X., Riceberg, J., Pulukuri, S.M., Grossman, S., Shinde, V., Shah, P., Brownell, J.E., Dick, L., Newcomb, J., and Bence, N. (2015). Characterization of the loss of SUMO pathway function on cancer cells and tumor proliferation. PLoS One *10*, e0123882. 10.1371/journal.pone.0123882.

He, X., Riceberg, J., Soucy, T., Koenig, E., Minissale, J., Gallery, M., Bernard, H., Yang, X., Liao, H., Rabino, C., et al. (2017). Probing the roles of SUMOylation in cancer cell biology by using a selective SAE inhibitor. Nat Chem Biol *13*, 1164-1171. 10.1038/nchembio.2463.

Heining, C., Horak, P., Uhrig, S., Codo, P.L., Klink, B., Hutter, B., Frohlich, M., Bonekamp, D., Richter, D., Steiger, K., et al. (2018). NRG1 Fusions in KRAS Wild-Type Pancreatic Cancer. Cancer Discov *8*, 1087-1095. 10.1158/2159-8290.CD-18-0036.

Hendriks, I.A., and Vertegaal, A.C. (2016). A comprehensive compilation of SUMO proteomics. Nat Rev Mol Cell Biol *17*, 581-595. 10.1038/nrm.2016.81.

Hingorani, S.R., Petricoin, E.F., Maitra, A., Rajapakse, V., King, C., Jacobetz, M.A., Ross, S., Conrads, T.P., Veenstra, T.D., Hitt, B.A., et al. (2003). Preinvasive and invasive ductal pancreatic cancer and its early detection in the mouse. Cancer Cell *4*, 437-450. 10.1016/s1535-6108(03)00309-x.

Hoellein, A., Fallahi, M., Schoeffmann, S., Steidle, S., Schaub, F.X., Rudelius, M., Laitinen, I., Nilsson, L., Goga, A., Peschel, C., et al. (2014). Myc-induced SUMOylation is a therapeutic vulnerability for B-cell lymphoma. Blood *124*, 2081-2090. 10.1182/blood-2014-06-584524.

Hofmann, M.H., Gerlach, D., Misale, S., Petronczki, M., and Kraut, N. (2022). Expanding the Reach of Precision Oncology by Drugging All KRAS Mutants. Cancer Discovery *12*, 924-937. 10.1158/2159-8290.Cd-21-1331.

Hruban, R.H., Goggins, M., Parsons, J., and Kern, S.E. (2000). Progression model for pancreatic cancer. Clin Cancer Res *6*, 2969-2972.

Hruban, R.H., Maitra, A., Kern, S.E., and Goggins, M. (2007). Precursors to pancreatic cancer. Gastroenterol Clin North Am *36*, 831-849, vi. 10.1016/j.gtc.2007.08.012.

Infante, J.R., Somer, B.G., Park, J.O., Li, C.P., Scheulen, M.E., Kasubhai, S.M., Oh, D.Y., Liu, Y., Redhu, S., Steplewski, K., and Le, N. (2014). A randomised, double-blind, placebo-controlled trial of trametinib, an oral MEK inhibitor, in combination with gemcitabine for patients with untreated metastatic adenocarcinoma of the pancreas. Eur J Cancer *50*, 2072-2081. 10.1016/j.ejca.2014.04.024.

Jackson, E.L., Willis, N., Mercer, K., Bronson, R.T., Crowley, D., Montoya, R., Jacks, T., and Tuveson, D.A. (2001). Analysis of lung tumor initiation and progression using conditional expression of oncogenic K-ras. Genes Dev *15*, 3243-3248. 10.1101/gad.943001.

Janes, M.R., Zhang, J., Li, L.S., Hansen, R., Peters, U., Guo, X., Chen, Y., Babbar, A., Firdaus, S.J., Darjania, L., et al. (2018). Targeting KRAS Mutant Cancers with a Covalent G12C-Specific Inhibitor. Cell *172*, 578-589 e517. 10.1016/j.cell.2018.01.006.

Janku, F., Yap, T.A., and Meric-Bernstam, F. (2018). Targeting the PI3K pathway in cancer: are we making headway? Nat Rev Clin Oncol *15*, 273-291. 10.1038/nrclinonc.2018.28.

Jiang, X., Xie, H., Dou, Y., Yuan, J., Zeng, D., and Xiao, S. (2020). Expression and function of FRA1 protein in tumors. Mol Biol Rep *47*, 737-752. 10.1007/s11033-019-05123-9.

Jones, S., Zhang, X., Parsons, D.W., Lin, J.C., Leary, R.J., Angenendt, P., Mankoo, P., Carter, H., Kamiyama, H., Jimeno, A., et al. (2008). Core signaling pathways in human pancreatic cancers revealed by global genomic analyses. Science *321*, 1801-1806. 10.1126/science.1164368.

Jung, L.A., Gebhardt, A., Koelmel, W., Ade, C.P., Walz, S., Kuper, J., von Eyss, B., Letschert, S., Redel, C., d'Artista, L., et al. (2017). OmoMYC blunts promoter invasion by oncogenic MYC to inhibit gene expression characteristic of MYC-dependent tumors. Oncogene *36*, 1911-1924. 10.1038/onc.2016.354.

Kamerkar, S., LeBleu, V.S., Sugimoto, H., Yang, S., Ruivo, C.F., Melo, S.A., Lee, J.J., and Kalluri, R. (2017). Exosomes facilitate therapeutic targeting of oncogenic KRAS in pancreatic cancer. Nature *546*, 498-503. 10.1038/nature22341.

Kessler, J.D., Kahle, K.T., Sun, T., Meerbrey, K.L., Schlabach, M.R., Schmitt, E.M., Skinner, S.O., Xu, Q., Li, M.Z., Hartman, Z.C., et al. (2012). A SUMOylation-dependent transcriptional subprogram is required for Myc-driven tumorigenesis. Science *335*, 348-353. 10.1126/science.1212728.

Knudsen, E.S., O'Reilly, E.M., Brody, J.R., and Witkiewicz, A.K. (2016). Genetic Diversity of Pancreatic Ductal Adenocarcinoma and Opportunities for Precision Medicine. Gastroenterology *150*, 48-63. 10.1053/j.gastro.2015.08.056.

Kroonen, J.S., and Vertegaal, A.C.O. (2021). Targeting SUMO Signaling to Wrestle Cancer. Trends Cancer *7*, 496-510. 10.1016/j.trecan.2020.11.009.

Kumar, S., Schoonderwoerd, M.J.A., Kroonen, J.S., de Graaf, I.J., Sluijter, M., Ruano, D., González-Prieto, R., Verlaan-de Vries, M., Rip, J., Arens, R., et al. (2022). Targeting

pancreatic cancer by TAK-981: a SUMOylation inhibitor that activates the immune system and blocks cancer cell cycle progression in a preclinical model. Gut, gutjnl-2021-324834. 10.1136/gutjnl-2021-324834.

Kurimchak, A.M., Shelton, C., Herrera-Montávez, C., Duncan, K.E., Chernoff, J., and Duncan, J.S. (2019). Intrinsic Resistance to MEK Inhibition through BET Protein-Mediated Kinome Reprogramming in NF1-Deficient Ovarian Cancer. Mol Cancer Res *17*, 1721-1734. 10.1158/1541-7786.MCR-18-1332.

Lake, D., Correa, S.A., and Muller, J. (2016). Negative feedback regulation of the ERK1/2 MAPK pathway. Cell Mol Life Sci *73*, 4397-4413. 10.1007/s00018-016-2297-8.

Langmead, B., and Salzberg, S.L. (2012). Fast gapped-read alignment with Bowtie 2. Nature Methods *9*, 357-359. 10.1038/nmeth.1923.

Langston, S.P., Grossman, S., England, D., Afroze, R., Bence, N., Bowman, D., Bump, N., Chau, R., Chuang, B.C., Claiborne, C., et al. (2021). Discovery of TAK-981, a First-in-Class Inhibitor of SUMO-Activating Enzyme for the Treatment of Cancer. J Med Chem *64*, 2501-2520. 10.1021/acs.jmedchem.0c01491.

Lee, C.L., Moding, E.J., Huang, X., Li, Y., Woodlief, L.Z., Rodrigues, R.C., Ma, Y., and Kirsch, D.G. (2012). Generation of primary tumors with Flp recombinase in FRT-flanked p53 mice. Dis Model Mech *5*, 397-402. 10.1242/dmm.009084.

Li, Y.J., Du, L., Wang, J., Vega, R., Lee, T.D., Miao, Y., Aldana-Masangkay, G., Samuels, E.R., Li, B., Ouyang, S.X., et al. (2019). Allosteric Inhibition of Ubiquitin-like Modifications by a Class of Inhibitor of SUMO-Activating Enzyme. Cell Chem Biol *26*, 278-288 e276. 10.1016/j.chembiol.2018.10.026.

Lightcap, E.S., Yu, P., Grossman, S., Song, K., Khattar, M., Xega, K., He, X., Gavin, J.M., Imaichi, H., Garnsey, J.J., et al. (2021). A small-molecule SUMOylation inhibitor activates antitumor immune responses and potentiates immune therapies in preclinical models. Science Translational Medicine *13*, eaba7791. doi:10.1126/scitranslmed.aba7791.

Lin, W.-c., Rajbhandari, N., Liu, C., Sakamoto, K., Zhang, Q., Triplett, A.A., Batra, S.K., Opavsky, R., Felsher, D.W., DiMaio, D.J., et al. (2013). Dormant cancer cells contribute to residual disease in a model of reversible pancreatic cancer. Cancer research *73*, 1821-1830. 10.1158/0008-5472.CAN-12-2067.

Lito, P., Saborowski, A., Yue, J., Solomon, M., Joseph, E., Gadal, S., Saborowski, M., Kastenhuber, E., Fellmann, C., Ohara, K., et al. (2014). Disruption of CRAF-mediated MEK activation is required for effective MEK inhibition in KRAS mutant tumors. Cancer Cell *25*, 697-710. 10.1016/j.ccr.2014.03.011.

Littler, S., Sloss, O., Geary, B., Pierce, A., Whetton, A.D., and Taylor, S.S. (2019). Oncogenic MYC amplifies mitotic perturbations. Open Biol *9*, 190136. 10.1098/rsob.190136.

Liu, X., Xu, Y., Pang, Z., Guo, F., Qin, Q., Yin, T., Sang, Y., Feng, C., Li, X., Jiang, L., et al. (2015). Knockdown of SUMO-activating enzyme subunit 2 (SAE2) suppresses cancer malignancy and enhances chemotherapy sensitivity in small cell lung cancer. J Hematol Oncol *8*, 67. 10.1186/s13045-015-0164-y.

Livak, K.J., and Schmittgen, T.D. (2001). Analysis of Relative Gene Expression Data Using Real-Time Quantitative PCR and the 2−ΔΔCT Method. Methods *25*, 402-408. https://doi.org/10.1006/meth.2001.1262.

Lord, C.J., and Ashworth, A. (2017). PARP inhibitors: Synthetic lethality in the clinic. Science *355*, 1152-1158. 10.1126/science.aam7344.

Lou, K., Steri, V., Ge, A.Y., Hwang, Y.C., Yogodzinski, C.H., Shkedi, A.R., Choi, A.L.M., Mitchell, D.C., Swaney, D.L., Hann, B., et al. (2019). KRAS(G12C) inhibition produces a driver-limited state revealing collateral dependencies. Sci Signal *12*. 10.1126/scisignal.aaw9450.

Love, M.I., Huber, W., and Anders, S. (2014). Moderated estimation of fold change and dispersion for RNA-seq data with DESeq2. Genome Biol *15*, 550. 10.1186/s13059-014-0550-8.

Lu, H., Liu, C., Velazquez, R., Wang, H., Dunkl, L.M., Kazic-Legueux, M., Haberkorn, A., Billy, E., Manchado, E., Brachmann, S.M., et al. (2019). SHP2 Inhibition Overcomes RTK-Mediated Pathway Reactivation in KRAS-Mutant Tumors Treated with MEK Inhibitors. Molecular Cancer Therapeutics *18*, 1323. 10.1158/1535-7163.MCT-18-0852.

Lv, Z., Yuan, L., Atkison, J.H., Williams, K.M., Vega, R., Sessions, E.H., Divlianska, D.B., Davies, C., Chen, Y., and Olsen, S.K. (2018). Molecular mechanism of a covalent allosteric inhibitor of SUMO E1 activating enzyme. Nat Commun *9*, 5145. 10.1038/s41467-018-07015-1.

Maddipati, R., Norgard, R.J., Baslan, T., Rathi, K.S., Zhang, A., Saeid, A., Higashihara, T., Wu, F., Kumar, A., Annamalai, V., et al. (2021). MYC levels regulate metastatic heterogeneity in pancreatic adenocarcinoma. Cancer Discov. 10.1158/2159-8290.Cd-20-1826.

Magen, A., Das Sahu, A., Lee, J.S., Sharmin, M., Lugo, A., Gutkind, J.S., Schäffer, A.A., Ruppin, E., and Hannenhalli, S. (2019). Beyond Synthetic Lethality: Charting the Landscape of Pairwise Gene Expression States Associated with Survival in Cancer. Cell Reports *28*, 938-948.e936. https://doi.org/10.1016/j.celrep.2019.06.067.

Mazur, P.K., Herner, A., Mello, S.S., Wirth, M., Hausmann, S., Sánchez-Rivera, F.J., Lofgren, S.M., Kuschma, T., Hahn, S.A., Vangala, D., et al. (2015). Combined inhibition of BET family proteins and histone deacetylases as a potential epigenetics-based therapy for pancreatic ductal adenocarcinoma. Nat Med *21*, 1163-1171. 10.1038/nm.3952.

Mendoza, M.C., Er, E.E., and Blenis, J. (2011). The Ras-ERK and PI3K-mTOR pathways: cross-talk and compensation. Trends Biochem Sci *36*, 320-328. 10.1016/j.tibs.2011.03.006.

Moffitt, R.A., Marayati, R., Flate, E.L., Volmar, K.E., Loeza, S.G., Hoadley, K.A., Rashid, N.U., Williams, L.A., Eaton, S.C., Chung, A.H., et al. (2015). Virtual microdissection identifies distinct tumor- and stroma-specific subtypes of pancreatic ductal adenocarcinoma. Nat Genet *47*, 1168-1178. 10.1038/ng.3398.

Moore, A.R., Rosenberg, S.C., McCormick, F., and Malek, S. (2020). RAS-targeted therapies: is the undruggable drugged? Nat Rev Drug Discov *19*, 533-552. 10.1038/s41573-020-0068-6.

Moore, M.J., Goldstein, D., Hamm, J., Figer, A., Hecht, J.R., Gallinger, S., Au, H.J., Murawa, P., Walde, D., Wolff, R.A., et al. (2007). Erlotinib plus gemcitabine compared with gemcitabine alone in patients with advanced pancreatic cancer: a phase III trial of the National Cancer Institute of Canada Clinical Trials Group. J Clin Oncol *25*, 1960-1966. 10.1200/JCO.2006.07.9525.

Mueller, S., Engleitner, T., Maresch, R., Zukowska, M., Lange, S., Kaltenbacher, T., Konukiewitz, B., Öllinger, R., Zwiebel, M., Strong, A., et al. (2018). Evolutionary routes and KRAS dosage define pancreatic cancer phenotypes. Nature *554*, 62-68. 10.1038/nature25459.

Mukhopadhyay, D., and Dasso, M. (2017). The SUMO Pathway in Mitosis. Adv Exp Med Biol *963*, 171-184. 10.1007/978-3-319-50044-7_10.

Muthalagu, N., Monteverde, T., Raffo-Iraolagoitia, X., Wiesheu, R., Whyte, D., Hedley, A., Laing, S., Kruspig, B., Upstill-Goddard, R., Shaw, R., et al. (2020). Repression of the Type I Interferon Pathway Underlies MYC- and KRAS-Dependent Evasion of NK and B Cells in Pancreatic Ductal Adenocarcinoma. Cancer Discovery *10*, 872. 10.1158/2159-8290.CD-19-0620.

Nabet, B., Roberts, J.M., Buckley, D.L., Paulk, J., Dastjerdi, S., Yang, A., Leggett, A.L., Erb, M.A., Lawlor, M.A., Souza, A., et al. (2018). The dTAG system for immediate and target-specific protein degradation. Nat Chem Biol *14*, 431-441. 10.1038/s41589-018-0021-8.

Nakhai, H., Sel, S., Favor, J., Mendoza-Torres, L., Paulsen, F., Duncker, G.I.W., and Schmid, R.M. (2007). Ptf1a is essential for the differentiation of GABAergic and glycinergic amacrine cells and horizontal cells in the mouse retina. Development *134*, 1151-1160. 10.1242/dev.02781.

Navas, C., Hernández-Porras, I., Schuhmacher, A.J., Sibilia, M., Guerra, C., and Barbacid, M. (2012). EGF receptor signaling is essential for k-ras oncogene-driven pancreatic ductal adenocarcinoma. Cancer cell *22*, 318-330. 10.1016/j.ccr.2012.08.001.

Nevala-Plagemann, C., Hidalgo, M., and Garrido-Laguna, I. (2020). From state-of-the-art treatments to novel therapies for advanced-stage pancreatic cancer. Nat Rev Clin Oncol *17*, 108-123. 10.1038/s41571-019-0281-6.

Neyret-Kahn, H., Benhamed, M., Ye, T., Le Gras, S., Cossec, J.C., Lapaquette, P., Bischof, O., Ouspenskaia, M., Dasso, M., Seeler, J., et al. (2013). Sumoylation at chromatin governs coordinated repression of a transcriptional program essential for cell growth and proliferation. Genome Res *23*, 1563-1579. 10.1101/gr.154872.113.

O'Kane, G.M., Grunwald, B.T., Jang, G.H., Masoomian, M., Picardo, S., Grant, R.C., Denroche, R.E., Zhang, A., Wang, Y., Lam, B., et al. (2020). GATA6 Expression Distinguishes Classical and Basal-like Subtypes in Advanced Pancreatic Cancer. Clin Cancer Res *26*, 4901-4910. 10.1158/1078-0432.CCR-19-3724.

Obenauf, A.C., Zou, Y., Ji, A.L., Vanharanta, S., Shu, W., Shi, H., Kong, X., Bosenberg, M.C., Wiesner, T., Rosen, N., et al. (2015). Therapy-induced tumour secretomes promote resistance and tumour progression. Nature *520*, 368-372. 10.1038/nature14336.

Ozkan-Dagliyan, I., Diehl, J.N., George, S.D., Schaefer, A., Papke, B., Klotz-Noack, K., Waters, A.M., Goodwin, C.M., Gautam, P., Pierobon, M., et al. (2020). Low-Dose Vertical Inhibition of the RAF-MEK-ERK Cascade Causes Apoptotic Death of KRAS Mutant Cancers. Cell Rep *31*, 107764. 10.1016/j.celrep.2020.107764.

Parekh, S., Ziegenhain, C., Vieth, B., Enard, W., and Hellmann, I. (2016). The impact of amplification on differential expression analyses by RNA-seq. Scientific Reports *6*, 25533. 10.1038/srep25533.

Perkhofer, L., Gout, J., Roger, E., Kude de Almeida, F., Baptista Simoes, C., Wiesmuller, L., Seufferlein, T., and Kleger, A. (2021). DNA damage repair as a target in pancreatic cancer: state-of-the-art and future perspectives. Gut *70*, 606-617. 10.1136/gutjnl-2019-319984.

Pettazzoni, P., Viale, A., Shah, P., Carugo, A., Ying, H., Wang, H., Genovese, G., Seth, S., Minelli, R., Green, T., et al. (2015). Genetic events that limit the efficacy of MEK and RTK inhibitor therapies in a mouse model of KRAS-driven pancreatic cancer. Cancer research *75*, 1091-1101. 10.1158/0008-5472.CAN-14-1854.

Pilie, P.G., Tang, C., Mills, G.B., and Yap, T.A. (2019). State-of-the-art strategies for targeting the DNA damage response in cancer. Nat Rev Clin Oncol *16*, 81-104. 10.1038/s41571-018-0114-z.

Pishvaian, M.J., Bender, R.J., Halverson, D., Rahib, L., Hendifar, A.E., Mikhail, S., Chung, V., Picozzi, V.J., Sohal, D., Blais, E.M., et al. (2018a). Molecular Profiling of Patients with Pancreatic Cancer: Initial Results from the Know Your Tumor Initiative. Clin Cancer Res *24*, 5018-5027. 10.1158/1078-0432.CCR-18-0531.

Pishvaian, M.J., Blais, E.M., Brody, J.R., Lyons, E., DeArbeloa, P., Hendifar, A., Mikhail, S., Chung, V., Sahai, V., Sohal, D.P.S., et al. (2020). Overall survival in patients with pancreatic cancer receiving matched therapies following molecular profiling: a retrospective analysis of the Know Your Tumor registry trial. Lancet Oncol *21*, 508-518. 10.1016/S1470-2045(20)30074-7.

Pishvaian, M.J., Rolfo, C.D., Liu, S.V., Multani, P.S., Maneval, E.C., and Garrido-Laguna, I. (2018b). Clinical benefit of entrectinib for patients with metastatic pancreatic cancer who harbor NTRK and ROS1 fusions. Journal of Clinical Oncology *36*, 521-521. 10.1200/JCO.2018.36.4_suppl.521.

Ponz-Sarvise, M., Corbo, V., Tiriac, H., Engle, D.D., Frese, K.K., Oni, T.E., Hwang, C.-I., Öhlund, D., Chio, I.I.C., Baker, L.A., et al. (2019). Identification of Resistance Pathways Specific to Malignancy Using Organoid Models of Pancreatic Cancer. Clinical cancer research : an official journal of the American Association for Cancer Research *25*, 6742-6755. 10.1158/1078-0432.CCR-19-1398.

Poulikakos, P.I., and Solit, D.B. (2011). Resistance to MEK inhibitors: should we co-target upstream? Sci Signal *4*, pe16. 10.1126/scisignal.2001948.

Quante, A.S., Ming, C., Rottmann, M., Engel, J., Boeck, S., Heinemann, V., Westphalen, C.B., and Strauch, K. (2016). Projections of cancer incidence and cancer-related deaths in Germany by 2020 and 2030. Cancer Med *5*, 2649-2656. 10.1002/cam4.767.

Rahib, L., Smith, B.D., Aizenberg, R., Rosenzweig, A.B., Fleshman, J.M., and Matrisian, L.M. (2014). Projecting cancer incidence and deaths to 2030: the unexpected burden of thyroid, liver, and pancreas cancers in the United States. Cancer Res *74*, 2913-2921. 10.1158/0008-5472.CAN-14-0155.

Rahib, L., Wehner, M.R., Matrisian, L.M., and Nead, K.T. (2021). Estimated Projection of US Cancer Incidence and Death to 2040. JAMA Netw Open *4*, e214708. 10.1001/jamanetworkopen.2021.4708.

Raphael, B.J., Hruban, R.H., Aguirre, A.J., Moffitt, R.A., Yeh, J.J., Stewart, C., Robertson, A.G., Cherniack, A.D., Gupta, M., Getz, G., et al. (2017). Integrated Genomic Characterization of Pancreatic Ductal Adenocarcinoma. Cancer Cell *32*, 185-203.e113. 10.1016/j.ccell.2017.07.007.

Rohrberg, J., Van de Mark, D., Amouzgar, M., Lee, J.V., Taileb, M., Corella, A., Kilinc, S., Williams, J., Jokisch, M.L., Camarda, R., et al. (2020). MYC Dysregulates Mitosis, Revealing Cancer Vulnerabilities. Cell Rep *30*, 3368-3382 e3367. 10.1016/j.celrep.2020.02.041.

Ruess, D.A., Heynen, G.J., Ciecielski, K.J., Ai, J., Berninger, A., Kabacaoglu, D., Görgülü, K., Dantes, Z., Wörmann, S.M., Diakopoulos, K.N., et al. (2018). Mutant KRAS-driven cancers depend on PTPN11/SHP2 phosphatase. Nat Med *24*, 954-960. 10.1038/s41591-018-0024-8.

Ryan, M.B., Der, C.J., Wang-Gillam, A., and Cox, A.D. (2015). Targeting RAS-mutant cancers: is ERK the key? Trends Cancer *1*, 183-198. 10.1016/j.trecan.2015.10.001.

Saborowski, M., Saborowski, A., Morris, J.P.t., Bosbach, B., Dow, L.E., Pelletier, J., Klimstra, D.S., and Lowe, S.W. (2014). A modular and flexible ESC-based mouse model of pancreatic cancer. Genes & development *28*, 85-97. 10.1101/gad.232082.113.

Samarasinghe, K.T.G., and Crews, C.M. (2021). Targeted protein degradation: A promise for undruggable proteins. Cell Chemical Biology *28*, 934-951. 10.1016/j.chembiol.2021.04.011.

Savoia, P., Fava, P., Casoni, F., and Cremona, O. (2019). Targeting the ERK Signaling Pathway in Melanoma. Int J Mol Sci *20*. 10.3390/ijms20061483.

Schlieman, M.G., Fahy, B.N., Ramsamooj, R., Beckett, L., and Bold, R.J. (2003). Incidence, mechanism and prognostic value of activated AKT in pancreas cancer. Br J Cancer *89*, 2110-2115. 10.1038/sj.bjc.6601396.

Schneeweis, C., Hassan, Z., Schick, M., Keller, U., and Schneider, G. (2021). The SUMO pathway in pancreatic cancer: insights and inhibition. Br J Cancer *124*, 531-538. 10.1038/s41416-020-01119-6.

Schneeweis, C., Wirth, M., Saur, D., Reichert, M., and Schneider, G. (2018). Oncogenic KRAS and the EGFR loop in pancreatic carcinogenesis-A connection to licensing nodes. Small GTPases *9*, 457-464. 10.1080/21541248.2016.1262935.

Schneider, G., Wirth, M., Keller, U., and Saur, D. (2021). Rationale for MYC imaging and targeting in pancreatic cancer. EJNMMI Res *11*, 104-104. 10.1186/s13550-021-00843-1.

Schönhuber, N., Seidler, B., Schuck, K., Veltkamp, C., Schachtler, C., Zukowska, M., Eser, S., Feyerabend, T.B., Paul, M.C., Eser, P., et al. (2014). A next-generation dual-recombinase system for time- and host-specific targeting of pancreatic cancer. Nature Medicine *20*, 1340-1347. 10.1038/nm.3646.

Seeler, J.S., and Dejean, A. (2017). SUMO and the robustness of cancer. Nat Rev Cancer *17*, 184-197. 10.1038/nrc.2016.143.

Semaan, A., Bernard, V., Lee, J.J., Wong, J.W., Huang, J., Swartzlander, D.B., Stephens, B.M., Monberg, M.E., Weston, B.R., Bhutani, M.S., et al. (2021). Defining the Comprehensive Genomic Landscapes of Pancreatic Ductal Adenocarcinoma Using Real-World Endoscopic Aspiration Samples. Clin Cancer Res *27*, 1082-1093. 10.1158/1078-0432.CCR-20-2667.

Settleman, J., Neto, J.M.F., and Bernards, R. (2021). Thinking Differently about Cancer Treatment Regimens. Cancer Discovery *11*, 1016. 10.1158/2159-8290.CD-20-1187.

Shaul, Y.D., and Seger, R. (2007). The MEK/ERK cascade: from signaling specificity to diverse functions. Biochim Biophys Acta *1773*, 1213-1226. 10.1016/j.bbamcr.2006.10.005.

Siegel, R.L., Miller, K.D., Fuchs, H.E., and Jemal, A. (2021). Cancer Statistics, 2021. CA Cancer J Clin *71*, 7-33. 10.3322/caac.21654.

Singhi, A.D., Ali, S.M., Lacy, J., Hendifar, A., Nguyen, K., Koo, J., Chung, J.H., Greenbowe, J., Ross, J.S., Nikiforova, M.N., et al. (2017). Identification of Targetable ALK Rearrangements in Pancreatic Ductal Adenocarcinoma. J Natl Compr Canc Netw *15*, 555-562. 10.6004/jnccn.2017.0058.

Singhi, A.D., George, B., Greenbowe, J.R., Chung, J., Suh, J., Maitra, A., Klempner, S.J., Hendifar, A., Milind, J.M., Golan, T., et al. (2019). Real-Time Targeted Genome Profile Analysis of Pancreatic Ductal Adenocarcinomas Identifies Genetic Alterations That Might Be Targeted With Existing Drugs or Used as Biomarkers. Gastroenterology *156*, 2242-2253 e2244. 10.1053/j.gastro.2019.02.037.

Skoulidis, F., Li, B.T., Dy, G.K., Price, T.J., Falchook, G.S., Wolf, J., Italiano, A., Schuler, M., Borghaei, H., Barlesi, F., et al. (2021). Sotorasib for Lung Cancers with KRAS p.G12C Mutation. N Engl J Med *384*, 2371-2381. 10.1056/NEJMoa2103695.

Sodir, N.M., Kortlever, R.M., Barthet, V.J.A., Campos, T., Pellegrinet, L., Kupczak, S., Anastasiou, P., Swigart, L.B., Soucek, L., Arends, M.J., et al. (2020). MYC Instructs and Maintains Pancreatic Adenocarcinoma Phenotype. Cancer Discovery *10*, 588. 10.1158/2159-8290.CD-19-0435.

Sodir, N.M., Swigart, L.B., Karnezis, A.N., Hanahan, D., Evan, G.I., and Soucek, L. (2011). Endogenous Myc maintains the tumor microenvironment. Genes & development *25*, 907-916. 10.1101/gad.2038411.

Soucek, L., Whitfield, J., Martins, C.P., Finch, A.J., Murphy, D.J., Sodir, N.M., Karnezis, A.N., Swigart, L.B., Nasi, S., and Evan, G.I. (2008). Modelling Myc inhibition as a cancer therapy. Nature *455*, 679-683. 10.1038/nature07260.

Stöckel, D., Kehl, T., Trampert, P., Schneider, L., Backes, C., Ludwig, N., Gerasch, A., Kaufmann, M., Gessler, M., Graf, N., et al. (2016). Multi-omics enrichment analysis using the GeneTrail2 web service. Bioinformatics *32*, 1502-1508. 10.1093/bioinformatics/btv770.

Subramanian, A., Tamayo, P., Mootha, V.K., Mukherjee, S., Ebert, B.L., Gillette, M.A., Paulovich, A., Pomeroy, S.L., Golub, T.R., Lander, E.S., and Mesirov, J.P. (2005). Gene set enrichment analysis: a knowledge-based approach for interpreting genome-wide expression profiles. Proc Natl Acad Sci U S A *102*, 15545-15550. 10.1073/pnas.0506580102.

Sulahian, R., Kwon, J.J., Walsh, K.H., Pailler, E., Bosse, T.L., Thaker, M., Almanza, D., Dempster, J.M., Pan, J., Piccioni, F., et al. (2019). Synthetic Lethal Interaction of SHOC2 Depletion with MEK Inhibition in RAS-Driven Cancers. Cell Reports *29*, 118-134.e118. https://doi.org/10.1016/j.celrep.2019.08.090.

Swayden, M., Alzeeb, G., Masoud, R., Berthois, Y., Audebert, S., Camoin, L., Hannouche, L., Vachon, H., Gayet, O., Bigonnet, M., et al. (2019). PML hyposumoylation is responsible for the resistance of pancreatic cancer. FASEB J *33*, 12447-12463. 10.1096/fj.201901091R.

Talotta, F., Casalino, L., and Verde, P. (2020). The nuclear oncoprotein Fra-1: a transcription factor knocking on therapeutic applications' door. Oncogene *39*, 4491-4506. 10.1038/s41388-020-1306-4.

Thng, D.K.H., Toh, T.B., and Chow, E.K.-H. (2021). Capitalizing on Synthetic Lethality of MYC to Treat Cancer in the Digital Age. Trends in Pharmacological Sciences *42*, 166-182. 10.1016/j.tips.2020.11.014.

Topham, C., Tighe, A., Ly, P., Bennett, A., Sloss, O., Nelson, L., Ridgway, R.A., Huels, D., Littler, S., Schandl, C., et al. (2015). MYC Is a Major Determinant of Mitotic Cell Fate. Cancer Cell *28*, 129-140. 10.1016/j.ccell.2015.06.001.

Trusolino, L., and Bertotti, A. (2012). Compensatory pathways in oncogenic kinase signaling and resistance to targeted therapies: six degrees of separation. Cancer Discov *2*, 876-880. 10.1158/2159-8290.CD-12-0400.

Uphoff, C.C., and Drexler, H.G. (2011). Detecting mycoplasma contamination in cell cultures by polymerase chain reaction. Methods Mol Biol *731*, 93-103. 10.1007/978-1-61779-080-5_8.

Vallejo, A., Perurena, N., Guruceaga, E., Mazur, P.K., Martinez-Canarias, S., Zandueta, C., Valencia, K., Arricibita, A., Gwinn, D., Sayles, L.C., et al. (2017a). An integrative approach unveils FOSL1 as an oncogene vulnerability in KRAS-driven lung and pancreatic cancer. Nat Commun *8*, 14294. 10.1038/ncomms14294.

Vallejo, A., Valencia, K., and Vicent, S. (2017b). All for one and FOSL1 for all: FOSL1 at the crossroads of lung and pancreatic cancer driven by mutant KRAS. Mol Cell Oncol *4*, e1314239. 10.1080/23723556.2017.1314239.

Van Cutsem, E., Hidalgo, M., Canon, J.L., Macarulla, T., Bazin, I., Poddubskaya, E., Manojlovic, N., Radenkovic, D., Verslype, C., Raymond, E., et al. (2018). Phase I/II trial of pimasertib plus gemcitabine in patients with metastatic pancreatic cancer. Int J Cancer *143*, 2053-2064. 10.1002/ijc.31603.

Vaseva, A.V., Blake, D.R., Gilbert, T.S.K., Ng, S., Hostetter, G., Azam, S.H., Ozkan-Dagliyan, I., Gautam, P., Bryant, K.L., Pearce, K.H., et al. (2018). KRAS Suppression-Induced Degradation of MYC Is Antagonized by a MEK5-ERK5 Compensatory Mechanism. Cancer cell *34*, 807-822.e807. 10.1016/j.ccell.2018.10.001.

Waddell, N., Pajic, M., Patch, A.M., Chang, D.K., Kassahn, K.S., Bailey, P., Johns, A.L., Miller, D., Nones, K., Quek, K., et al. (2015). Whole genomes redefine the mutational landscape of pancreatic cancer. Nature *518*, 495-501. 10.1038/nature14169.

Walz, S., Lorenzin, F., Morton, J., Wiese, K.E., von Eyss, B., Herold, S., Rycak, L., Dumay-Odelot, H., Karim, S., Bartkuhn, M., et al. (2014). Activation and repression by oncogenic MYC shape tumour-specific gene expression profiles. Nature *511*, 483-487. 10.1038/nature13473.

Wang, B., Krall, E.B., Aguirre, A.J., Kim, M., Widlund, H.R., Doshi, M.B., Sicinska, E., Sulahian, R., Goodale, A., Cowley, G.S., et al. (2017). ATXN1L, CIC, and ETS Transcription Factors Modulate Sensitivity to MAPK Pathway Inhibition. Cell reports *18*, 1543-1557. 10.1016/j.celrep.2017.01.031.

Waters, A.M., and Der, C.J. (2018). KRAS: The Critical Driver and Therapeutic Target for Pancreatic Cancer. Cold Spring Harb Perspect Med *8*. 10.1101/cshperspect.a031435.

Waters, A.M., Khatib, T.O., Papke, B., Goodwin, C.M., Hobbs, G.A., Diehl, J.N., Yang, R., Edwards, A.C., Walsh, K.H., Sulahian, R., et al. (2021). Targeting p130Cas- and microtubule-dependent MYC regulation sensitizes pancreatic cancer to ERK MAPK inhibition. Cell Reports *35*. 10.1016/j.celrep.2021.109291.

Wee, S., Jagani, Z., Xiang, K.X., Loo, A., Dorsch, M., Yao, Y.M., Sellers, W.R., Lengauer, C., and Stegmeier, F. (2009). PI3K pathway activation mediates resistance to MEK inhibitors in KRAS mutant cancers. Cancer Res *69*, 4286-4293. 10.1158/0008-5472.CAN-08-4765.

Werner, J., Combs, S.E., Springfeld, C., Hartwig, W., Hackert, T., and Buchler, M.W. (2013). Advanced-stage pancreatic cancer: therapy options. Nat Rev Clin Oncol *10*, 323-333. 10.1038/nrclinonc.2013.66.

Wirth, M., Mahboobi, S., Krämer, O.H., and Schneider, G. (2016). Concepts to Target MYC in Pancreatic Cancer. Mol Cancer Ther *15*, 1792-1798. 10.1158/1535-7163.Mct-16-0050.

Wirth, M., and Schneider, G. (2016). MYC: A Stratification Marker for Pancreatic Cancer Therapy. Trends in Cancer *2*, 1-3. 10.1016/j.trecan.2015.12.002.

Witkiewicz, A.K., McMillan, E.A., Balaji, U., Baek, G., Lin, W.C., Mansour, J., Mollaee, M., Wagner, K.U., Koduru, P., Yopp, A., et al. (2015). Whole-exome sequencing of pancreatic cancer defines genetic diversity and therapeutic targets. Nat Commun *6*, 6744. 10.1038/ncomms7744.

Wolf, E., and Eilers, M. (2020). Targeting MYC Proteins for Tumor Therapy. Annual Review of Cancer Biology *4*, 61-75. 10.1146/annurev-cancerbio-030518-055826.

Xue, Y., Martelotto, L., Baslan, T., Vides, A., Solomon, M., Mai, T.T., Chaudhary, N., Riely, G.J., Li, B.T., Scott, K., et al. (2017). An approach to suppress the evolution of resistance in BRAF(V600E)-mutant cancer. Nat Med *23*, 929-937. 10.1038/nm.4369.

Yaeger, R., and Corcoran, R.B. (2019). Targeting Alterations in the RAF-MEK Pathway. Cancer Discov *9*, 329-341. 10.1158/2159-8290.CD-18-1321.

Yang, Y., Xia, Z., Wang, X., Zhao, X., Sheng, Z., Ye, Y., He, G., Zhou, L., Zhu, H., Xu, N., and Liang, S. (2018). Small-Molecule Inhibitors Targeting Protein SUMOylation as Novel Anticancer Compounds. Mol Pharmacol *94*, 885-894. 10.1124/mol.118.112300.

Yoon, S., and Seger, R. (2006). The extracellular signal-regulated kinase: multiple substrates regulate diverse cellular functions. Growth Factors *24*, 21-44. 10.1080/02699050500284218.

Young, M.R., and Colburn, N.H. (2006). Fra-1 a target for cancer prevention or intervention. Gene *379*, 1-11. 10.1016/j.gene.2006.05.001.

Zhang, X., Wu, J., Luo, S., Lechler, T., and Zhang, J.Y. (2016). FRA1 promotes squamous cell carcinoma growth and metastasis through distinct AKT and c-Jun dependent mechanisms. Oncotarget *7*, 34371-34383. 10.18632/oncotarget.9110.

Zhao, X. (2018). SUMO-Mediated Regulation of Nuclear Functions and Signaling Processes. Mol Cell *71*, 409-418. 10.1016/j.molcel.2018.07.027.

Acknowledgements

First, I would like to thank Professor Günter Schneider for giving me the opportunity to work on these research projects, the freedom to pursue and explore novel ideas and above all his constant support, scientific guidance and encouragement.

I would also like to thank Professor Roland Schmid and the Klinik und Poliklinik

für Innere Medizin II for providing an excellent research environment.

Next, I would like to express my sincere gratitude to Professor Bernhard Küster and Professor Dieter Saur for agreeing to supervise and mentor me as part of my thesis advisory committee.

I furthermore would like to thank Prof. Dr. Erwin Wagner for providing us with the Fra1lox mouse lines and Professor Ulrich Keller and his group – in particular Alexander and Markus – for the great and fruitful collaboration on the SUMO project.

Last but not least, I would like to thank all members of AG Schneider, AG Rad, AG Reichert, AG Geisler and AG Saur for the scientific discussions and their great help and support.

In particular, I am deeply grateful to Sandra – who started the FRA1 research project and KCF mouse lines and who introduced me to all the necessary techniques – and especially to Zonera for her collaborative scientific spirit and her great invaluable work and support across our many shared projects. I furthermore would like to thank Rupert for the RNA-sequencing, Matthias and Lukas for the bioinformatics analysis, Roman and Sebastian W. for their help with plasmids and cloning, Hannah for her help with the drug screen analysis, Aylin for great technical support and Chiara for the many critical discussions and feedback and her invaluable scientific input.